U.S. - JAPAN COORDINATED PROGRAM
FOR
MASONRY BUILDING RESEARCH

REPORT NO. 3.1(a)-2

RESPONSE OF SINGLE-STORY REINFORCED MASONRY SHEAR WALLS TO IN-PLANE LATERAL LOADS

by

P. Benson Shing
James L. Noland
Hannes P. Spaeh
Eric W. Klamerus
Michael P. Schuller

January 1991

supported by:

NATIONAL SCIENCE FOUNDATION

GRANT NO. ECE-8517024

Department of Civil, Environmental,
and Architectural Engineering
University of Colorado at Boulder
Boulder, Colorado 80309-0428

ACKNOWLEDGMENTS

The study presented in this paper is financially supported by the National Science Foundation under Grant No. ECE-8517024. The partial support of the Concrete Masonry Association of California and Nevada, the Western States Clay Products Association, the Masonry Institute of America, and the Colorado Masonry Association is also gratefully acknowledged. Furthermore, the writers would like to thank members of the Technical Coordinating Committee on Masonry Research (TCCMAR) and the advisory panel for their valuable advice and contribution to this project. Some of the experimental work and data reduction were carried out by Shankar Hoskere and Edward Carter, who are former graduate research assistants, and also with the dedicated assistance of Craig Kitzman, Susan Huey, Daniel Hogan, and Daniel Burrroughs. The construction of the wall specimens was professionally done by Michael Stein as well as with the support of local contractors. Finally, the assistance of Jeffrey Smith in preparing the tables and figures for this report is also appreciated. However, opinions expressed in this report are those of the writers, and do not necessarily represent those of the National Science Foundation and other sponsors.

RESPONSE OF SINGLE-STORY REINFORCED MASONRY SHEAR WALLS TO IN-PLANE LATERAL LOADS

by

P. Benson Shing
James L. Noland
Hannes P. Spaeh
Eric W. Klamerus
Michael P. Schuller

A Report to Sponsor
National Science Foundation
Grant No. ECE-8517024

Report No. 3.1(a)-2
U.S.-Japan Coordinated Program for Masonry Building Research

Department of Civil, Environmental,
and Architectural Engineering
University of Colorado at Boulder
Boulder, Colorado 80309-0428

January 1991

ABSTRACT

Twenty-four single-story reinforced masonry shear walls were tested at the University of Colorado at Boulder as part of the U.S.-Japan Coordinated Program for Masonry Building Research. The objective of this study is to provide relevant experimental data for the development and calibration of analytical models and improved design recommendations for reinforced masonry shear walls. In this study, the influence of the axial compressive stress, quantity of vertical and horizontal reinforcement, and load/displacement history on the lateral resistance, failure mechanism, ductility, and energy-dissipation capability of a wall panel has been examined. Eighteen of the wall specimens were hollow concrete unit masonry and six were hollow clay unit masonry. It has been shown that the flexural strength increases with the axial compressive stress and the quantity of vertical reinforcement. However, the flexural ductility decreases as the axial compressive stress increases. The shear strength, dominated by diagonal cracking, increases with the quantity of vertical and horizontal steel, as well as with the axial compressive stress. Nevertheless, the axial compressive stress has a more significant influence on the flexural strength than on the shear strength. Furthermore, the increase of the shear strength is not directly proportional to the increase of horizontal steel. In spite of this, increasing the quantity of horizontal as well as vertical reinforcement can substantially improve the postcracked ductility and energy-dissipation capability of a shear-dominated wall panel.

TABLE OF CONTENTS

LIST OF FIGURES

LIST OF TABLES

1 INTRODUCTION

1.1 Statement of Problem

Reinforced masonry buildings can be frequently found in regions of high seismicity. Such structures are usually constructed as "box systems," in which walls resist the gravity loads as well as the vertical and lateral in-plane loads induced by wind and earthquake ground motions. Depending on the structural configuration, effective aspect ratio of wall components, and quantity of vertical and horizontal reinforcement, two distinct inelastic deformation mechanisms can be exhibited by shear walls subjected to seismic loads. One is the in-plane flexural mechanism that is characterized by the tensile yielding of vertical reinforcement and/or compressive crushing of masonry. The other is the shear mechanism that is characterized by diagonal tensile cracking. The former can be developed in slender cantilever walls connected by flexible floor slabs, whereas the latter often occurs in strongly coupled shear walls connected by stiff spandrels (Priestley 1987), or in walls with a low height-to-length ratio. A detailed discussion of these mechanisms will be presented in Chapter 5 of this report.

While both of the aforementioned wall systems can be found in masonry construction, systems with stiff spandrels are common among existing masonry structures and are also frequently used in current construction. Nevertheless, observations from past earthquake damage and results of recent research (Priestley 1987) have indicated that the shear mechanism is less desirable than the flexural mechanism. Experimental results (Mayes et al. 1976a; Hidalgo et al. 1978, 1979; Chen et al. 1978; Priestley and Bridgeman 1974; Priestley 1977; Priestley and Elder 1982; Sveinsson et al. 1985; Wakabayashi and Nakamura 1984) have indicated that wall components dominated by the shear mechanism are more brittle than those dominated by flexure. Furthermore, structures with stiff spandrels have a high tendency to form soft stories once severe diagonal cracks have developed in the piers. This will reduce the overall ductility of a structural system, and, thereby, severely jeopardize the seismic resistance of a structure.

To avoid undesirable brittle shear behavior in reinforced masonry design, it is necessary to know the strength and deformation capability of wall panels under different behavior modes. The latter is important for seismic resistance design where the design load, stipulated in most building codes, increases as the expected ductility or deformation capability of a structure decreases. To this end, extensive experimental studies, some of which are indicated above, have been carried out by numerous researchers. Unfortunately, owing to the large number of design parameters involved and the specific load conditions introduced in some of the test procedures, the existing data do not lead to definitive conclusions. Hence, the design of reinforced masonry structures in the U.S. has been predominantly based on the working stress approach, which does not explicitly require the above considerations. The first major change of the design methodology for masonry in this country was introduced in the 1988 edition of the Uniform Building Code (UBC), in which provisions for the strength design of reinforced masonry shear walls are provided as an alternative to the working stress approach.

Because of insufficient experimental data and the lack of a validated theoretical model, the 1988 UBC provisions for the shear strength of reinforced masonry wall panels could be over-conservative. Moreover, information on the ductility of reinforced masonry structures is very limited. Therefore, the values of the R_W factor for the equivalent static load recommended by the UBC for masonry structures have not been fully validated. To enhance the data base and improve current design methodology, tests of reinforced masonry shear walls were included as important components of the U.S. Coordinated Program for Masonry Building Research (Noland 1987). In this program, tests of full-size, single-story, two-story (Merryman et al. 1990), and three-story (Hegemier et al. 1990) reinforced masonry shear walls were carried out. The results of the single-story shear wall tests, which were conducted at the University of Colorado, are summarized in this report.

1.2 Review of Previous Research

Experimental studies of reinforced masonry shear walls have been conducted by numerous researchers in different countries, notably in Chile (Luders and Hildago 1988), Greece (Tassios, Vintzeleou, and Trohanis 1984), Italy (Giuffre', Macchi, and Modena 1984; Macchi 1982; Cantu and Macchi 1979), Japan (Matsumura 1988; Kaminosono et al. 1988; Wakabayashi and Nakamura 1984), Mexico

(Meli 1983), New Zealand (Priestley and Elder 1982; Priestley 1977; Priestley and Bridgeman 1974; Williams and Scrivener 1973; Scrivener 1969), the United States (Sveinsson et al. 1985; Woodward and Rankin 1985; Hidalgo et al. 1978, 1979; Chen et al. 1978; Mayes et al. 1976a, 1976b; Schneider 1956), and Yugoslavia (Tomazevic and Lutman 1988; Tomazevic et al. 1986). In spite of the different unit types and construction techniques used in different countries, some of the observations are quite similar. In general, reinforced masonry wall panels have demonstrated substantially higher ductility than unreinforced panels. Furthermore, walls exhibiting a flexure-dominated mechanism have a more ductile behavior than those which exhibit a shear-dominated mechanism.

Nevertheless, because of widely scattered material properties, reinforcing schemes and testing techniques, results obtained by different researchers are not always consistent or comparable. In particular, test results have indicated a large variation of the observed influence of horizontal reinforcement on the shear strength and ductility of a wall panel. Some of these results will be briefly reviewed here. However, to present a concise overview, only those results relevant to the construction practice in the U.S. will be discussed.

In early studies, the strength and ductility of reinforced masonry walls were evaluated by racking tests (Schneider 1956; Scrivener 1969), in which a specimen is held down to the test floor on one side by an external vertical compressive force or an internal steel rod and the horizontal load is gradually increased until failure occurs (see Fig. 1.1a). While such tests can be effectively used to evaluate and compare the diagonal cracking strength and ductility of wall panels tested under similar loads, they do not reflect the wall behavior under actual seismic load conditions. In particular, the test setup does not allow the free development of the flexural mechanism and causes an unrealistic stress distribution. Scrivener (1969) has observed from these tests that the vertical and horizontal reinforcing bars are equally effective in improving postcracked shear behavior, and that the shear strength increases with the amount of reinforcement. However, the maximum effective steel ratio, with respect to the gross cross-sectional area of a wall, is 0.3%, beyond which no further increase of the failure load could be observed. Moreover, walls with evenly distributed reinforcement have a better performance than those with concentrated reinforcement.

Diagonal compression tests (see Fig. 1.1b) were used by Blume et al. (1968) to study the cracking strength of reinforced brick panels. However, similarly to racking tests, diagonal compression tests introduce a stress field that could be very different from those induced by seismic loads. Moreover, while these tests are useful for determining the critical tensile strength of masonry, the interpretation of test data is difficult due to the complexity of the diagonal tension field induced in the test panels (Hegemier, Nunn, and Arya 1978) and the sensitivity of test results to the loading condition.

A series of wall tests were conducted at the University of California at Berkeley (Sveinsson et al. 1985; Hidalgo et al. 1978, 1979; Chen et al. 1978; Mayes et al. 1976a, 1976b). In these tests, the top and bottom of a masonry pier were fixed against rotation, simulating a wall component in a typical masonry building with stiff spandrels, and a horizontal cyclic load was applied at the top of the pier (see Fig. 1.1c). The loading conditions in these tests closely resembled those induced by earthquake ground motions. Both double (Mayes et al. 1976a, 1976b) and single (Hidalgo et al. 1978, 1979; Chen et al. 1978; Sveinsson et al. 1985) piers were tested. The specimens were constructed with hollow concrete blocks and hollow clay bricks. The parameters investigated included the quantity and distribution of vertical and horizontal reinforcement, the axial compressive stress, full and partial grouting, and the height/length ratio of a pier.

In the above tests, it was observed that decreasing the height/length ratio increased the shear strength. Moreover, the shear strength and ductility tended to increase with the amount of horizontal reinforcement. However, the above improvement did not appear to be consistent. For walls dominated by the shear mechanism, full grouting led to a more ductile behavior than partial grouting. Walls with partial grouting also appeared to have a lower shear strength, evaluated with respect to the net cross-sectional area of a wall, than those with full grouting. However, the latter trend was not consistent. There was a distinct tendency that increasing the axial compressive stress and the quantity of vertical steel increased the flexural strength. Unfortunately, in all the early single-pier tests (Hidalgo et al. 1978, 1979; Chen et al. 1978), a pair of stiff pinned-end steel struts were used to restrain the end rotations of the pier (see Fig. 1.1c). These struts acted as rigid links and could induce a large com-

pressive force onto the pier specimen as they rotated about the bottom hinge to accommodate the lateral deflection of the specimen. Since the compressive force changed with the amount of lateral deflection, results of these tests did not lead to definitive conclusions.

In later tests conducted by Sveinsson et al. (1985), the steel struts were replaced by two load-controlled servo-hydraulic actuators (see Fig. 1.1d). The actuators were used to fix the rotation at the top of the pier specimens, while maintaining a constant axial compressive load during a test. Several observations have been made. Increasing the compressive axial stress increases the shear strength. Walls with a high axial compressive stress tend to fail in the shear mode, while those with a low compressive stress tend to fail in the flexural mode. Horizontal reinforcement improves the shear strength and ductility. However, similarly to prior results, this improvement is not consistent. Similar observations have also been obtained by Wakabayashi and Nakamura (1984) and Tomazevic et al. (1986). Furthermore, it has been observed that no further improvement of shear behavior can be achieved when the horizontal steel ratio is increased beyond 0.3%. Shear ductility is increased when the horizontal reinforcement is evenly distributed. The results also indicated that horizontal reinforcement with 180-degree anchoring hooks leads to better shear strength and ductility than those with 90-degree hooks. The influence of the distribution of vertical reinforcement is, however, found to be insignificant. Nevertheless, because of the large number of variables involved in these studies and the limited number of test specimens, the results did not lead to quantitative conclusions.

Tests of cantilever walls with cyclic lateral loads were conducted by Priestley et al. (1974, 1977, 1982). It was shown that the opening of diagonal shear cracks can be effectively prohibited by horizontal reinforcement (Priestley 1977). Moreover, Priestley and Bridgeman (1974) have demonstrated that horizontal reinforcement is about three times more effective than vertical reinforcement in carrying the shear force across a diagonal crack because the latter carries the shear mainly by dowel action. As a result, it has been suggested that shear reinforcement exceeding the maximum effective quantity observed by Sveinsson et al. (1985) could be beneficial. This seemingly contradictory observations, in fact, address two separate issues. While Sveinsson's results indicate the influence of shear reinforcement on the shear-dominated behavior, Priestley's results show that shear-dominated

behavior can be effectively suppressed by horizontal steel. Nevertheless, the latter results do not indicate the minimum shear reinforcement required to achieve that. Most of Priestley's studies have been focussed on the flexural behavior. It has been shown that the introduction of steel plates into the bed joints in a flexural compression zone can provide a confining effect on masonry and thus substantially improve the flexural ductility of a wall (Priestley 1981).

While it has been demonstrated by prior studies (e.g., Priestley 1986) that the flexural strength of a reinforced masonry wall panel can be accurately evaluated with formulas based on the simple flexure theory, no theoretical formulation has been developed to give an accurate prediction of the shear strength dominated by diagonal cracking. It has been observed that the shear strength of a wall panel depends on many factors, such as the tensile or compressive strength of masonry, amount of horizontal reinforcement, dowel action of the vertical steel, applied axial stress, and aggregate-interlock mechanism. The difficulty in predicting shear behavior can be largely attributed to the complex interaction of these mechanisms.

In general, studies have suggested that shear-dominated behavior should be avoided in design. However, to achieve that, the shear strength of a wall panel has to be assessed by a reliable formula. A physical model based on the analogy of combined truss and arch mechanisms has been proposed by Wakabayashi and Nakamura (1984) for reinforced masonry shear walls. However, this model is based mainly on test results obtained from wall panels with effective aspect ratios less than one. Empirical formulations based on the regression analysis of experimental data have also been proposed (Matsumura 1988); the validation of these formulas requires a large amount of experimental data.

1.3 Objectives and Scope

The main objective of this study was to provide a systematic experimental investigation of the inelastic performance of reinforced masonry shear walls, with an emphasis on shear behavior. In particular, the influence of shear reinforcement on the shear strength was further investigated. This was intended to obtain definitive information on avoiding brittle shear behavior in design. To this end, the influence of various parameters on the shear strength and ductility was examined to clarify some of the aforementioned issues. It is anticipated that results of this study will enhance the current data base

on the inelastic behavior of reinforced masonry shear walls, and will support the evaluation and improvement of the current design methodology for masonry structures. To this end, the study has been closely coordinated with the other tasks of the coordinated research program. In particular, the test results presented here have provided a data base for the calibration of analytical models developed in Task 2 of the coordinated research program (Noland 1987) and will be eventually used in Task 10 for the development of design recommendations and criteria.

A total of twenty-four story-height reinforced masonry cantilever shear walls were tested. To allow a meaningful analysis of test data, the number of design variables considered in this study was carefully limited. The major parameters investigated were the amount of vertical and horizontal reinforcement, and the axial compressive stress. To obtain a better understanding of the shear mechanism, a majority of the specimens were designed to exhibit a shear-dominated behavior. The specimens were constructed with hollow concrete blocks and hollow clay bricks. All specimens were fully grouted and had reinforcing steel uniformly distributed in each direction. Most of the tests were conducted with a standard cyclic displacement history, except for three specimens, two of which were subjected to monotonic displacements. The axial compressive load was maintained constant during each test although different amounts of compression were used in different tests. The test procedure and results are documented in this report.

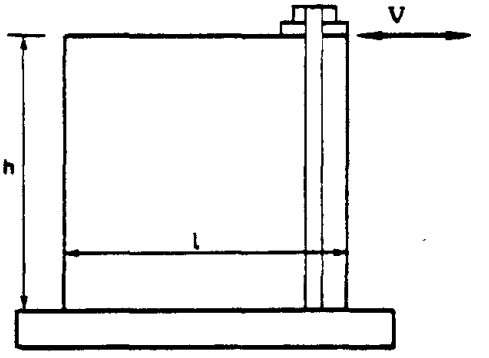

(a) Racking Test

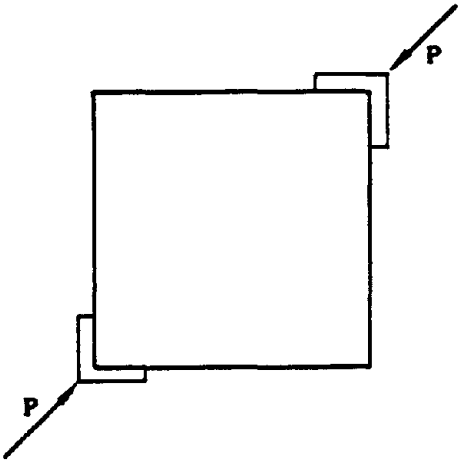

(b) Diagonal Compression Test

Figure 1.1 - Tests of Masonry Walls

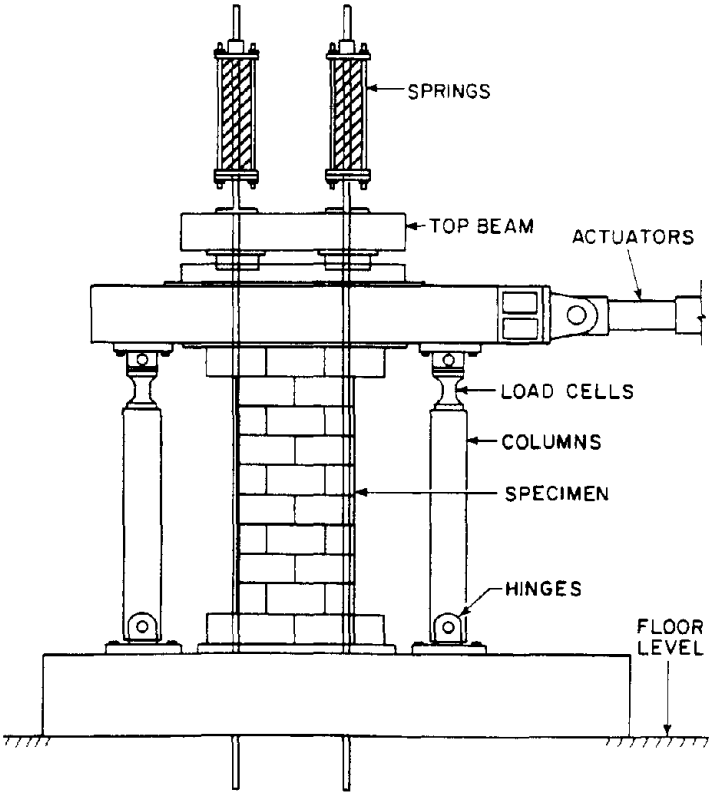

(c) Test of Single Pier (Hidalgo et al. 1979)

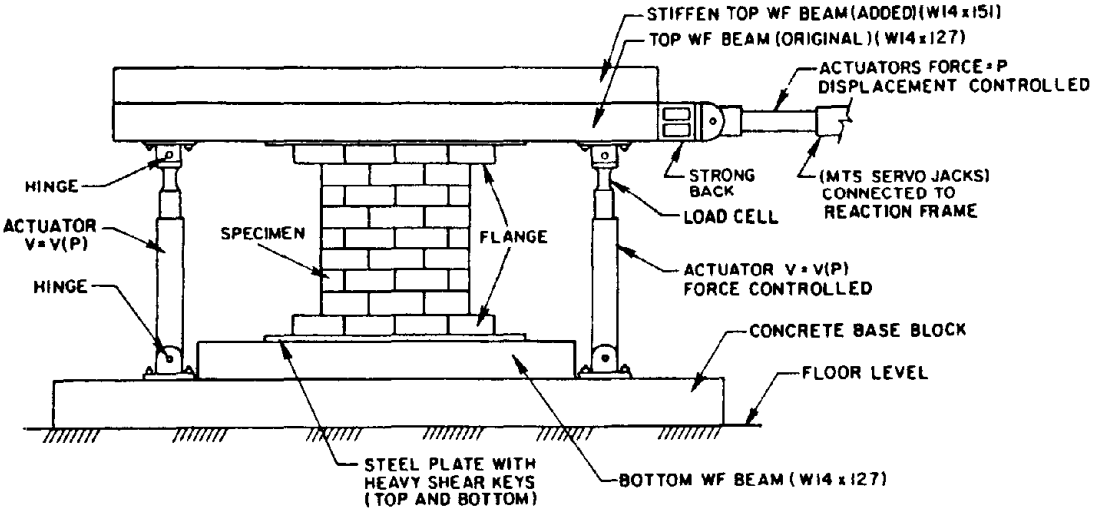

(d) Test of Single Pier (Sveinsson et al. 1985)

Figure 1.1 - Tests of Masonry Walls

2 TEST SPECIMENS

Twenty-four cantilever wall panels were tested. The design of the specimens was based on several considerations. It is known that the inelastic behavior of a reinforced masonry wall panel is influenced by many factors, such as the effective aspect ratio, quantity and arrangement of steel reinforcement, applied axial stress, grouting pattern, properties of masonry materials, and load or displacement history. However, because of the limited number of specimens, the number of variables had to be restricted in this study. After reviewing results of prior studies and identifying the current objectives, it was decided that the quantities of vertical and horizontal reinforcement and the magnitude of axial compressive stress be selected as major parameters in this study. In addition, two types of masonry units, namely, hollow concrete blocks and hollow clay bricks, were used. All the specimens, except three, were subjected to a standard displacement history, and one specimen had confinement steel at its compression toes.

2.1 Design of Test Specimens

As mentioned in the previous chapter, the study of the shear mechanism was one of the prime objectives of this investigation. In particular, there was a need to obtain some quantitative information about the influence of reinforcing steel on the shear strength and ductility of a wall panel. Furthermore, the influence of reinforcement content and axial compressive stress on the failure mechanism has to be identified. For these reasons, a majority of the specimens were selected to exhibit a shear-dominated behavior, while a few specimens were designed to have a flexural or mixed flexural/shear behavior. The latter were intended for comparison purpose as well as for identifying the parameters that influence the failure mechanism. The aspect ratio was kept constant for all panels. To allow the possibility that both the flexure and shear mechanisms could occur, all specimens had a height/length (h / l) ratio of one. Results of prior studies (Priestley 1981; Hidalgo et al. 1978, 1979; Sveinsson et al. 1985) have indicated that fully grouted walls tend to have better inelastic behavior than partially grouted walls, and that uniformly distributed reinforcing steel results in better ductility than concentrated steel. Therefore, it was decided that all of the specimens would be fully grouted with reinforcing steel uniformly distributed in each direction.

As shown in Table 2.1, eighteen of the twenty-four specimens were fabricated with 6x8x16-in. hollow concrete blocks and six with 6x4x16-in. hollow clay bricks. The shapes and dimensions of the hollow units are shown in Figs. 2.1a and 2.1b. To allow the placement of horizontal steel and enhance the continuity of the grout, the cross webs were partially removed from the units to form bond-beam units, as shown in Figs. 2.1c and 2.1d, which were used throughout a wall specimen. A typical concrete masonry wall specimen is shown in Fig. 2.2. It was 6-ft. high and 6-ft. long, with a reinforced concrete top beam and base slab. Every specimen, except one (Specimen 2), had five vertical and five horizontal reinforcing bars, with a center-to-center spacing of 16 in. The vertical steel ran continuously from the base slab to the top beam with 180-degree anchoring hooks. The horizontal reinforcement had 180-degree hooks around the extreme vertical steel. The hooks were bent in accordance with ACI standards (ACI 318-83). It has been observed by Sveinsson et al. (1985) that 180-degree hooks result in better shear ductility than 90-degree hooks. Furthermore, it has been verified by Soric and Tulin (1987) that standard 180-degree hooks provide sufficient anchorage to allow the reinforcing bar to develop its yield capacity.

The design of the clay masonry specimens was the same as of concrete masonry specimens. However, the vertical steel in three of the flexure-dominated clay masonry specimens had 32-in.-long lap splices at the base (which conform to UBC provisions). One of these specimens had wire-mesh-type toe confinement extending 24 in. from each side of the wall in the bed joints of the first six courses from the base. The reinforcement details of this specimen are shown in Fig. 2.3. The wire-mesh confinement was fabricated from standard DUR-O-WAL joint reinforcement by welding additional steel wires across the width of the wire mesh to provide the confinement effect.

The design details of the twenty-four specimens are summarized in Table 2.1. The quantity of vertical steel was selected to be about 0.38, 0.54, and 0.74% of the net horizontal cross-sectional area of a wall by using No. 4, 5, and 6 bars, respectively. The quantity of horizontal steel was around 0.14 and 0.24%, corresponding to No. 3 and 4 bars, respectively. In general, three specimens were tested for each type of reinforcement content, with an axial compressive stress of 0, 100, and 270 psi, respectively. Since no adequate guidelines were available to determine the shear strength, the design of the test specimens followed a trial-and-error approach, with the first two specimens shown in Table 2.1

being selected as initial trials. It was found that the response of the specimens with 0.38% vertical steel was dominated by flexure, while the response of those with 0.54 and 0.74% was dominated by either a flexure/shear or shear mode.

All reinforcing bars used were Grade 60, except the No. 3 bars which were available in Grade 40 only. The mortar mix consisted of $1{:}\frac{1}{2}{:}4\frac{1}{2}$ proportions of Portland cement, hydrated lime, and sand by volume, which conform to ASTM Type S. The grout mix consisted of 1:3:2 proportions of Portland cement, sand, and coarse aggregate by volume, with SIKA grout aid added as expanding agent (Type I for clay masonry and Type II for concrete masonry). The grout was specified to have a slump of 8 to 10 in. Material tests were conducted for each batch of specimens in accordance with the ASTM and UBC specifications. The results of these tests are presented in Chapter 4.

2.2 Specimen Construction

The specimens were constructed three at a time by an experienced mason. The reinforcement details of the top beam and base slab are shown in Fig. 2.4. As shown in Fig. 2.4, the base slab consisted of three separate, trapezoidal, reinforced concrete blocks tied together by eight horizontal, post-tensioned, high-strength steel rods. The outer blocks could be saved and reused for subsequent specimens. During a test, the wall specimen was tied down to the strong floor by high-strength steel rods passing through the post-tensioning holes located in the outer blocks. The vertical reinforcing bars of a wall panel were installed in place before the center block was cast. The three base blocks were separated by corrugated steel. The corrugated steel served as dividers and also provided shear keys, which prevented the horizontal sliding of the center block. The steel cage for the base slab during its initial construction is shown in Fig. 2.5. For subsequent tests, the outer blocks were recovered from the tested specimens and used as formwork for the center block.

About ten minutes after the center block was cast, the concrete surface was roughened by a high-pressure water jet to have approximately a 1/4-in. amplitude of the aggregate exposed. This was done to increase the base shear friction. Except for the first two specimens, "cleanouts" were made in the first course by removing the face shells of the hollow units at cells containing vertical reinforcement, which is required by the UBC for any grout pour above 5 ft. All units were laid in running bond.

The construction process is shown in Fig. 2.6. During construction, mortar protruding from the bed and head joints was carefully removed. After all units had been laid, the mortar droppings were removed via the cleanouts. The cleanouts were then sealed with the original face shells, which were supported in place by a wood plank.

To prevent the bursting of mortar joints under the hydrostatic pressure of the grout, the grout was poured with high-lifts the following day after wall construction. The grout was supplied by a single commercial vendor, in accordance with the above specification. Grout aid was dissolved in water at the site before being added into the mixer. Slump tests were conducted to ensure an 8- to 10-in. slump. Immediately after pouring, the grout was consolidated once by an 8-in.-long and 7/8-in.-diameter mechanical vibrator. The specimens were cured for at least 28 days before testing. Specimens for material tests were prepared at the same time with the same materials used for the wall panels and were tested exactly on the 28th day.

Table 2.1 - Reinforced Masonry Shear Wall Specimens

Wall Spec.	Unit Type[1]	Vert. Steel	ρ_v (%)	Horiz. Steel	ρ_h (%)	Axial Comp. Stress (psi)	S[2]	C[3]	Displ. Hist.[4]
1	HCBL	5 x #5	0.38	5 x #4	0.24	200	N	N	SC
2	HCBL	5 x #5	0.38	9 x #3	0.24	270	N	N	SC
3	HCBL	5 x #7	0.74	5 x #3	0.14	270	N	N	SC
4	HCBL	5 x #7	0.74	5 x #3	0.14	0	N	N	SC
5	HCBL	5 x #7	0.74	5 x #3	0.14	100	N	N	SC
6	HCBL	5 x #5	0.38	5 x #3	0.14	0	N	N	SC
7	HCBL	5 x #7	0.74	5 x #3	0.14	100	N	N	C
8	HCBL	5 x #5	0.38	5 x #4	0.24	0	N	N	SC
9	HCBL	5 x #5	0.38	5 x #3	0.14	270	N	N	SC
10	HCBL	5 x #5	0.38	5 x #3	0.14	100	N	N	SC
11	HCBL	5 x #7	0.74	5 x #4	0.24	0	N	N	SC
12	HCBL	5 x #5	0.38	5 x #4	0.24	100	N	N	SC
13	HCBL	5 x #6	0.54	5 x #4	0.24	270	N	N	SC
14	HCBL	5 x #6	0.54	5 x #3	0.14	270	N	N	SC
15	HCBL	5 x #6	0.54	5 x #4	0.24	100	N	N	SC
16	HCBL	5 x #7	0.74	5 x #4	0.24	270	N	N	SC
17	HCBR	5 x #5	0.40	5 x #4	0.26	280	N	N	SC
18	HCBR	5 x #5	0.40	5 x #4	0.26	280	Y	N	SC
19	HCBR	5 x #5	0.40	5 x #4	0.26	280	Y	Y	SC
20	HCBR	5 x #5	0.40	5 x #4	0.26	280	Y	N	SC
21	HCBR	5 x #6	0.56	5 x #3	0.14	280	N	N	SC
22	HCBR	5 x #6	0.56	5 x #3	0.14	100	N	N	SC
23	HCBL	5 x #6	0.54	5 x #3	0.14	270	N	N	M
24	HCBL	5 x #6	0.54	5 x #4	0.24	270	N	N	M

1 HCBL: Hollow Concrete Blocks; HCBR: Hollow Clay Bricks
2 Y: With Lap Splices; N: Without Lap Splices
3 Y: With Confinement; N: Without Confinement
4 SC: Standard Cyclic History; C: Cyclic History; M: Monotonic

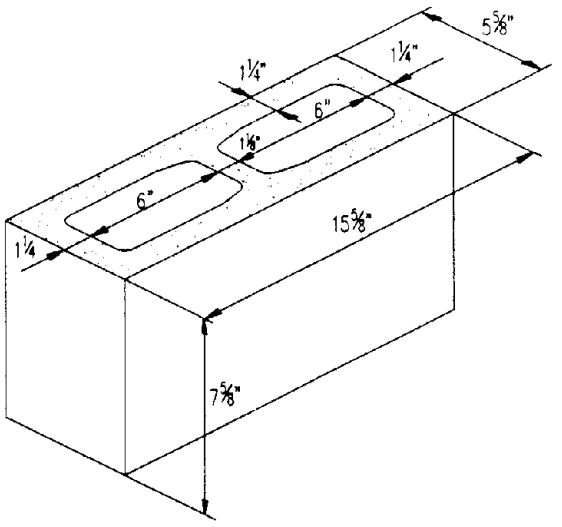

(a) 6x8x16-in. Hollow Concrete Block

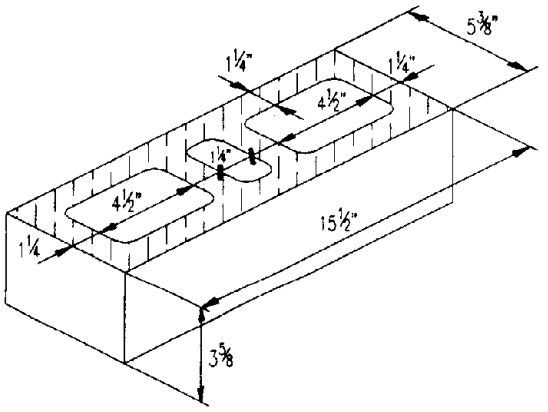

(b) 6x4x16-in. Hollow Clay Brick

Figure 2.1 - Hollow Masonry Units

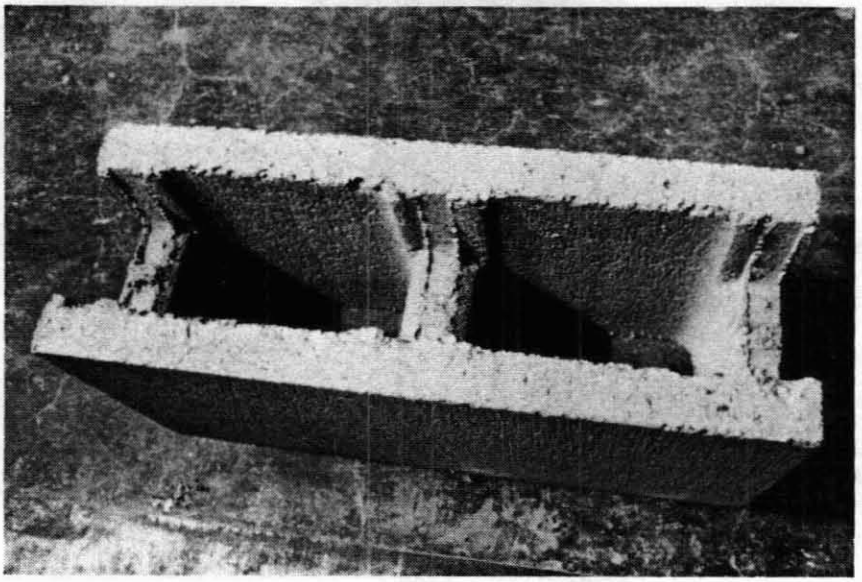

(c) Hollow Concrete Block - Bond-Beam Unit

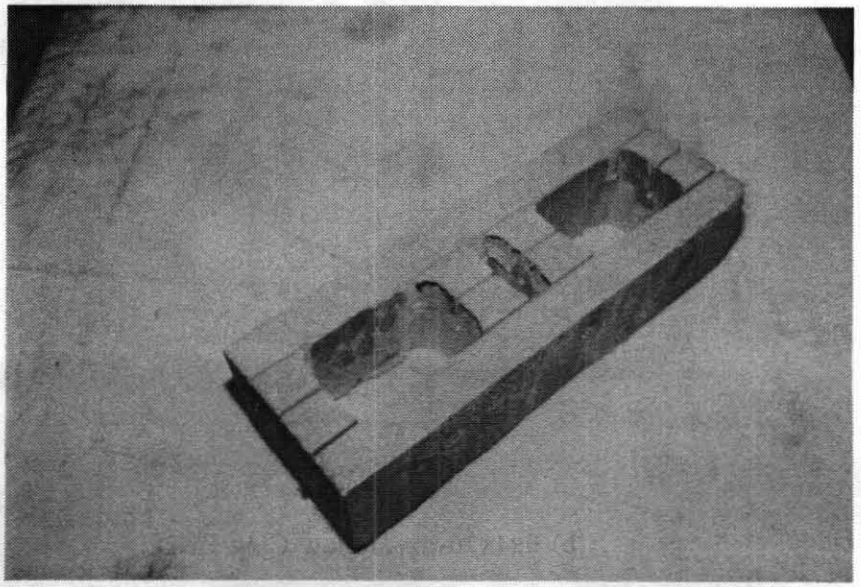

(d) Hollow Clay Brick (cross webs partially cut to enable bond-beam units to be formed)

Figure 2.1 - Hollow Masonry Units

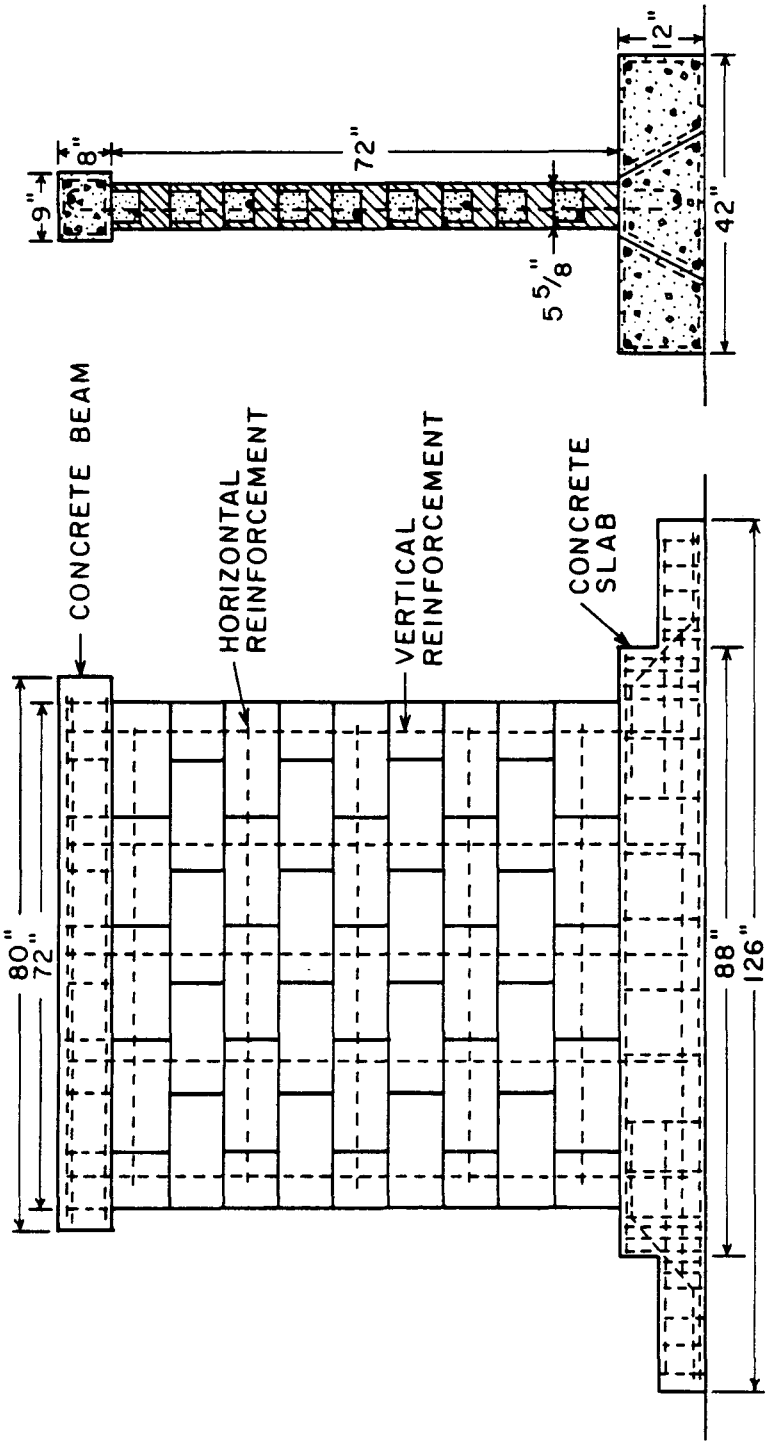

Figure 2.2 - Concrete Masonry Wall Specimen

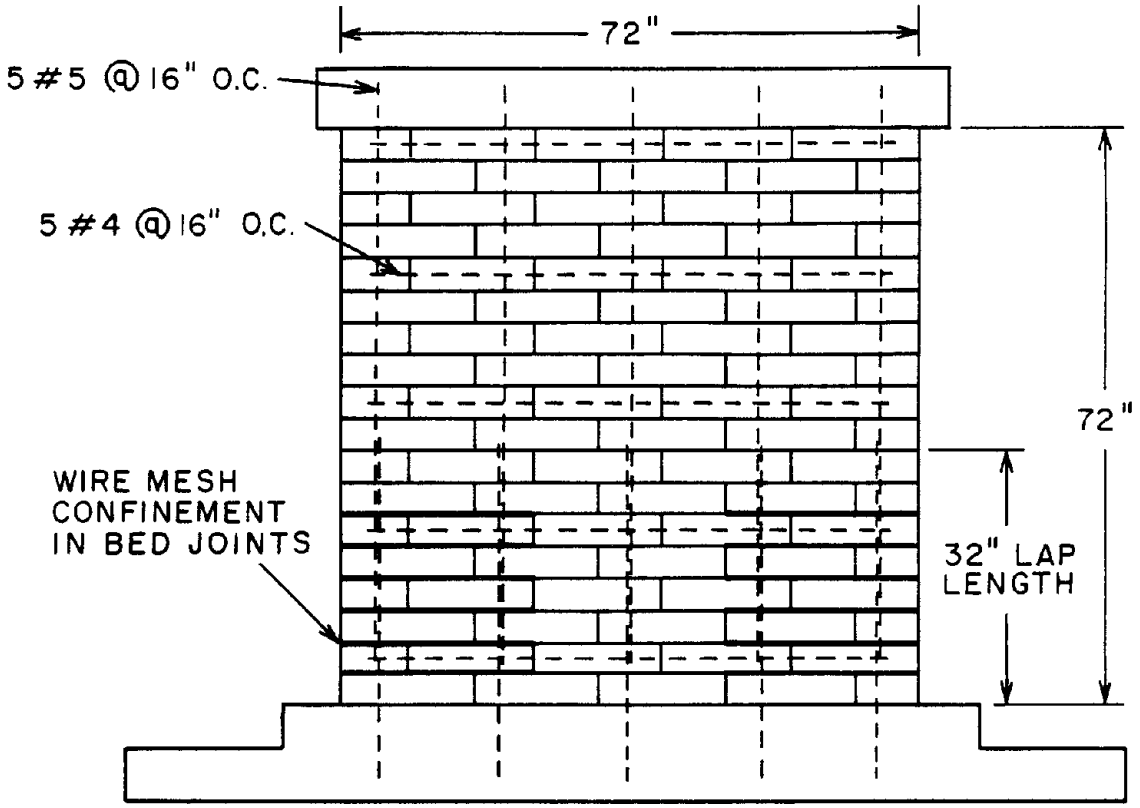

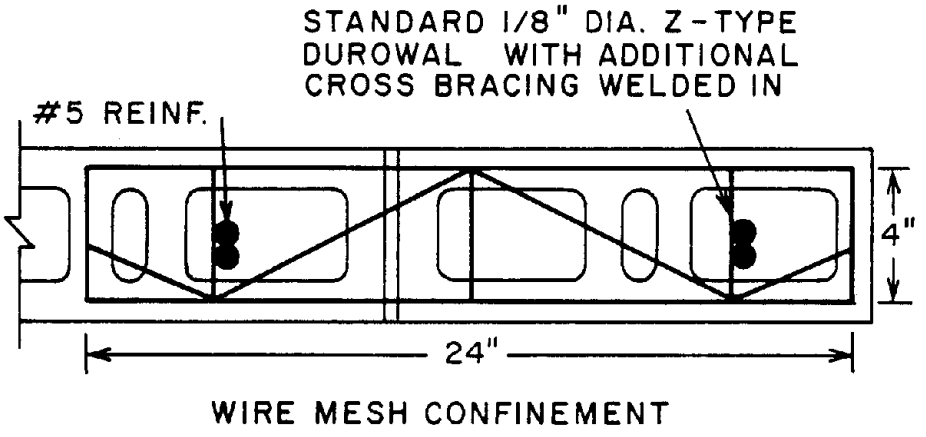

WIRE MESH CONFINEMENT

Figure 2.3 - Clay Masonry Wall Specimen

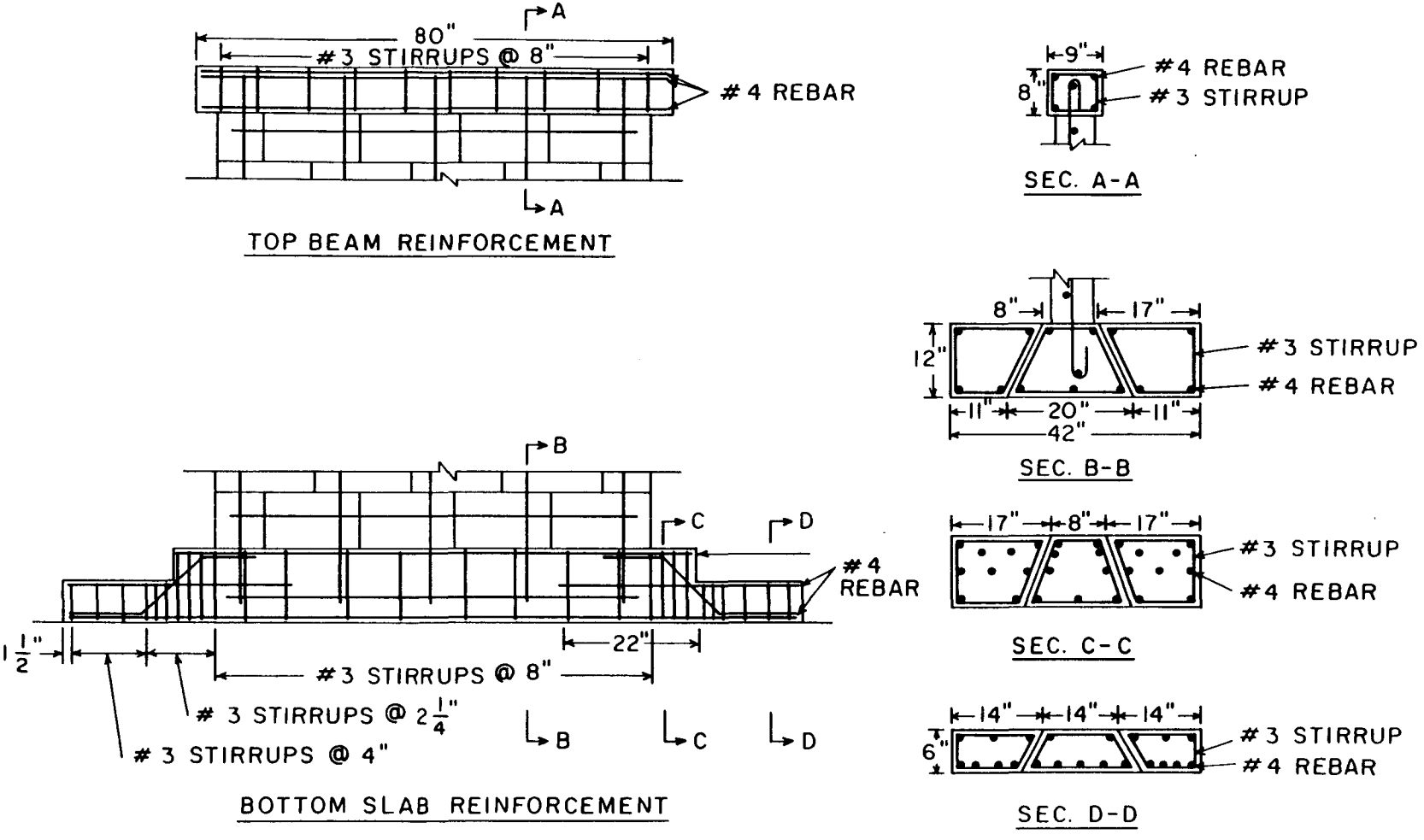

Figure 2.4 - Design of Top Beam and Base Slab

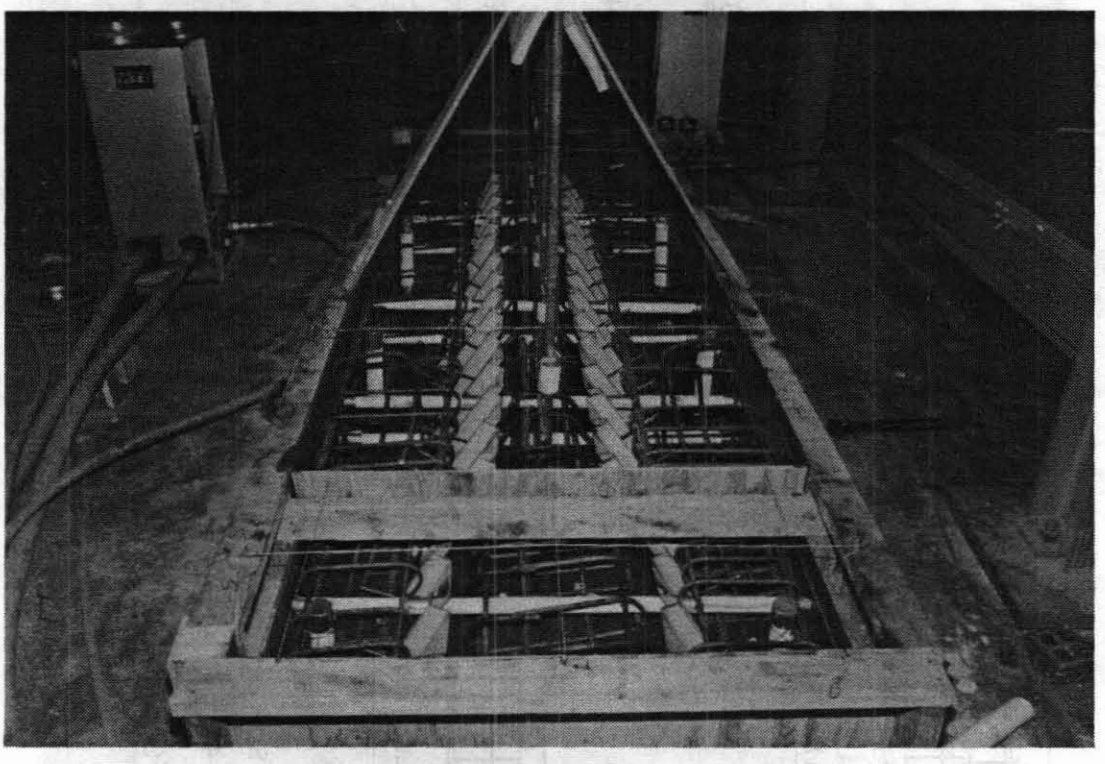

Figure 2.5 - Construction of Base Slab

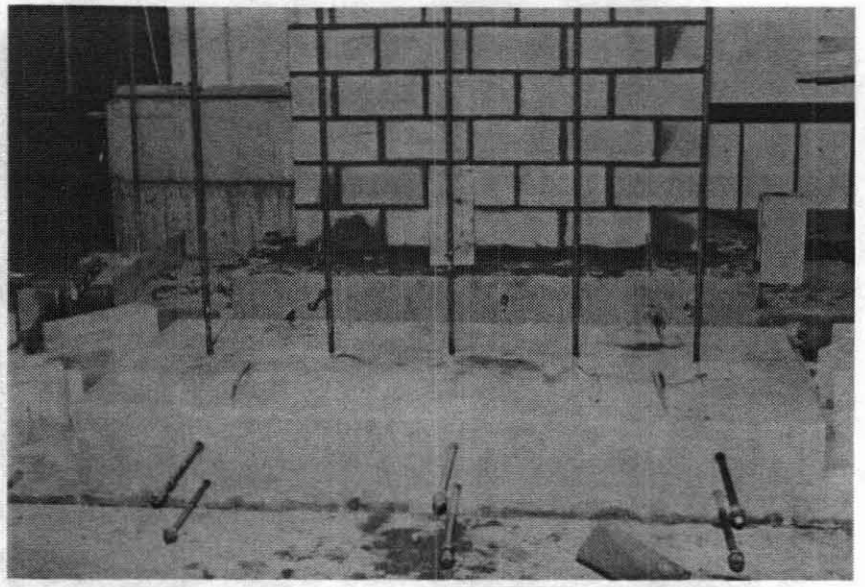

(a) Base Slab

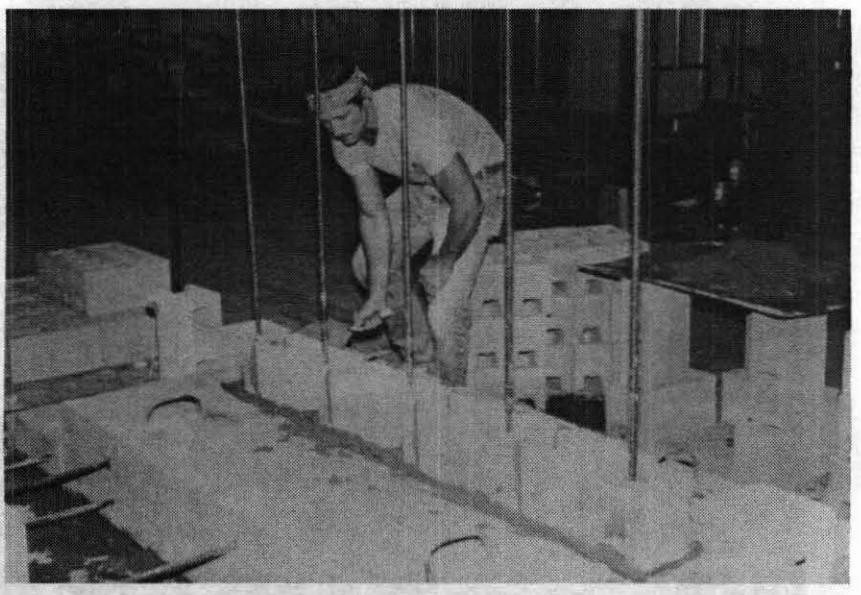

(b) First Course

Figure 2.6 - Construction of Wall Specimen

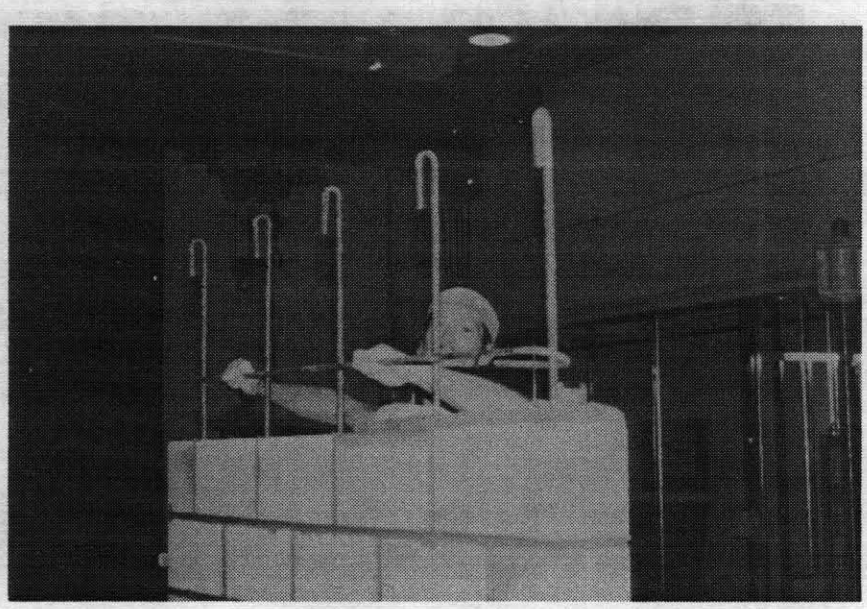

(c) Horizontal Steel

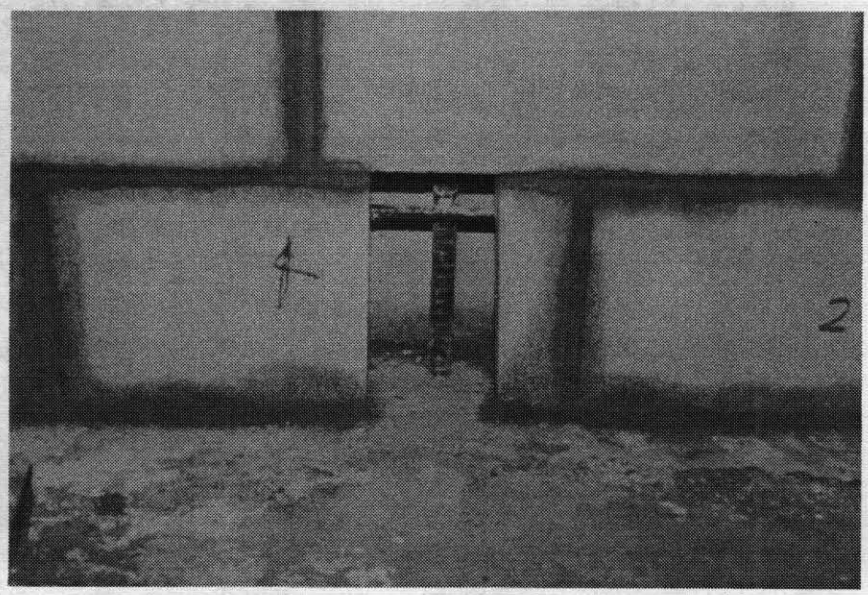

(d) Cleanout

Figure 2.6 - Construction of Wall Specimen

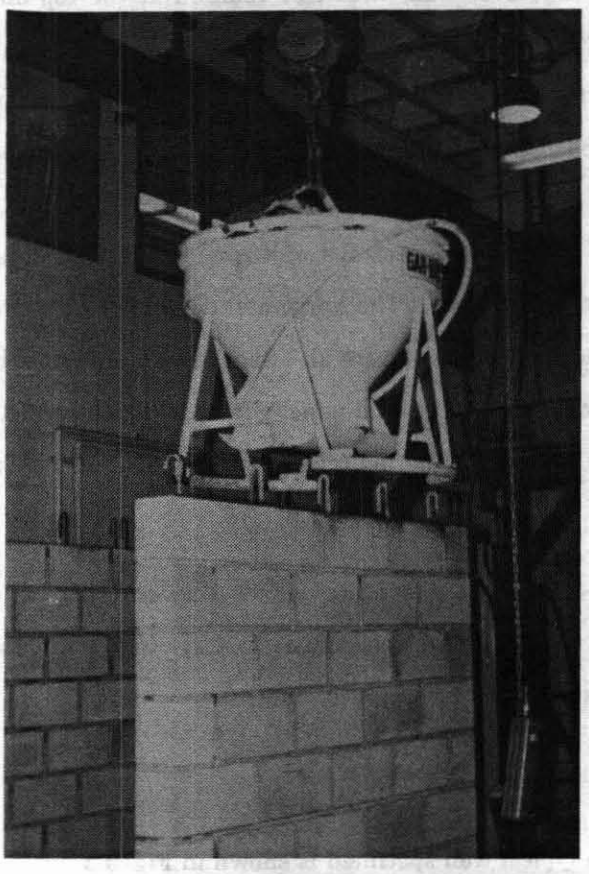

(e) Grout Pour

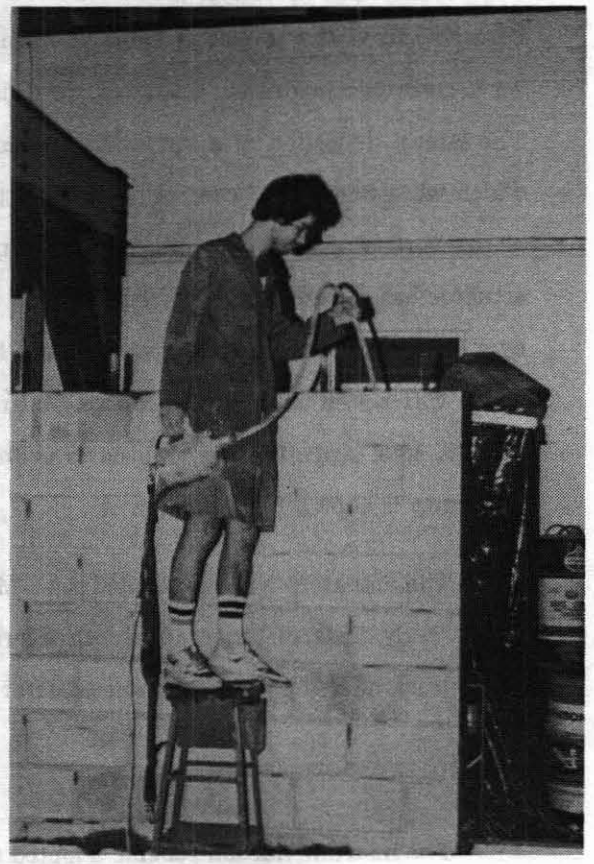

(f) Grout Consolidation

Figure 2.6 - Construction of Wall Specimen

3 TEST SETUP AND LOADING PROCEDURE

3.1 Test Apparatus and Setup

Each specimen was loaded in-plane as a cantilever wall, with free rotation at the top and the base slab fixed to the strong floor. The schematic of the test setup is shown in Fig. 3.1. Three MTS servo-controlled hydraulic actuators were used to apply the axial and lateral loads to the specimens. The lateral deflection of a specimen was controlled by a horizontal actuator. Two vertical actuators, which were under load control, were used to exert constant axial compression during each test. Each of the vertical actuators has a load capacity of 55 kips and a stroke of ±3 in., while the horizontal actuator has a load capacity of 165 kip and a stroke of ±2.5 in. The horizontal actuator was supported by a steel reaction frame. The vertical and horizontal actuators were all attached to a stiff steel beam, which was bolted down to the concrete beam on the top of the wall panel with ten high-strength steel bolts. A steel space frame was used to prevent the out-of-plane deflection of the specimen. The actual test setup is shown in Fig. 3.2.

The actuators were controlled with MTS 458 analog controllers, which were manually adjusted in the early tests in accordance with a predefined load or displacement history. In later tests, the analog controller for the horizontal actuator was switched to computer control.

3.2 Instrumentation

The instrumentation scheme adopted for a typical wall specimen is shown in Fig. 3.3. In addition to the internal LVDT's of the actuators, twenty-five displacement transducers were used to monitor the lateral deflection, flexural deformation, shear deformation, base slip, and base uplift of each specimen.

As shown in Fig. 3.3a, the flexural curvature was monitored by the displacement transducers (L1 to L12) installed along the two vertical edges of a wall specimen. Additional transducers (L13 to 16) were installed near the wall base to measure the flexural strain profile. The base uplift was monitored by four transducers (L19 to L22) installed very close to the base. The diagonal transducers

(L23 and L24) were used to measure the average shear distortion. Transducer L25 was attached to a fixed support to measure the absolute wall deflection, and was used to correct the measurement obtained from the internal LVDT of the horizontal actuator, which was also influenced by the deformation of the reaction frame. The readings from the external transducer (L25) were not used directly because of possible errors that might be caused by external disturbances. Instead, the stiffness of the reaction frame was calculated from the two different transducer readings and then used to correct the internal transducer after each test. The displacement transducers were attached to aluminum supports glued onto the wall specimen as shown in Fig. 3.4. Each actuator had a load cell to measure the load applied onto a specimen.

As shown in Fig. 3.3b, a strain gage was attached to each of the vertical reinforcing bars near the base of a wall panel to monitor initial yielding as well as the distribution of the flexural strain in the vertical steel. The gages were glued to the reinforcing bars and covered by a protective material, as shown in Fig. 3.5. In Specimens 1, 7, 9, 23, and 24, strain gages were also attached to the horizontal steel near one of the wall diagonals. They were intended to detect the change of tensile strain due to diagonal cracking. The data were collected by a computer-controlled, high-speed, data-acquisition system.

As shown in Fig. 3.6, 81 photogrammetry targets were attached to monitor wall deformation. Pictures were taken at the peaks of selected displacement cycles. The positions of the targets with respect to the reference points (located on two fixed poles shown in Fig. 3.6) could be digitized from the pictures. However, since the resolution of the procedure was found to be unsatisfactory for strain measurement, digitization was carried out only for the first two specimens. However, the pictures recorded the progressive crack development in the wall panels.

3.3 Load Sequence

Each specimen was subjected to a prescribed lateral displacement history under a constant axial load. The axial compression applied to each specimen is shown in Table 2.1. Furthermore, as indicated in Table 2.1, all specimens, except Specimens 7, 23, and 24 were subjected to a standard lateral displacement history shown in Fig. 3.7. The displacement history consisted of sequences of fully-reversed

displacement cycles. The displacement amplitude of the first cycle of each sequence was identical to the maximum amplitude of the previous sequence. It was then followed by three to four cycles with an increased amplitude, and finally by three cycles with decaying amplitudes. The last decaying cycle had an amplitude of one-quarter of the maximum amplitude of that sequence. The purpose of the decaying cycles was to measure the degradation of the elastic stiffness of a specimen. The sequence was repeated, with an amplitude increment each time, until the specimen lost at least 50% of its maximum load resistance or the displacement limit (±2.5 in.) of the horizontal actuator was reached.

Specimen 7 had the same design as Specimen 5, but was initially subjected to three large-amplitude cycles that passed the ultimate resistance of the specimen, before being subjected to the standard displacement sequences described above. The purpose was to examine the influence of the displacement history on the hysteretic behavior of a wall panel. Specimens 23 and 24 were subjected to monotonic displacement increments until failure.

To ensure the uniformity of the displacement histories and increments applied to different specimens, the displacement amplitude of each cycle was specified in terms of an integer multiple of a critical displacement (Δ_{cr}), which was defined as the displacement at which the first major event occurred. For shear-dominated specimens, the first major event was defined as the occurrence of the first major diagonal crack. For a flexure-dominated specimen, Δ_{cr} was obtained by extrapolating the initial stiffness to the predicted flexural strength of the specimen as shown in Fig. 3.8. The initial stiffness was defined as the average stiffness of the specimen measured at a load of about 75% of the predicted flexural strength. The horizontal actuator was under load control with gradually increasing load amplitudes up to the critical displacement Δ_{cr}, while the rest of the test was conducted under displacement control.

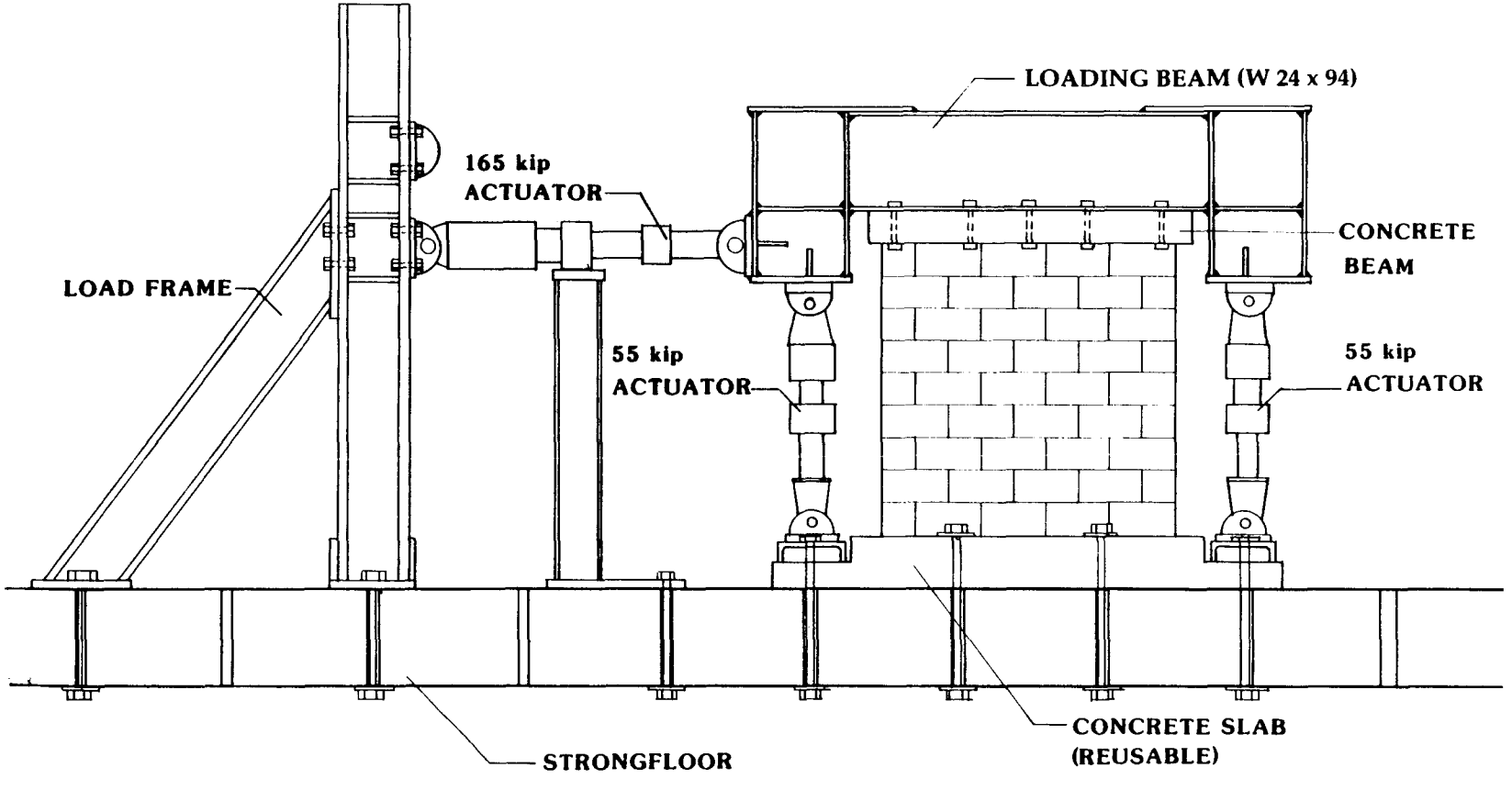

Figure 3.1 - Schematic of Test Setup and Apparatus

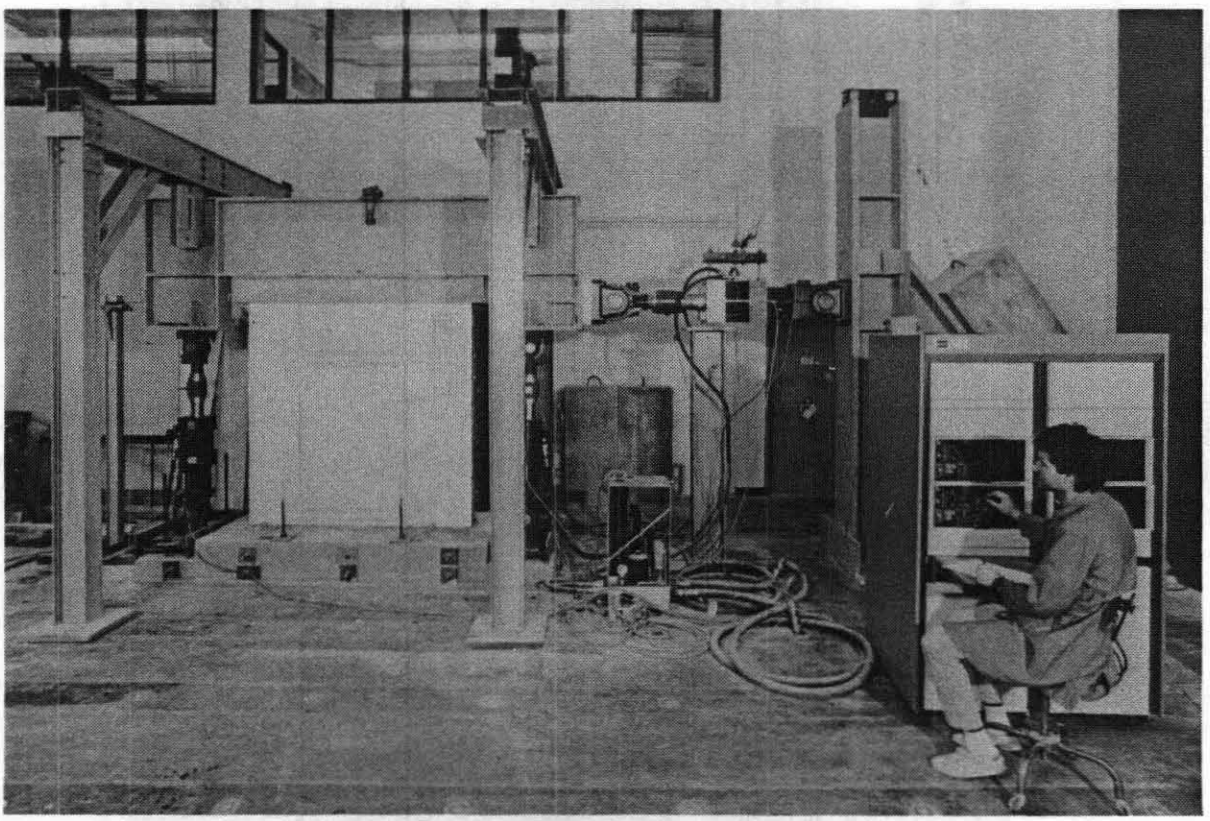

Figure 3.2 - Picture of Test Setup

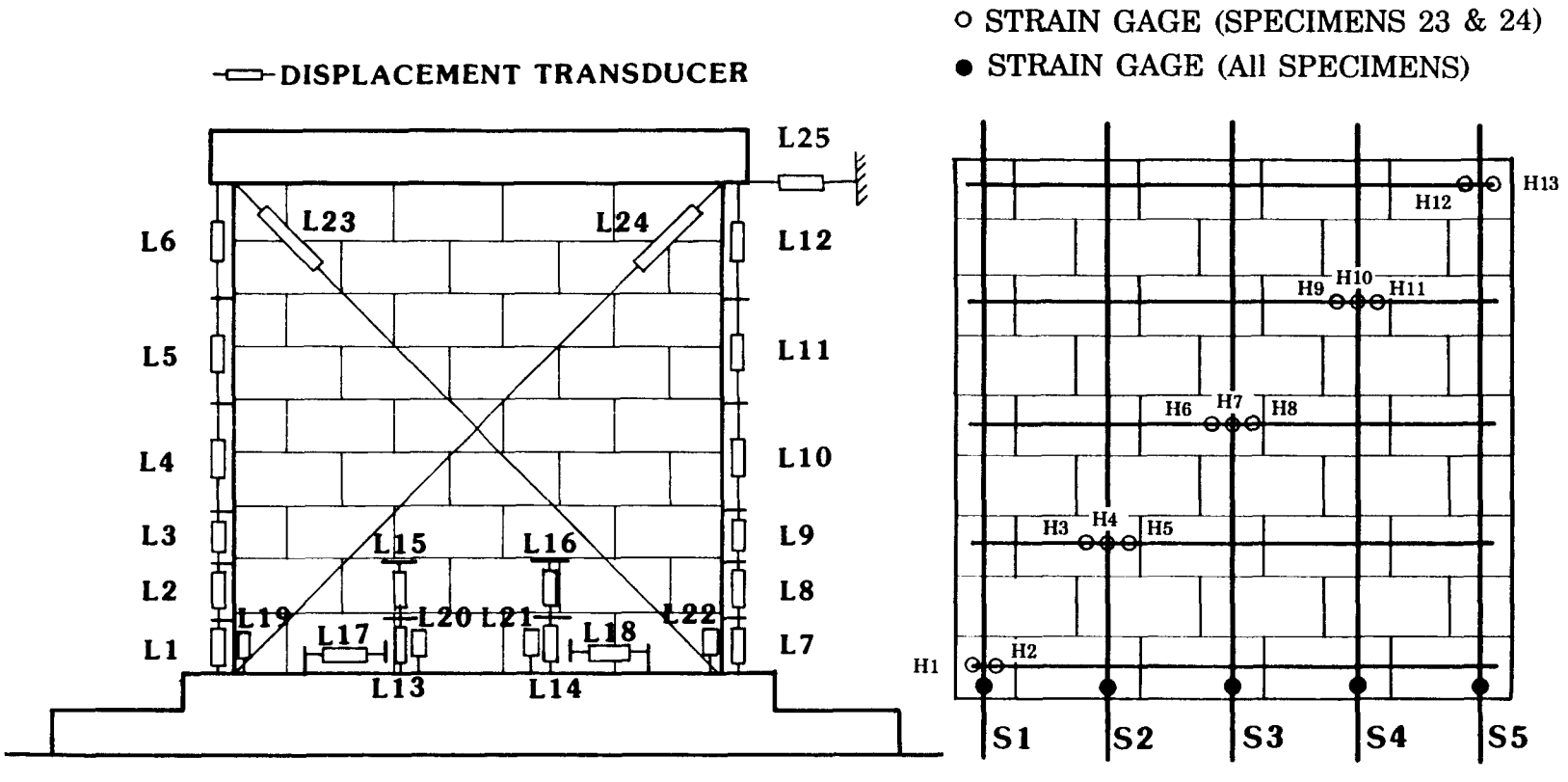

(a) Displacement Transducers

(b) Strain Gages

Figure 3.3 - Instrumentation

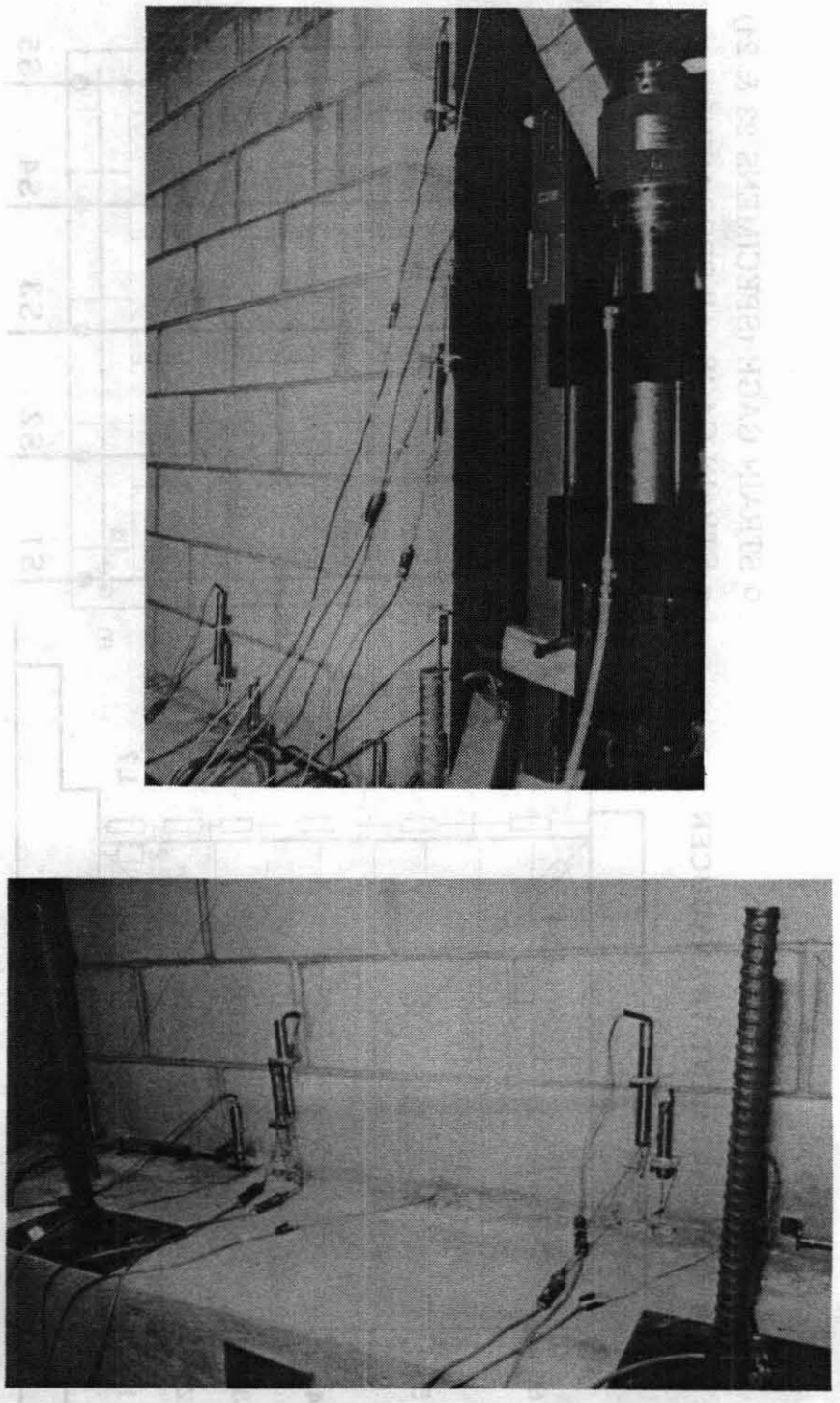

Figure 3.4 - Installation of Displacement Transducers

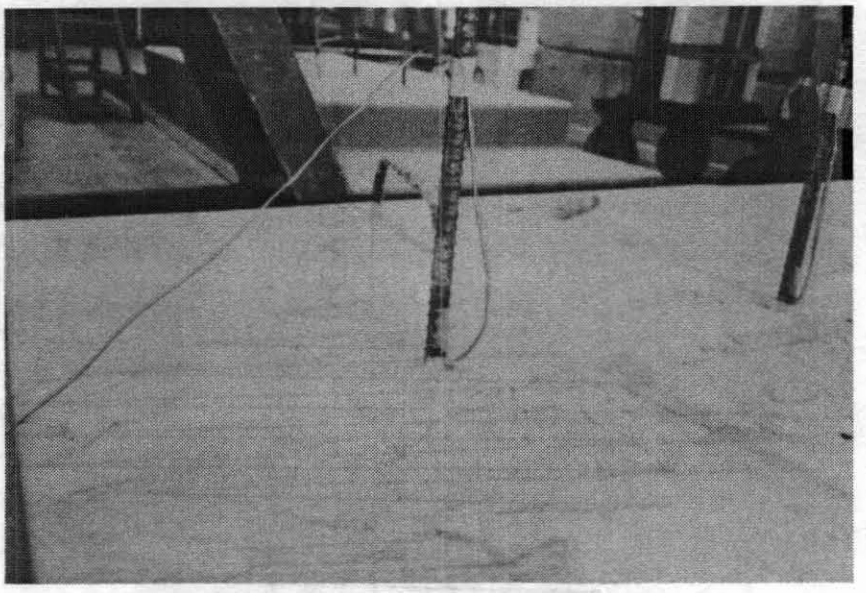

Figure 3.5 - Installation of Strain Gages

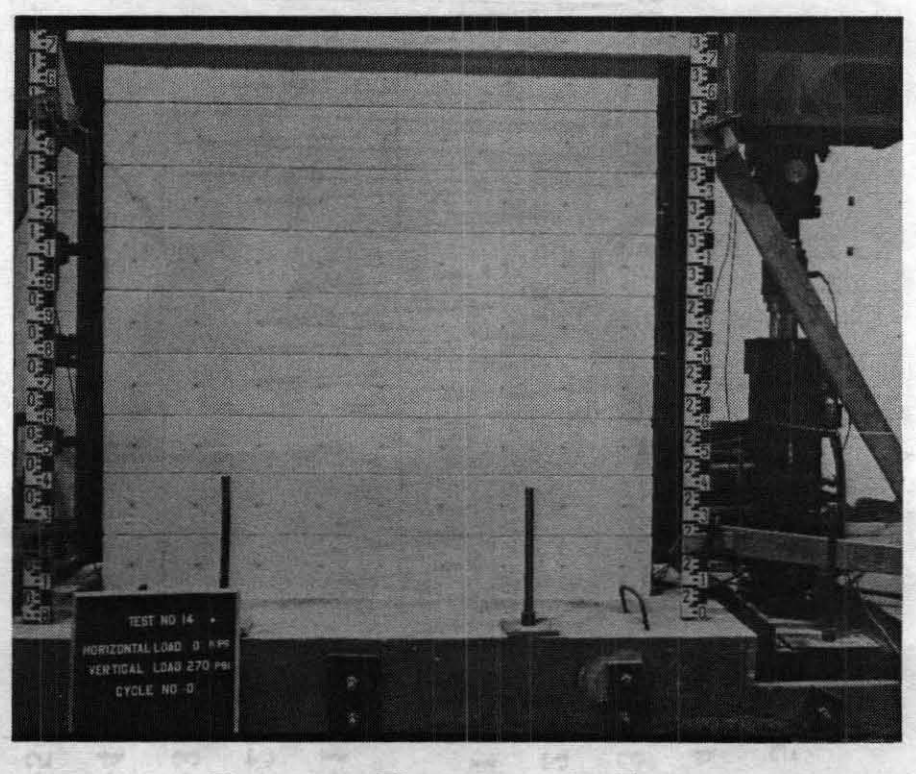

Figure 3.6 - Photogrammetry Targets

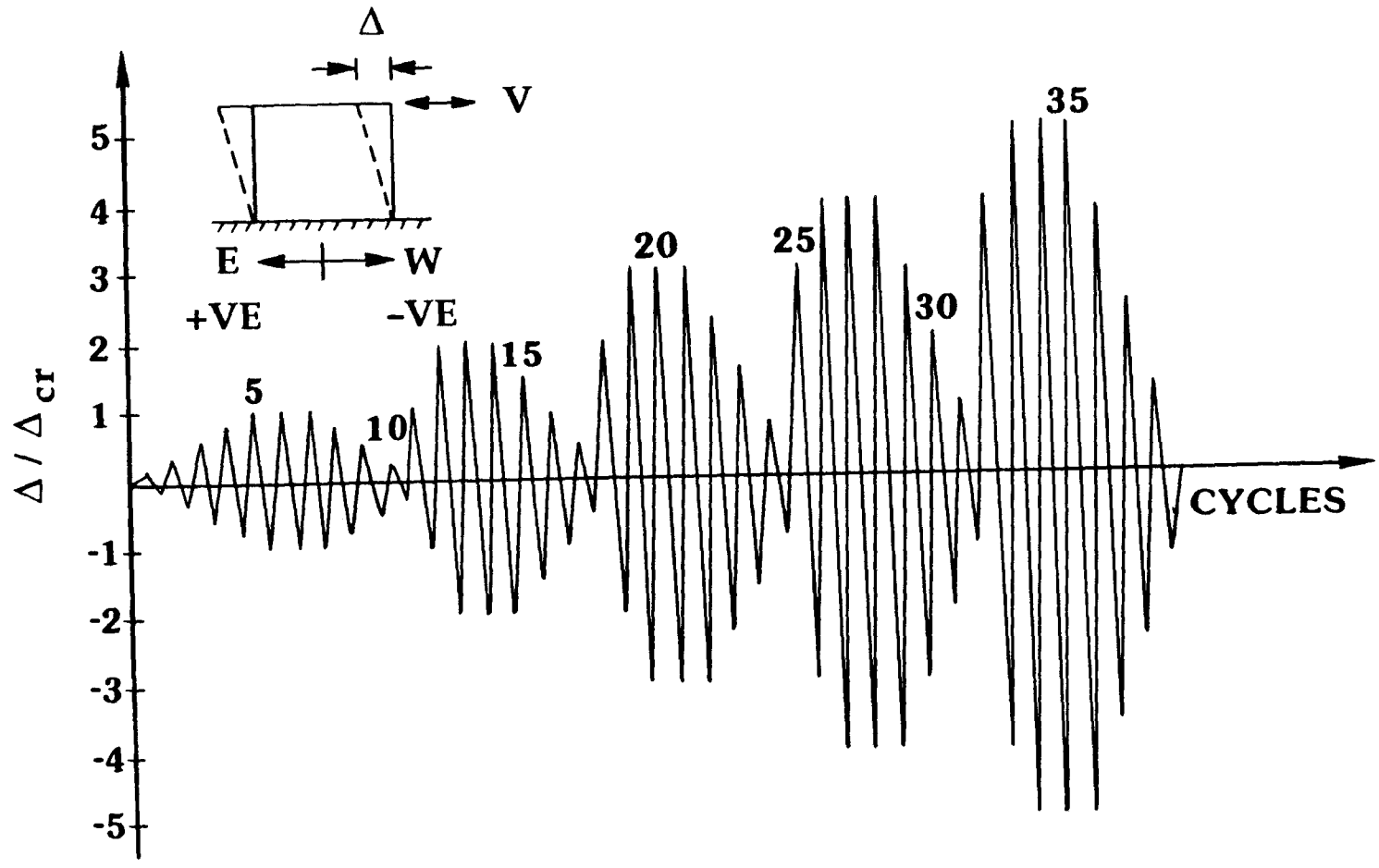

Figure 3.7 - Standard Displacement Sequence

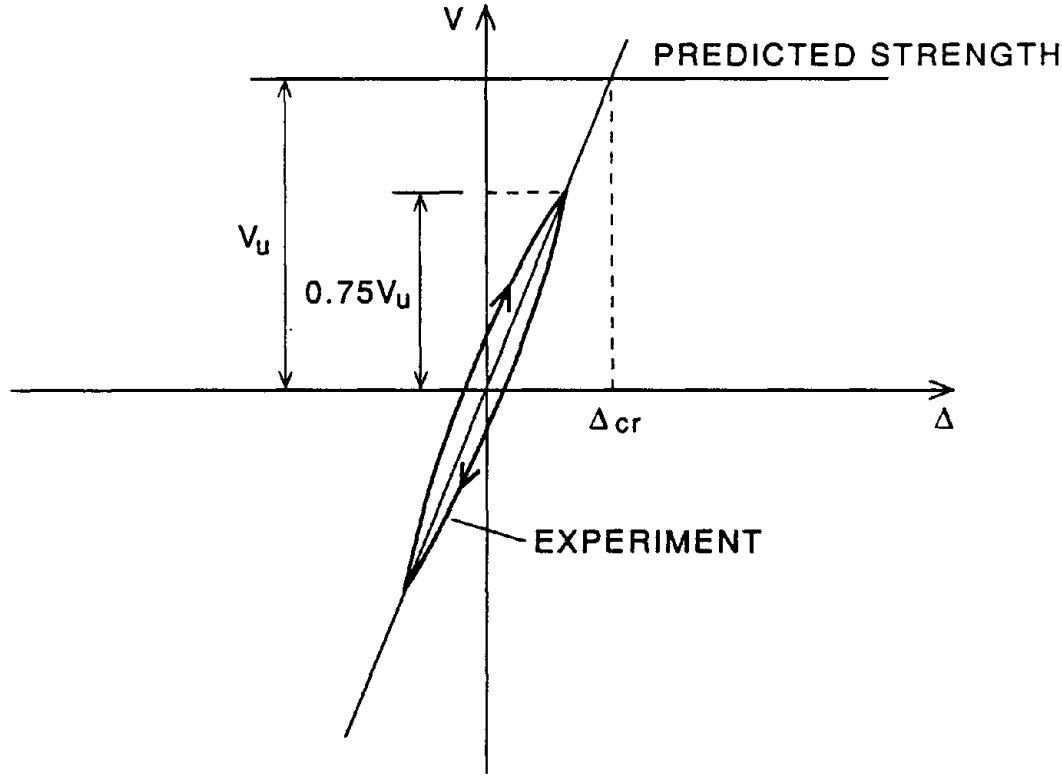

Figure 3.8 - Determination of Critical Displacement Δ_{cr} for Flexure-Dominated Walls

4 MATERIAL PROPERTIES

4.1 Material Tests

Most of the wall specimens were constructed in sets of three using the same batch of mortar and grout mixes in each set. The first specimen of each set was tested about 28 days after grouting, and the remaining ones were tested in consecutive weeks. Mortar specimens, grout specimens, and masonry prisms were prepared from the same batch of materials used for each set of wall specimens, and were tested on the 28th day after casting, in accordance with the ASTM Standards (1984) and UBC Standards (1985). In addition, some material tests were conducted with the procedures recommended by Task 1.1 of the TCCMAR program (Atkinson and Kingsley 1985). The tensile strength of the reinforcing steel was also obtained for each batch of reinforcing bars delivered. The test procedures and results are summarized in the following sections.

4.2 Masonry Units

Hollow concrete block and clay brick units were tested in compression in accordance with the ASTM Standards (1984) for each set of wall specimens. The units were capped with high-strength gypsum plaster (Hydrostone) to provide flat and smooth surfaces. They were loaded in a universal testing machine using a 4.5-in.-thick steel bearing plate at each end. A thickness of 4.5 in. exceeds ASTM recommendations. It has been observed that this thickness is required to obtain a uniform stress distribution over hollow units whose length is greater than the diameter of the testing machine platens (Atkinson and Kingsley 1985). The average uniaxial compressive strength obtained from sample units for each set of wall specimens is shown in Table 4.1. The compressive strength was calculated with the average net cross-sectional area of a unit.

4.3 Mortar

The mortar mix consisted of $1:\frac{1}{2}:4\frac{1}{2}$ proportions of Portland cement, hydrated lime, and sand by volume, which conform to ASTM Type S. For accuracy, the ingredients were proportioned by weight with a cement:lime:sand ratio of 1:0.212:3.83, which corresponds to the above volume ratio. Two types of mortar specimens were tested. One was 2-in. mortar cubes prepared in accordance with the ASTM Standards (1984), and the other was 2x4-in. mortar cylinders cast in plastic molds in accordance with the UBC Standards (1985). The cubes were submerged in a saturated lime solution for 28 days before testing, while the cylinders were cured in a fog room. Three tests were conducted for each type of mortar specimens, and the average compressive strength corresponding to each set of wall specimens is shown in Table 4.2. In general, the cylinders appeared to have a lower compressive strength than the cubes.

4.4 Grout

The grout mix consisted of 1:3:2 proportions of Portland cement, sand, and coarse aggregate by volume, with SIKA Grout Aid (Type II for concrete masonry and Type I for clay masonry) added as an expanding agent. The ingredients were proportioned by weight with a cement:sand:aggregate ratio of 1:2.71:1.71, which corresponds to the volume proportions shown above. The largest aggregate size was 3/8 in. The grout was ordered from a commercial supplier. One pound of grout aid was added to every 94 pounds of cement right before grouting. The grout aid was mixed with water before being added into the mixer.

The grout was checked to ensure an 8- to 10-in. slump as measured by the truncated cone test. Grout prisms of 3x3x6-in. were prepared in accordance with the UBC Standards (1985) and subjected to uniaxial compression tests. Additionally, 2x4-in. grout cores were drilled directly from grouted hollow units and tested as recommended by TCCMAR Task 1.1 (Atkinson and Kingsley 1985). The latter has been found to be more reflective of the actual grout strength in masonry (Kingsley et al.

1985). In general, three specimens of each type were tested for each batch of grout mix. Their ends were smoothed and capped with high-strength gypsum plaster (Hydrostone). The average compressive strength of the grout is shown in Table 4.3.

4.5 Masonry Prisms

Twenty-four-inch-high, stack-bond prisms were constructed with the aid of a jig, as shown in Fig. 4.1, which was designed to assure the alignment and the uniformity of mortar-joint thickness (Atkinson and Kingsley 1985). The prisms were fully grouted. The concrete block prisms consisted of 3 courses of units, while the clay brick prisms consisted of 6 courses. The prisms were capped with high-strength gypsum plaster with the aid of a glass plate to obtain smooth surfaces. Two to three prisms were tested for each set of wall specimens. They were loaded to the maximum compressive stress by a universal testing machine with a 4.5-in.-thick steel bearing plate at each end. Because of the large number of tests involved, the detailed stress-strain relations were not monitored in most of the tests. Most of the concrete block prisms exhibited a compression-shear failure, as shown in Fig. 4.2, while the failure of the clay brick prisms was initiated by the spalling of the face shell and followed by the crushing of the grout core. The test results are summarized in Table 4.4.

4.6 Reinforcing Steel

All reinforcing bars used were Grade 60, except the No. 3 bars which were available in Grade 40 only. Bars of each size used for each set of wall specimens were ordered and delivered at the same time. They were delivered with the mill report to ensure uniform properties as possible. Tests were conducted to obtain the actual yield and ultimate tensile strengths of the reinforcing bars sampled from the same batch of steel used in each set of wall specimens. The typical stress-strain relations obtained are shown in Fig. 4.3. The average tensile strength for each bar size is shown in Table 4.5, and the dispersion of test results is indicated by the standard deviations shown. With the exception of the No. 6 bars in Specimen 23, it was found that bars of the same size had almost the same tensile strength. The No. 6 bars in Specimen 23 had a yield strength of 74 ksi and ultimate strength of 107 ksi, which is not included in the calculation of the average strength listed in Table 4.5.

Table 4.1 - Compressive Strength of Masonry Units

Wall Specimen	*Compressive Strength (ksi)*			
	Spec 1	*Spec 2*	*Spec 3*	*Average*
1,2	*2.500*	*2.300*	*2.400*	*2.400*
3	*2.500*	*2.300*	*2.400*	*2.400*
4,5,6	*2.500*	*2.300*	*2.400*	*2.400*
7,8,9	*2.500*	*2.300*	*2.400*	*2.400*
10,11,12	*2.404*	*2.426*	*2.787*	*2.539*
13,14,15	*2.915*	*2.947*	*2.787*	*2.883*
16	*2.915*	*2.947*	*2.787*	*2.883*
17,18,19	*6.550*	*6.570*	*6.550*	*6.557*
20,21,22	*6.550*	*6.570*	*6.550*	*6.557*
23	*3.276*	*3.347*	*3.248*	*3.290*
24	*3.276*	*3.347*	*3.248*	*3.290*

Table 4.2 - Compressive Strength of Mortar

Wall Specimen	Test Method	Compressive Strength (ksi)			
		Spec 1	Spec 2	Spec 3	Average
1,2	Cubes	3.325	3.650	3.250	3.408
	Cylinders	3.739	3.351		3.545
3	Cubes	4.560	4.500	4.900	4.653
	Cylinders	3.023	3.820	3.250	3.364
4,5,6	Cubes	3.500	3.313	3.375	3.396
	Cylinders	2.865	2.387	2.546	2.599
7,8,9	Cubes	3.525	3.313	3.375	
		3.250	3.061	3.250	3.296
	Cylinders	2.674	2.642	2.785	2.700
10,11,12	Cubes	2.825	3.125	2.900	2.950
	Cylinders	2.700	2.350	2.515	2.522
13,14,15	Cubes	3.000	2.850	3.075	2.975
	Cylinders				
16	Cubes	2.400	2.475	2.425	2.433
	Cylinders				
17,18,19	Cubes	4.175	4.150	3.900	4.075
	Cylinders				
20,21,22	Cubes	3.200	3.440	3.240	3.293
	Cylinders	2.705	2.801	2.896	2.801
23	Cubes	2.588	2.750	2.688	2.675
	Cylinders	2.324	2.228	2.220	2.257
24	Cubes	2.813	2.963	2.875	2.884
	Cylinders	2.300	2.451	2.546	2.432

Table 4.3 - Compressive Strength of Grout

Wall Specimen	Test Method	Compressive Strength (ksi)			
		Spec 1	Spec 2	Spec 3	Average
1,2	Cubes	4.770	4.170		4.470
	Cores	3.819	4.774		4.297
3	Cubes	4.700	4.300		4.500
	Cores	4.100	4.530	4.200	4.277
4,5,6	Cubes	2.444	3.333		2.889
	Cores	3.183	2.865		3.024
7,8,9	Cubes				
	Cores	4.169	3.501	4.202	3.957
10,11,12	Cubes	3.778	3.333	3.778	3.630
	Cores	2.070	2.260	2.420	2.250
13,14,15	Cubes	4.170	3.950	4.740	4.287
	Cores	3.278	3.055	3.310	3.214
16	Cubes	6.250	6.070	5.775	6.032
	Cores	5.936	5.952	5.379	5.756
17,18,19	Cubes	3.550	3.900	4.286	3.912
	Cores	4.345	5.930	3.770	4.682
20,21,22	Cubes	4.131	4.477	3.132	3.913
	Cores	2.546	2.737		2.642
23	Cubes	5.185	5.435	5.391	5.337
	Cores	4.825	3.692	4.162	4.226
24	Cubes	3.149	2.782	2.892	2.941
	Cores	3.517	3.279	3.199	3.332

Table 4.4 - Compressive Strength of Masonry Prisms

Wall Specimen	*Compressive Strength (ksi)*			
	Spec 1	*Spec 2*	*Spec 3*	*Average*
1,2	*2.873*	*2.958*		*2.916*
3	*2.958*	*2.958*		*2.958*
4,5,6	*2.458*	*2.890*	*2.355*	
	2.844			*2.637*
7,8,9	*2.958*	*3.015*	*3.755*	*3.243*
10,11,12	*3.197*	*3.277*		*3.237*
13,14,15	*3.413*	*3.271*		*3.342*
16	*2.480*	*2.470*		*2.475*
17,18,19	*3.570*	*3.690*	*4.110*	*3.790*
20,21,22	*3.570*	*3.690*	*4.110*	*3.790*
23	*4.119*	*3.999*	*4.176*	*4.098*
24	*2.896*	*2.735*	*2.671*	*2.767*

Table 4.5 - Tensile Strength of Steel

BAR SIZE	GRADE	NO. OF SAMPLES	YIELD STRENGTH (ksi)		ULTIMATE STRENGTH (ksi)	
			Mean	Sample Standard Deviation	Mean	Sample Standard Deviation
3	40	12	57	1.07	82	1.60
4	60	2	67	0.40	107	0.50
5	60	5	64	0.33	104	0.88
6	60	3	65	0.53	107	1.07
7	60	9	72	2.00	105	4.20

Figure 4.1 - Construction of Masonry Prism

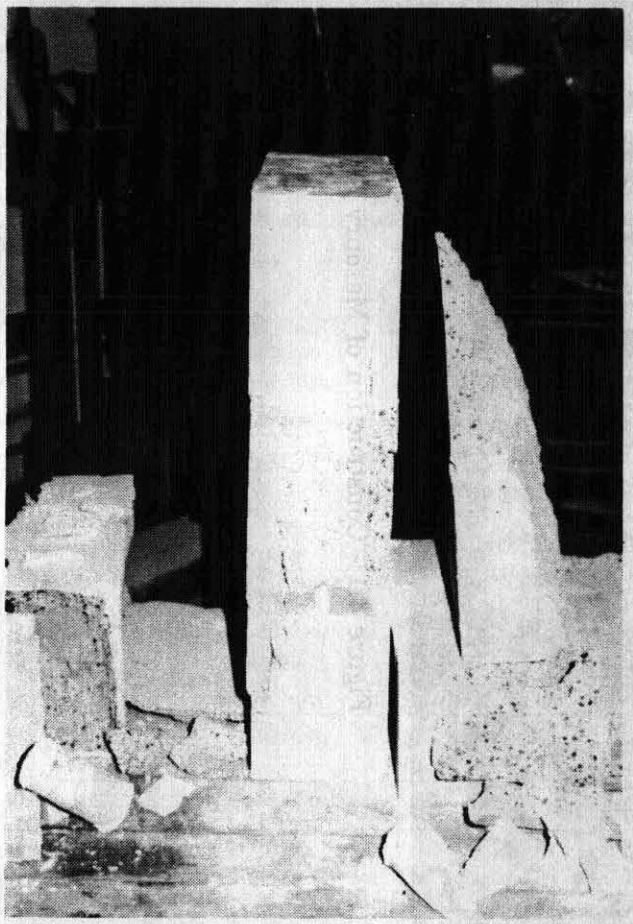

Figure 4.2 - Failure Mode of Concrete Masonry Prism

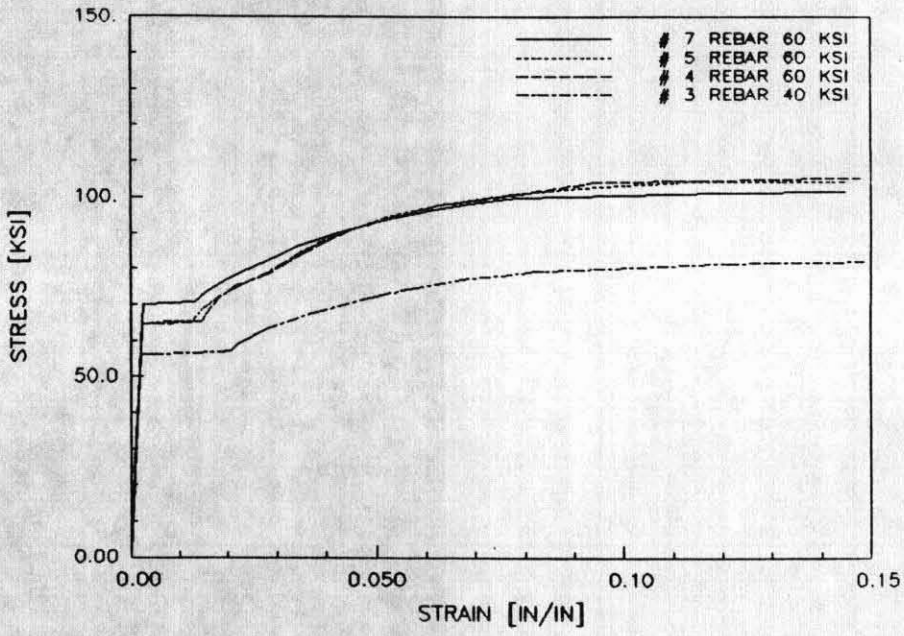

Figure 4.3 - Typical Stress-Strain Curves of Steel Reinforcement

5 GENERAL WALL BEHAVIOR

The general behavior and inelastic performance of the twenty-four wall specimens are presented in this chapter. The following discussions are organized in terms of the predominant failure mechanisms of the wall specimens, which are defined in the following section.

5.1 Strength and Failure Modes

The critical strengths of the twenty-four wall specimens are summarized in Table 5.1. They are classified as the yield strength, which is the lateral resistance developed at the first yield of the extreme vertical steel, the diagonal cracking strength, which is defined as the load at which a major diagonal crack extending over a length of at least two-third of the wall diagonal occurs, and the maximum strength, which is the maximum horizontal load resistance developed by a wall specimen.

In accordance with the governing load resistance mechanisms, two types of inelastic behavior modes can be identified from the wall specimens. One is the flexural mechanism, which is characterized by the tensile yielding of the vertical steel and compressive crushing of masonry at the wall toes. The other is the shear mechanism, which is characterized by diagonal tensile cracking. The different failure modes are illustrated in Fig. 5.1. In this study, the maximum lateral load resistance governed by the flexural mechanism is termed the flexural strength, whereas the resistance governed by diagonal tensile cracking is termed the shear strength of a wall specimen.

It has been found from the test results that the inelastic behavior of a wall panel is highly sensitive to the applied axial compressive stress and the quantity of vertical and horizontal reinforcement present. For example, specimens that had a vertical steel ratio of 0.38% and a horizontal steel ratio of 0.24% exhibited predominantly flexural behavior, while those with a higher content of vertical steel and/or a smaller quantity of horizontal steel tended to exhibit brittle shear behavior. In general, flexure-dominated specimens exhibited more ductile behavior than shear-dominated specimens.

As shown in Table 5.1, Specimens 1, 2, 8, 12, and 17 through 20 exhibited predominantly flexural behavior, while Specimens 3, 4, 5, 7, 9, 11, 13, 14, 16, and 21 through 24 exhibited predominantly

shear behavior. Specimens 6, 10 and 15 exhibited mixed flexural/shear behavior, which had significant flexural yielding, toe crushing, as well as diagonal cracking. In Specimens 6, 8, and 11, which were not subjected to any axial load, more than 10% of the total deformation at the maximum load was contributed by base sliding. At final stages of these tests, while base sliding constituted about 25% of the total deformation in Specimens 6 and 11, it constituted more than 50% of the total deformation in Specimen 8. Hence, it is expected that the load degradation and, to a lesser extent, the maximum strengths of these specimens could be affected by base sliding.

Specimens 17 through 22 were grouted hollow clay unit masonry specimens, whose behavior was very similar to that of the corresponding concrete masonry specimens. The overall performance of the wall specimens is described in the following sections. In the following discussions, the sign convention adopted for the lateral displacement and load is shown in Fig. 3.7.

5.2 Flexure-Dominated Specimens

Specimens 1, 2, 8, 12, and 17 through 20, which responded predominantly in flexure, had five #5 vertical reinforcing bars and five #4 horizontal reinforcing bars. Based on the net cross-sectional areas of the wall specimens, these correspond to a vertical steel ratio of 0.38% and a horizontal steel ratio of 0.24% for Specimens 1, 2, 8, and 12, which were concrete masonry, and to the respective steel ratios of 0.40% and 0.26% for Specimens 17 through 20, which were clay masonry. The concrete masonry specimens were subjected to three levels of axial compressive stress. All the clay masonry specimens had identical reinforcement content and axial stress, but some of them had lap splices and toe confinement near the base, as mentioned in Chapter 2.

5.2.1 Concrete Masonry Specimens

Specimen 8 was not subjected to axial compressive stress. The first yield of the extreme vertical steel occurred at a lateral load of about 35 kips. Some flexural-shear cracks developed, but no major diagonal crack occurred. As shown by the hysteresis curves in Fig. 5.2a, a maximum resistance of 50 kips occurred at a displacement of about 0.4 in. and remained almost constant thereafter for a number of cycles. Significant load degradation started at a lateral displacement of 1 in. Stiffness degradation

occurred at a very early stage, and the stiffness was almost zero at load reversal points. This was primarily due to base sliding. At the final stage, base sliding constituted more than 50% of the total displacement. The residual stiffness was mainly provided by the dowel action of the vertical steel, as well as the base friction. Significant base spalling occurred at the final stage, as shown in Fig. 5.2b. This was caused by the sliding action as well as the lateral compressive stress induced on masonry by the dowel action.

Specimen 12 was subjected to a 100-psi axial compressive stress. As shown by the hysteresis curves in Fig. 5.3a, the specimen exhibited a relatively ductile behavior. The load degradation of the specimen with respect to the increment of displacement amplitudes was relatively moderate. Nevertheless, because of the severe opening and closing of the flexural cracks, the hysteresis curves are pinched, with flat slopes at load-reversal points. Because of inoperable strain gages, the first yield of the extreme vertical steel could not be monitored during the test. However, based on analytical calculations, the first yield should have occurred at a lateral load of 46 kips. The first major diagonal crack was observed at a lateral load of 69 kips and a lateral displacement of 0.38 in. in the positive direction. The crack extended approximately at a 40-degree angle with respect to the horizontal from the left toe to the fifth course from the base. The diagonal crack in the other direction occurred at 70 kips and 0.57 in., extending from the upper left corner to the right toe. Toe crushing occurred at maximum loads of 71 kips in both directions, and lateral displacements of 0.62 and 0.87 in., respectively. Severe spalling was observed at the wall toes, and the extreme vertical steel had a fatigue rupture near the wall base during the final stage of the test. The maximum base sliding developed at the final stage was about 10% of the total deformation. The failure mode is shown in Fig. 5.3b.

Specimen 1 was subjected to a 200-psi axial compressive stress. As shown in Fig. 5.4a, the specimen had a more rapid load degradation with respect to the displacement cycle than Specimen 12. However, the hysteresis loops of Specimen 1 appear to be less pinched than those of the previous specimen. It is attributed to the fact that the opening of the flexural cracks had been significantly reduced by the high axial stress. The first yield of the extreme vertical steel occurred at a lateral load of 60 kips. The first major diagonal crack was observed at 82 kips and 0.56-in. lateral displacement in

the positive direction, and 76 kips and 0.35 in. in the other. Toe crushing was observed at the maximum strength of 87 kips and a lateral displacement of 0.82 in. in one direction, and 78 kips and 0.59 in. in the other. The weaker strength, which occurred in the negative direction, was due to small grout cavities located at the right toe. Severe base spalling was observed at the final stage of the test. The maximum base sliding was about 10% of the total deformation. The damage state of the specimen is shown in Fig. 5.4b.

Specimen 2 had an axial compressive stress of 270 psi. As shown in Fig. 5.5a, the specimen exhibited a rapid load degradation right after the maximum strength had been reached. The first yield occurred at 66 kips. The first major diagonal crack was observed at 82 kips and 0.35-in. displacement in the positive direction, and 84 kips and 0.50 in. in the other. However, the latter occurred during a load-degradation cycle after passing the maximum load of 98 kips. The maximum strengths were 83 and 98 kips in the positive and negative directions, respectively. The corresponding lateral displacements were 0.50 and 0.54 in. The discrepancy in the maximum strengths was again due to small grout cavities, which were located at the left toe of the specimen. The specimen failed in a very drastic fashion at a lateral displacement of 1.4 in. due to the severe base spalling and the loss of vertical stability under the high axial compressive load. Diagonal cracks in this specimen were more severe than those in Specimens 12 and 1. However, the opening of the diagonal cracks was well controlled by the horizontal steel. The maximum base sliding observed was about 7% of the total deformation. The damage state of the specimen is shown in Fig. 5.5b.

5.2.2 Clay Masonry Specimens

Specimens 17 through 20 were flexure-dominated clay masonry specimens that were subjected to a 280-psi axial compressive stress. Specimen 17 had the same reinforcement content as Specimen 2. As shown in Table 5.1, the maximum strength of Specimen 17 is slightly higher than that of Specimen 2. Furthermore, as shown by the hysteresis curves in Fig. 5.6a, Specimen 17 had a more ductile behavior than Specimen 2. Toe crushing occurred at a lateral displacement of about 0.9 in. in Specimen 17, whereas it occurred at about 0.5 in. in Specimen 2. This is probably due to the higher compressive strength of clay masonry. The higher strength of clay masonry also led to a higher diagonal cracking

strength, as shown in Table 5.1. The compressive failure of clay masonry was initiated by the spalling of the face shell from the grout core at the compression toe, which was subsequently followed by the crushing of the grout core. However, in the concrete masonry specimens, the crushing of the face shell and grout core occurred almost simultaneously. The final failure mode of Specimen 17 is shown in Fig. 5.6b.

Specimens 18, 19, and 20 had the same reinforcement content as Specimen 17, but the vertical steel in these specimens had 32-in. lap splices at the base. As shown in Table 5.1, their strengths are almost identical to that of Specimen 17. Specimens 18 and 20 had the same reinforcement layout, whereas Specimen 19 had wire-mesh-type confinement steel at the compression toe. However, Specimen 18 had severe grout cavities at the left toe, and therefore, exhibited a slightly lower strength and a comparatively brittle behavior, as shown by the hysteresis curves in Fig. 5.7a. The final failure mode of the specimen is shown in Fig. 5.7b. Specimen 20 exhibited a relatively ductile behavior, as shown by the hysteresis curves in Fig. 5.8a. In spite of the lap splices, its performance is very similar to that of Specimen 17. The final failure mode of the specimen is shown in Fig. 5.8b. As shown by the hysteresis curves in Fig. 5.9a, Specimen 19 had a very ductile behavior. Even though the first sign of toe crushing occurred at a lateral displacement of about 0.8 in., significant load degradation was observed at a lateral displacement of about 1.2 in. At the displacement of 1.5 in., the residual strength of the specimen was about 60 kips. As shown in Fig. 5.9b, base spalling at the final damage state was substantially reduced by the joint confinement.

5.3 Shear-Dominated Specimens

As shown in Table 5.1, the response of Specimens 3, 4, 5, 7, 9, 11, 13, 14, 16, and 21 through 24 to the applied loads was predominantly shear. The shear-dominated specimens had three vertical and two horizontal steel contents (i.e., reinforcement ratios), and were subjected to three axial compressive stress levels, as shown in Table 2.1. All specimens, except Specimens 23 and 24, were subjected to fully reversed displacement cycles. In the following discussions, the specimens are grouped in terms of the masonry unit type and vertical steel content.

5.3.1 Concrete Masonry Specimens

Vertical Steel Ratio of 0.74% (5 No. 7 Bars)

Specimens 3, 4, 5, and 7 had five No. 3 horizontal bars, while Specimens 11 and 16 had five No. 4 horizontal bars. The following discussions start with the specimens with No. 3 horizontal bars and proceed in order of increasing axial compressive loads that were applied to the specimens.

Specimen 4 was not subjected to axial compressive stress. The first major diagonal crack occurred at a lateral load of 51 kips and a displacement of 0.12 in. in the negative direction. The crack extended from the top left corner to the fifth course from the base at an approximately 50-degree angle with respect to the horizontal. The major diagonal crack occurred at 55 kips and 0.17 in. in the other direction. The first yield of the extreme vertical steel occurred at about 65 kips. The maximum strengths are 72 and 87 kips, occurring at 0.34- and 0.48-in. lateral displacements, in the positive and negative directions, respectively. Load degradation occurred soon after the maximum strengths had been reached. This is attributed to the opening of the diagonal cracks. The hysteresis curves and final failure state are shown in Fig. 5.10. The rapid stiffness degradation shown in the figure is probably due to the development and opening of diagonal cracks. Stiffness appears to be zero at load-reversal points due to the closing of the flexural cracks, which are usually severe when the axial stress is low. Because of the predominantly shear behavioral mode, base sliding was negligible.

Specimen 5 was subjected to a 100-psi axial compressive stress. The hysteresis curves are shown in Fig. 5.11a. They are very similar to those of Specimen 4, except that the load degradation in Specimen 5 appears to be slightly more rapid than that in Specimen 4. The flat slopes of the load-deflection curves at load-reversal points were due to the closing of the flexural cracks. The first major diagonal crack occurred at 60 kips and 0.16 in. in both directions. The first yield occurred at 82 kips. The maximum strengths are 89 and 84 kips, occurring at about 0.40-in. displacements, in the positive and negative directions, respectively. They were governed by the opening of the diagonal cracks. Numerous cracks parallel to the major diagonal ones were observed in both Specimens 4 and 5. However, as shown in Fig. 5.11b, the diagonal cracks in Specimen 5 were more severe and distinct than those in Specimen 4.

Specimen 7 contained the same reinforcement and was subjected to the same axial compressive load as Specimen 5. However, this specimen was subjected to a large displacement, attaining the maximum strength, right in the first cycle, as shown by the hysteresis curves in Fig. 5.12a. The first major diagonal crack occurred at 65 kips and 0.15 in. in one direction, and 60 kips and 0.10 in. in the other. The extreme vertical steel yielded at about 83 kips. The maximum strengths are 97 kips in both directions, which are about 12% (the average) higher than those of Specimen 5. Even though the average compressive strength of masonry prisms for Specimen 7 is about 15% higher than that for Specimen 5, the loads at first major diagonal cracking are almost the same in both specimens. Since the influence of material strength on the maximum strength of a wall panel should not be as significant as that on the load at first major cracking, the discrepancy in the maximum loads of the two specimens is primarily due to the different load histories and is not due to the material properties. Finally, as shown by the hysteresis curves in Fig. 5.12a, Specimen 7 exhibited a more rapid load degradation than Specimen 5. The final failure state of the specimen is shown in Fig. 5.12b.

Specimen 3 was subjected to a 270-psi axial compressive stress. The first major diagonal crack occurred at about 80 kips and 0.17-in. displacement. It extended from the top left corner to the base of the specimen at about a 45-degree angle with respect to the horizontal. The maximum strengths are 100 and 105 kips, occurring at lateral displacements of about 0.7 in. in both directions. As shown in Fig. 5.13a, the high axial compressive stress helped to sustain the maximum load for a number of displacement cycles, probably through the aggregate-interlock mechanism. However, the loss of the load resistance occurred very suddenly at a lateral displacement of 0.9 in. as the diagonal crack opened substantially. The crack was more distinct than those in Specimens 4 and 5. The vertical steel in Specimen 3 did not reach yield stress. The failure mode of the specimen is shown in Fig. 5.13b. It must also be noted that the diagonal crack intersected the wall base a few inches away from the lower right corner of the wall. This provided additional horizontal frictional resistance at the compression toe and, thereby, reduced the rate of load degradation.

Specimen 11 had the same amount of vertical reinforcement as the previous specimens, but had twice the amount of horizontal reinforcement. It was not subjected to axial compressive stress. The first diagonal crack was observed at a lateral load of about 55 kips, which is close to that of Specimen

4. However, the maximum loads developed were 89 and 95 kips in the positive and negative directions, respectively, which are higher than those of Specimen 4. The diagonal cracks were uniformly distributed throughout the wall panel. Moreover, as shown by the hysteresis curves in Fig. 5.14a, the load degradation was relatively mild when compared with Specimen 4. This is due to the fact that the maximum resistance of this specimen was governed by base sliding, rather than diagonal crack opening. As shown in Fig. 5.14b, the diagonal cracks remained close at the final stage. However, some sliding induced spalling was observed at the wall toes. Base sliding accounted for 25% of the lateral displacement at the final stage.

Specimen 16 had the same reinforcement content as Specimen 11, but was subjected to an axial compressive stress of 270 psi. The compressive stress substantially reduced the base sliding, and the final failure was governed by the shear cracks. The first major diagonal crack occurred at about 85 kips and 0.15-in. displacement in the negative direction, and 87 kips and 0.14-in. displacement in the other. The first yield occurred at about 100 kips. The maximum strengths reached are 120 kips in both directions, occurring at lateral displacements of about 0.6 in. They are 20% higher than those of Specimen 3, which had only half of the horizontal steel, while the diagonal cracking strengths are almost the same. This is evidently due to the larger amount of horizontal steel in Specimen 16. However, as shown in Fig. 5.15a, the load degradation of this specimen appears to be more rapid than that of Specimen 3. This is possibly due to the fact that the locations of the diagonal cracks in these two specimens were slightly different. While the major diagonal cracks extended right through the base corners of Specimen 16, as shown in Fig. 5.15b, the major crack intersected the base of Specimen 3 at a distance of about nine inches away from the base corner towards the interior of the wall, as shown in Fig. 5.13b. As a result, a large compression zone existed at the right corner of Specimen 3. The large compression zone could delay toe crushing, and, as a result, could lead to a higher deformation capability. Moreover, because of the larger amount of horizontal reinforcement, the shear cracks in Specimen 16 were more uniformly spread across the wall panel than those in Specimen 3.

Vertical Steel Ratio of 0.38% (5 No. 5 Bars)

Specimen 9 had the same amount of horizontal reinforcement and axial compressive stress, i.e., 270 psi, as Specimen 3. However, it had a vertical reinforcement ratio of 0.38%, which is about half of that in Specimen 3. The first yield occurred at 76 kips. The first major diagonal crack occurred at 92 kips in both directions. The maximum strengths are 96 kips, occurring at about 0.3-in. displacements in both directions. The specimen exhibited brittle behavior. As shown in Fig. 5.16a, the lateral resistance dropped rapidly immediately after the maximum strength had been attained due to the severe opening of the diagonal cracks. The horizontal steel ruptured near the center of the wall at the final stage of the test. The final failure state is shown in Fig. 5.16b.

Vertical Steel Ratio of 0.54% (5 No. 6 Bars)

Specimen 14 had 0.54% of vertical steel, but had the same amount of horizontal reinforcement and axial compressive stress as Specimen 9. As shown in Fig. 5.17a, its hysteresis curves are very similar to those of Specimen 9, exhibiting a very brittle behavior. The first yield occurred at 85 kips. The first major diagonal crack occurred at 98 and 105 kips in the positive and negative directions, respectively. The maximum strengths are 98 and 112 kips. A sudden drop of lateral resistance was observed at a displacement of about 0.5 in. due to the opening of the diagonal cracks. Its final failure mode was very similar to that of Specimen 9, as shown in Fig. 5.17b.

Specimen 13 was similar to Specimen 14, except that it had twice as much horizontal reinforcement. As shown in Fig. 5.18a, it exhibited a more ductile behavior than Specimen 14. The first yield occurred at 90 kips. The first major diagonal crack occurred at the maximum strengths of 109 and 115 kips in the positive and negative directions, respectively. The final failure state is shown in Fig. 5.18b. The axial compressive stress applied was 270 psi.

Specimens 23 and 24 had the same reinforcement content as Specimens 14 and 13, respectively. Axial compressive stress was 270 psi. However, the specimens were subjected to monotonic displacements. As a result, the failure mechanism, as well as the strain in the horizontal reinforcement, was easier to observe than that in the cyclically loaded specimens. For Specimen 23, the sequence of major diagonal cracking is indicated in the diagram in Fig. 5.19. The first crack occurred prematurely due to

the accidental loss of the vertical load. After the first two major cracks had occurred, a diagonal strut mechanism formed, sustaining the lateral and vertical loads. The occurrence of the strut mechanism is supported by the evidence that the horizontal steel in the compression strut region exhibited compression rather than tension. After the third major crack had occurred at a load of 119 kips, which extended from one corner to the other along the main diagonal, as shown in Fig. 5.19, the strut mechanism became ineffective and the shear resistance dropped rapidly. At this stage, the horizontal steel was subjected to severe tension in the vicinity of the crack. The monotonic load-displacement curve is shown in Fig. 5.20a. The hysteresis envelope of Specimen 14 is also plotted in the same figure. It is evident that the monotonically loaded specimen exhibited a much more ductile behavior than the cyclically loaded specimen. The final failure state is shown in Fig. 5.20b.

The monotonic load-displacement curve for Specimen 24 is shown in Fig. 5.21a. The crack sequence as indicated on the curve is similar to that shown in Fig. 5.19. However, the third crack developed more gradually, starting at a lateral displacement of about 0.45 in. Because of the large quantity of horizontal steel, the third major diagonal crack remained closed until shear-induced toe crushing occurred, after which the resistance dropped rapidly. The ductility of this specimen is slightly better than that of Specimen 23. The load-displacement envelope of Specimen 13 is also plotted in the same figure. It can be observed that the ductility of the cyclically loaded specimen is slightly lower than that of Specimen 24. The final failure mode of this specimen is shown in Fig. 5.21b.

5.3.2 Clay Masonry Specimens

Specimens 21 and 22, which had five No. 6 vertical bars and five No. 3 horizontal bars, were shear dominated clay masonry specimens. Specimen 21 was subjected to an axial compressive stress of 280 psi. As shown in Fig. 5.22a, the specimen exhibited a very brittle behavior and its hysteresis curves are very similar to those of Specimen 14, which had the same quantity of reinforcement and axial compressive stress but was fabricated with concrete blocks. The first major diagonal crack occurred at about 90 kips, which is very close to that of Specimen 14. The final failure state is shown in Fig. 22b.

Specimen 22 was subjected to an axial compressive stress of 100 psi. As shown by the hysteresis curves in Fig. 5.23a, the behavior is a lot more ductile than that of Specimen 21. The first yield occurred at about 62 kips and the first major diagonal crack occurred at about 85 kips. The maximum strength of this specimen was lower than that of Specimen 21. The final failure mode is shown in Fig. 5.23b; it is very similar to that of Specimen 21.

5.4 Flexure/Shear-Dominated Specimens

Specimens 6, 10, and 15 were concrete masonry walls which exhibited a mixed flexural/shear behavior. Specimen 6 had the same reinforcement content as Specimen 9, but it was not subjected to axial stress. The first yield occurred at about 30 kips and the first major diagonal crack at 45 kips. At a displacement amplitude of 0.6 in., about 18% of the total displacement was contributed by base sliding. As shown in Fig. 5.24a, the load degradation was slow and the stiffness decreased to zero at load-reversal points because of base sliding. The final failure state is shown in Fig. 5.24b. It had severe diagonal cracks and mild toe crushing.

Specimen 10 had the same reinforcement content as Specimen 6, but it was subjected to a 100-psi axial compressive stress. As shown by the hysteresis curves in Fig. 5.25a, it exhibited relatively ductile behavior. Because of inoperable strain gages, the yielding of the vertical steel could not be monitored in this specimen. Based on analytical calculations, the first yield should have occurred at 46 kips. The first major diagonal crack was observed at 60 kips in the positive direction and 58 kips in the other. The maximum strengths developed are 69 and 67 kips, respectively. The diagonal cracks had about a 35-degree angle with respect to the horizontal and extended from the base corners to the mid-height of the specimen. Toe crushing started at about 69 and 66 kips, and lateral displacements of 0.8 in. in the two directions. The load degradation was relatively moderate and was mainly caused by toe crushing, which was very significant at the final stage of the test, as shown in Fig. 5.25b. The extreme vertical steel ruptured near the left toe.

Specimen 15 had the same reinforcement content as Specimen 13, but it was subjected to a 100-psi, instead of 270 psi, axial compressive stress. It exhibited a much more ductile behavior than Specimen 13, as indicted by the curves in Fig. 5.26a. The first major diagonal crack occurred at 67 kips

in the positive direction and 80 kips in the other. The maximum strengths are 82 and 94 kips, respectively. The diagonal cracks extended from corner to corner. Toe crushing was first observed at 75 kips in the positive direction and 88 kips in the other. Severe toe crushing and base spalling were observed at the final stage, as shown in Fig. 5.26b.

Table 5.1 - Critical Strengths of Wall Specimens

Wall Specimen	Yield Strength (kips)	Diagonal Cracking Strength (kips)	Maximum Strength (kips)	Predominant Damage Mode
1	60	+82,-76	87,-78	Flexure
2	66	+82,-84	+83,-98	Flexure
3	-	-,-80	+100,-105	Shear
4	65	+55,-51	+72,-87	Shear
5	82	+60,-60	+89,-84	Shear
6	30	+52,-45	+52,-47	Flexure/Shear/Slide
7	83	+65,-60	+97,-97	Shear
8	35	-	+50,-47	Flexure/Slide
9	76	+92,-92	+96,-96	Shear
10	46*	+60,-58	+69,-67	Flexure/Shear
11	63*	+57,-55	+89,-95	Shear/Slide
12	46*	+69,-70	+71,-71	Flexure
13	90	+109,-115	+109,-116	Shear
14	85	+98,-105	+98,-112	Shear
15	58*	+67,-80	+82,-94	Flexure/Shear
16	101	+87,-85	+120,-121	Shear
17	65	+96,-103	+96,-103	Flexure
18	64	+90,-98	+90,-98	Flexure
19	65	+100,-99	+108,-104	Flexure
20	70	+108,-111	+108,-111	Flexure
21	-	+90,-105	+102,-109	Shear
22	62	+90,-85	+97,-86	Shear
23	89	119	119	Shear
24	100	115	116	Shear

* Analytical Predictions

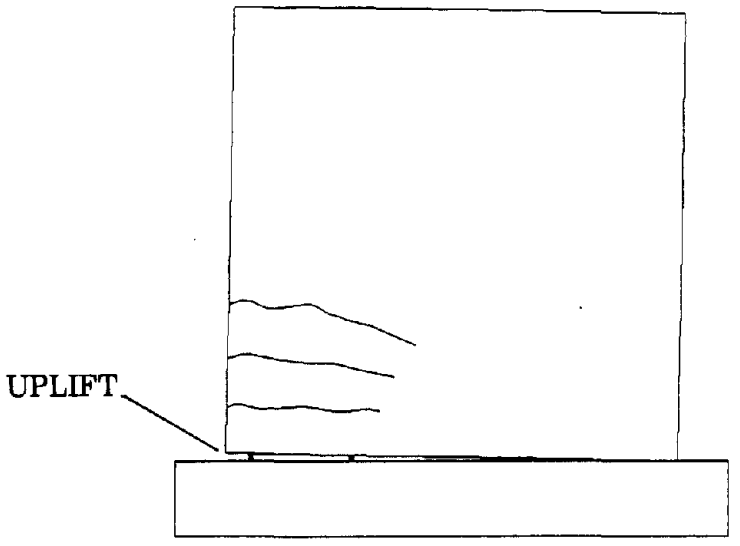

Flexural Failure

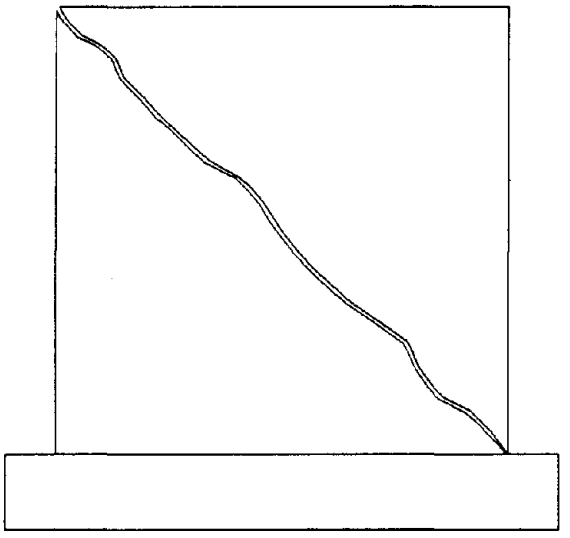

Shear Failure

Figure 5.1 - Failure Mechanisms of Masonry Wall Panels

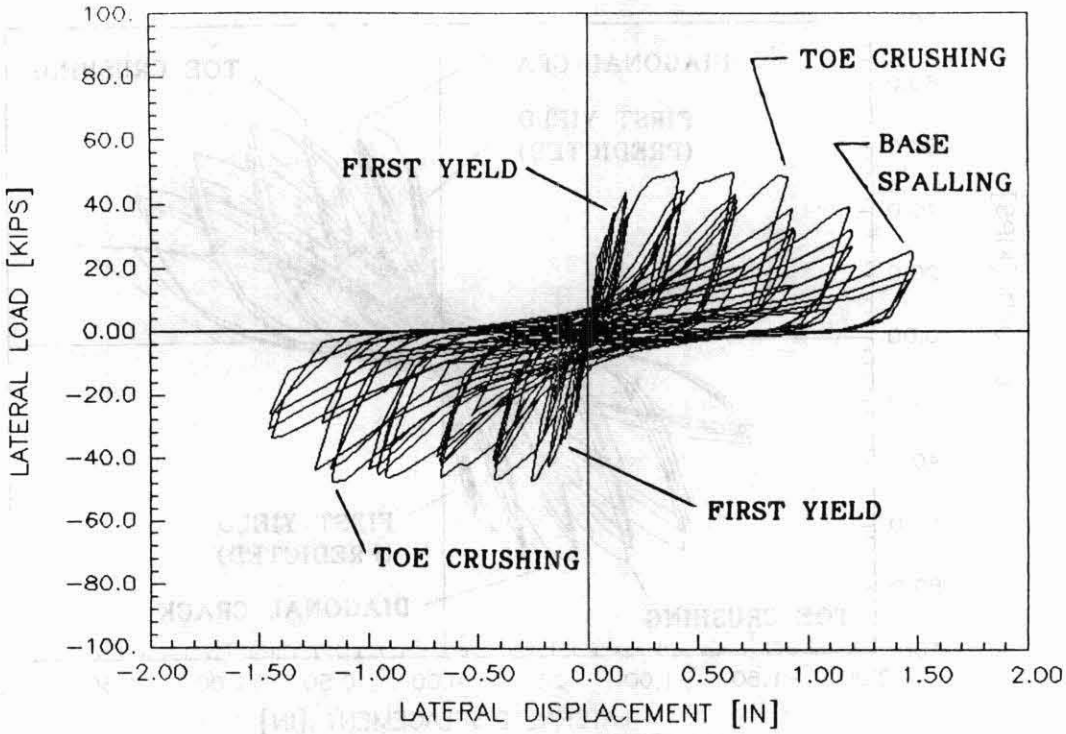

(a) Lateral Load Versus Lateral Displacement

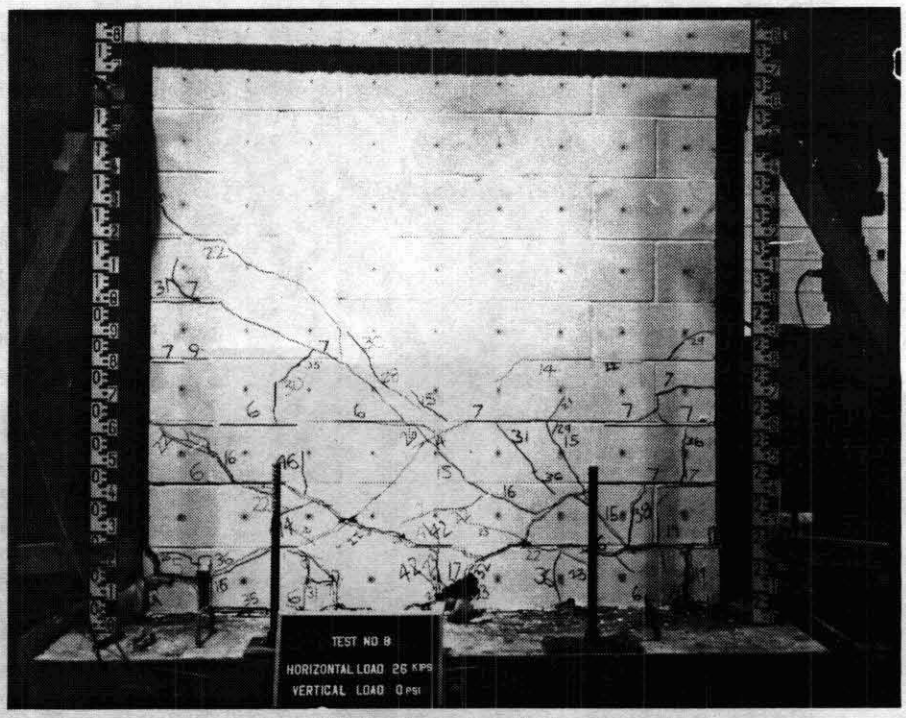

(b) Failure Mode

Figure 5.2 - Hysteresis Curves and Failure Mode of Specimen 8

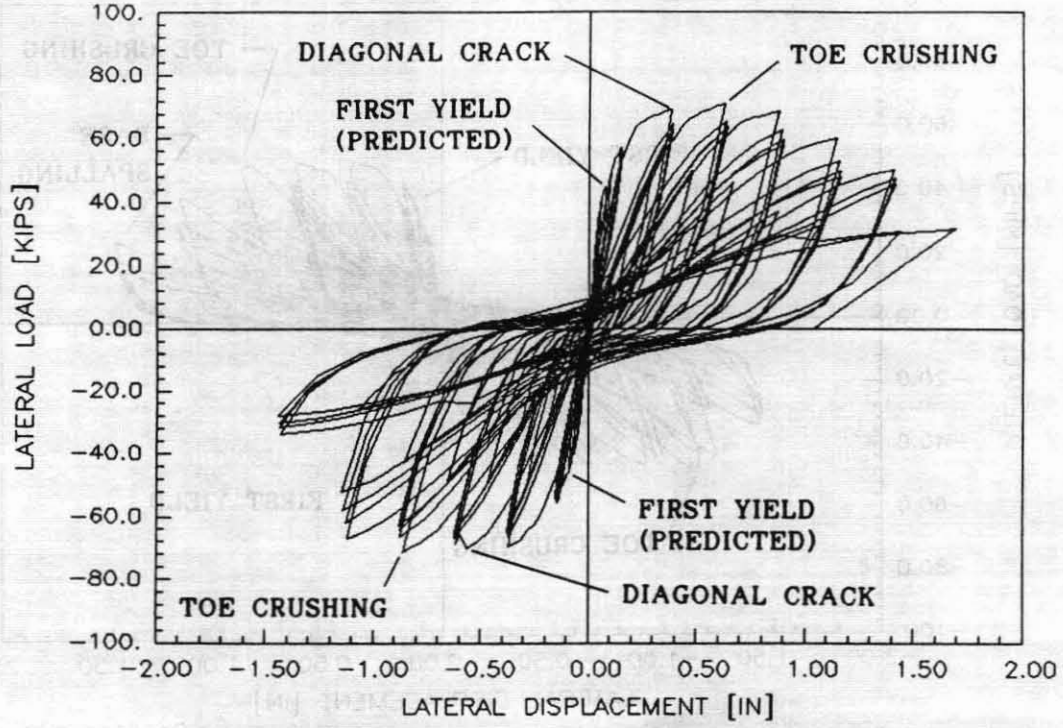

(a) Lateral Load Versus Lateral Displacement

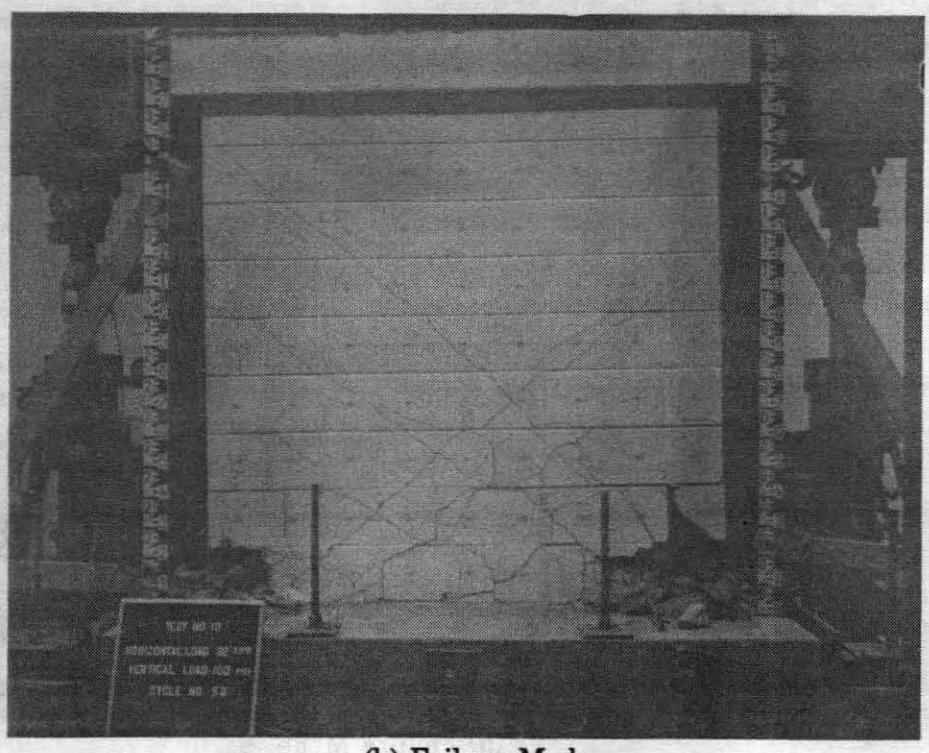

(b) Failure Mode

Figure 5.3 - Hysteresis Curves and Failure Mode of Specimen 12

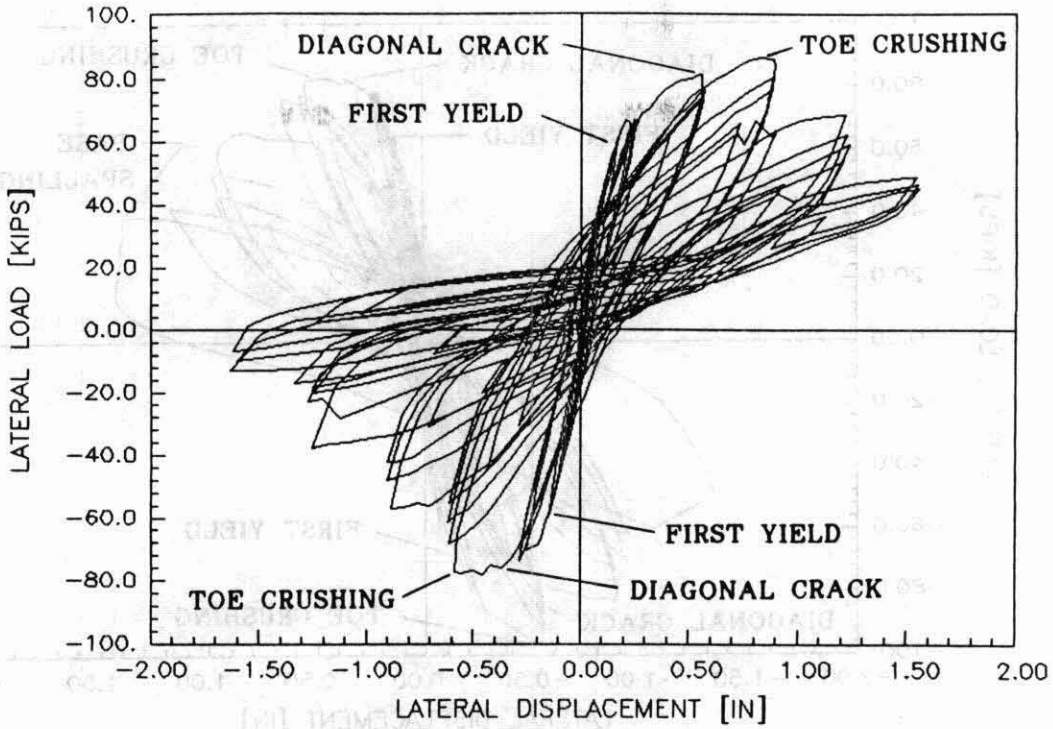

(a) Lateral Load Versus Lateral Displacement

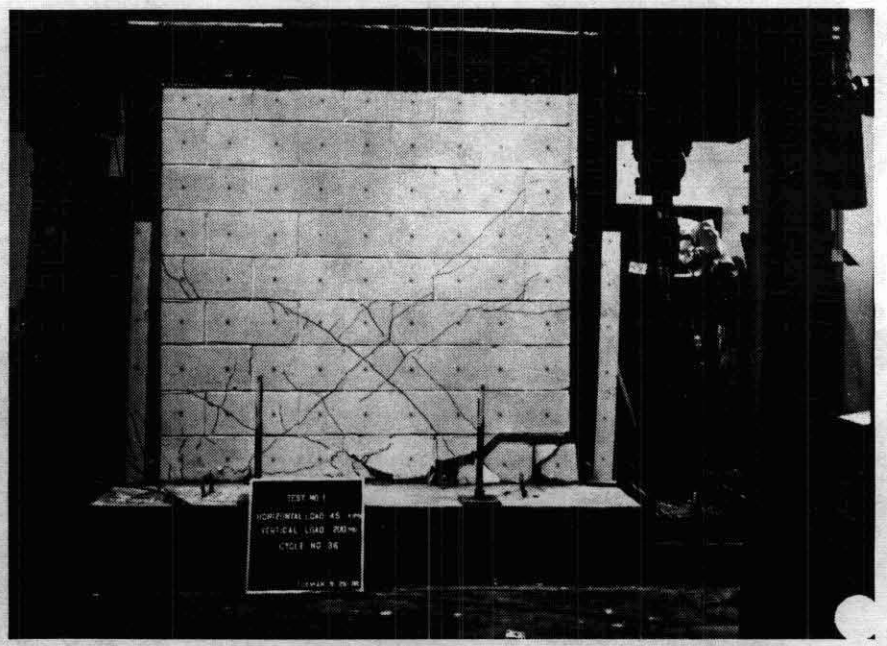

(b) Failure Mode

Figure 5.4 - Hysteresis Curves and Failure Mode of Specimen 1

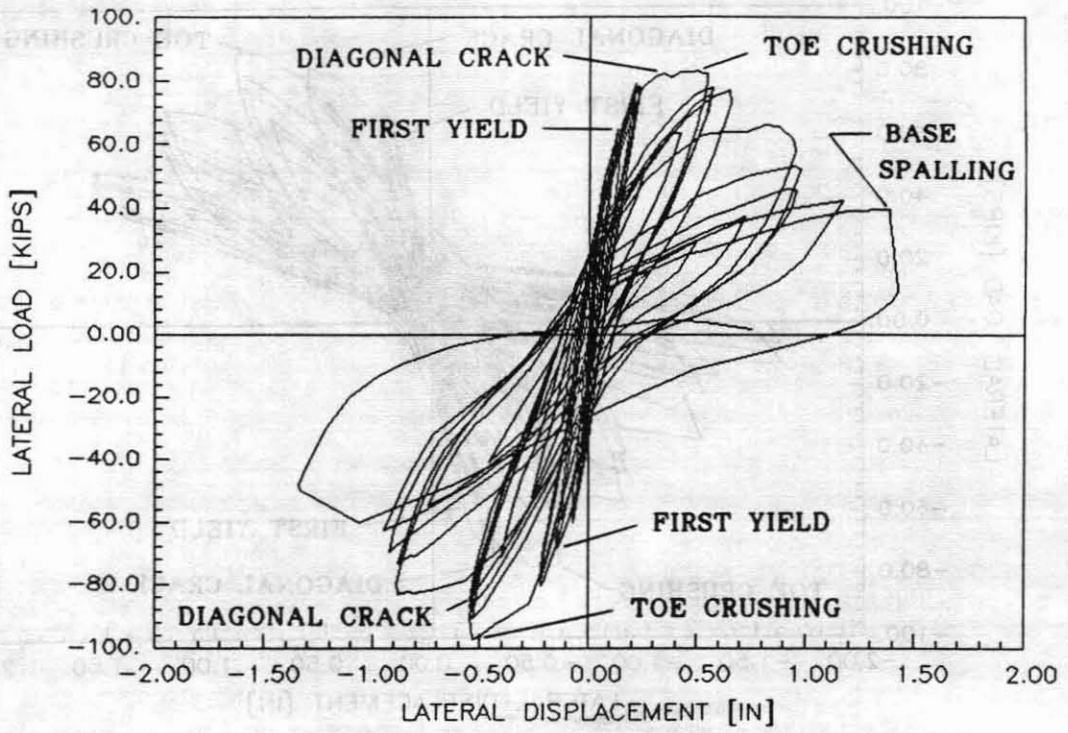

(a) Lateral Load Versus Lateral Displacement

(b) Failure Mode

Figure 5.5 - Hysteresis Curves and Failure Mode of Specimen 2

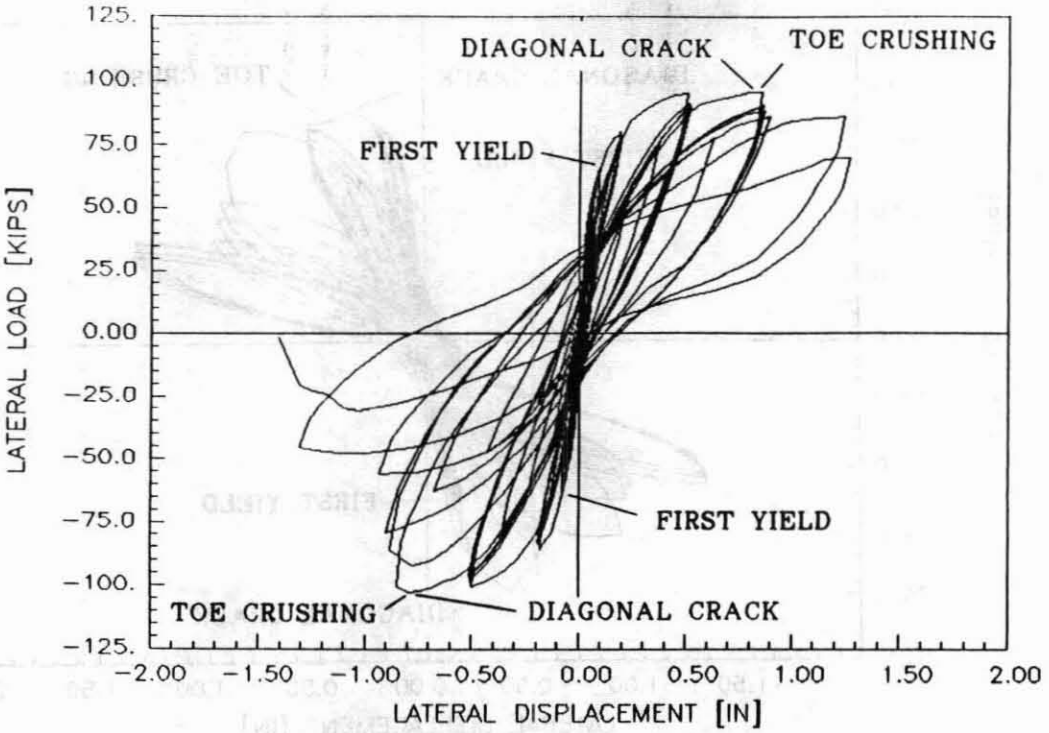

(a) Lateral Load Versus Lateral Displacement

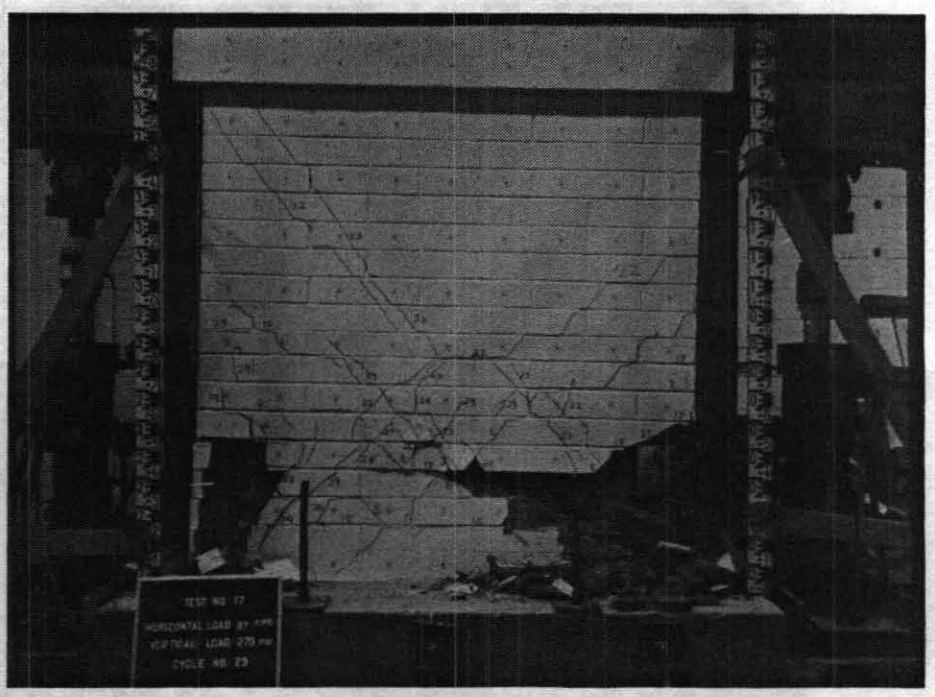

(b) Failure Mode

Figure 5.6 - Hysteresis Curves and Failure Mode of Specimen 17

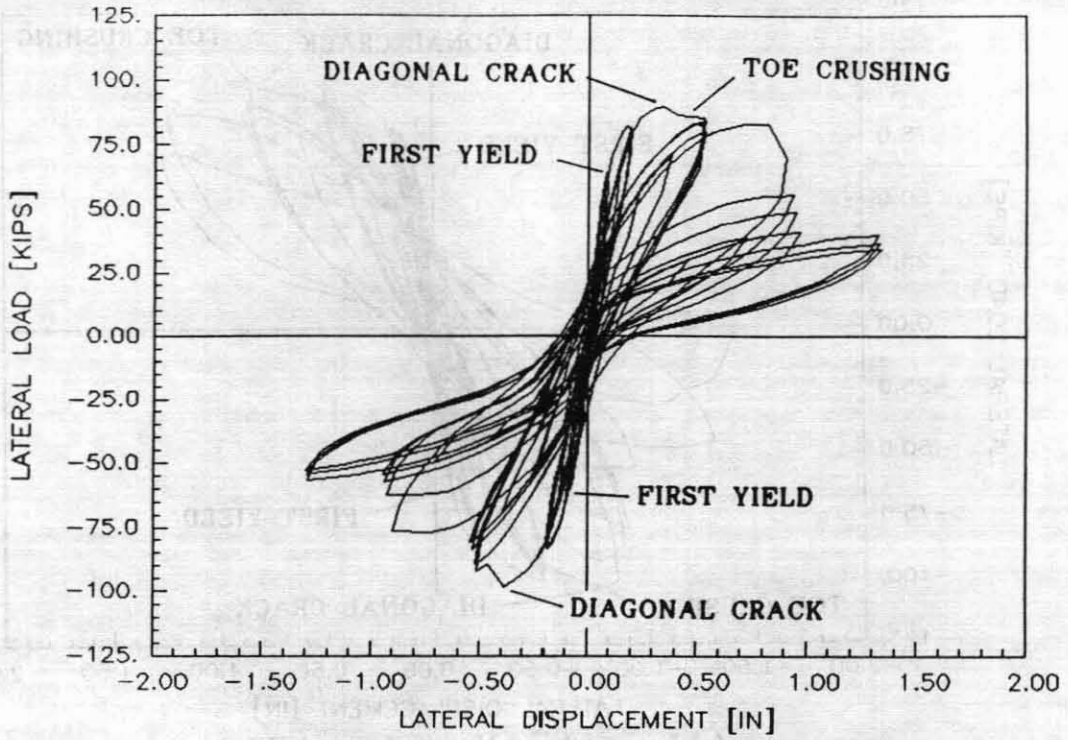

(a) Lateral Load Versus Lateral Displacement

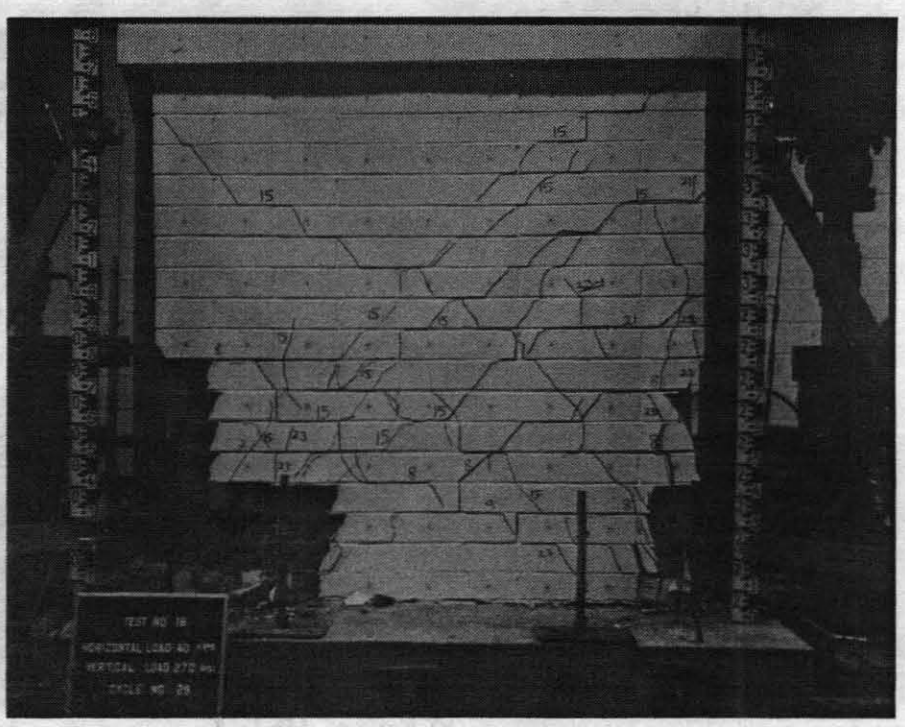

(b) Failure Mode

Figure 5.7 - Hysteresis Curves and Failure Mode of Specimen 18

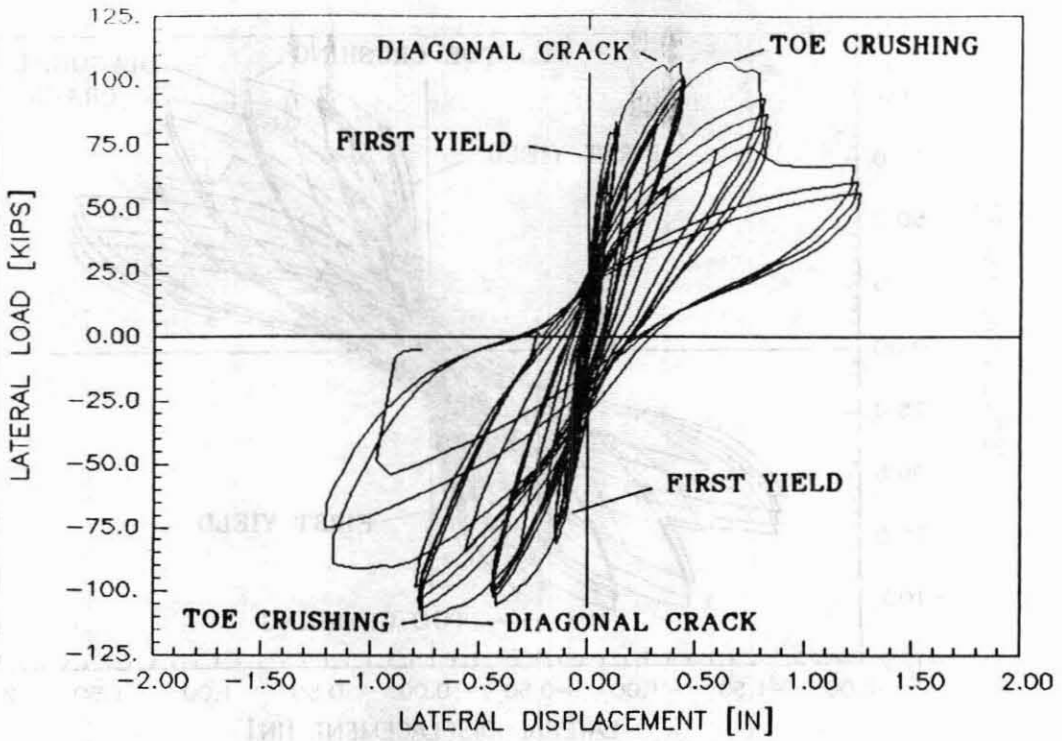

(a) Lateral Load Versus Lateral Displacement

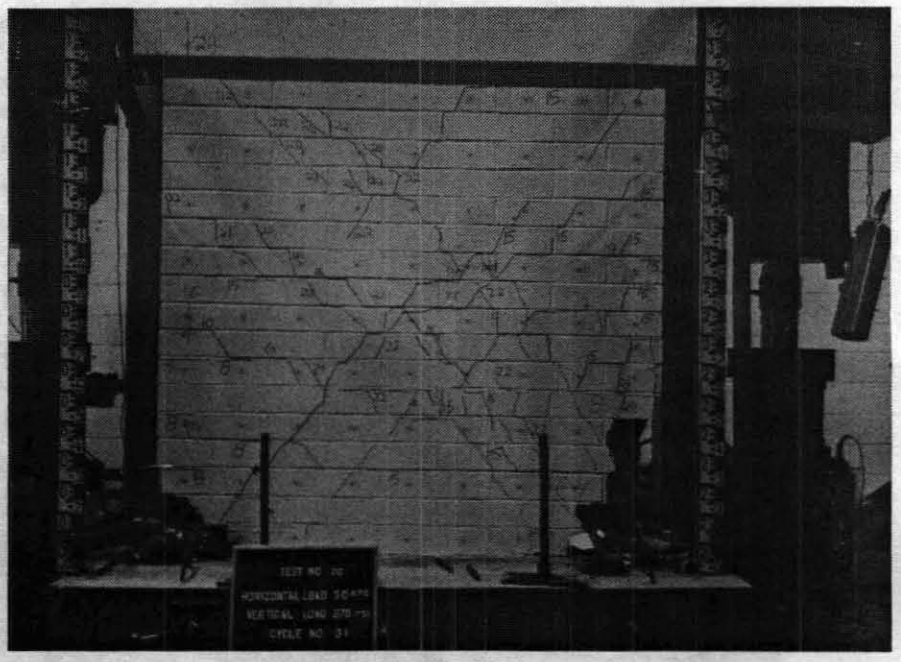

(b) Failure Mode

Figure 5.8 - Hysteresis Curves and Failure Mode of Specimen 20

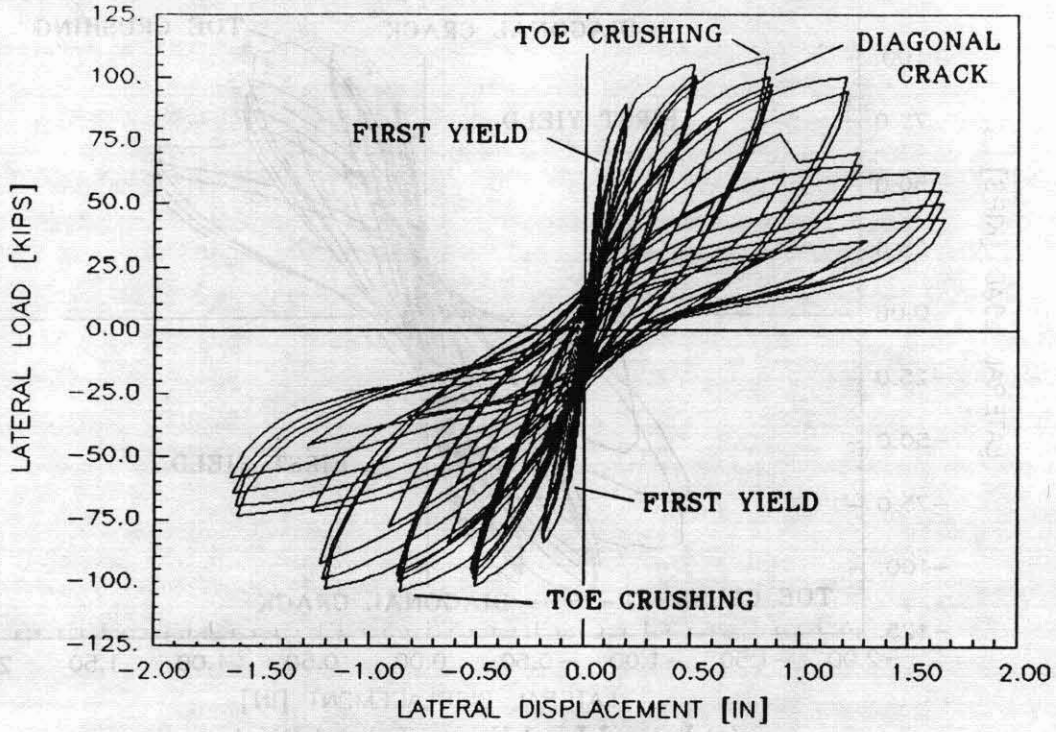

(a) Lateral Load Versus Lateral Displacement

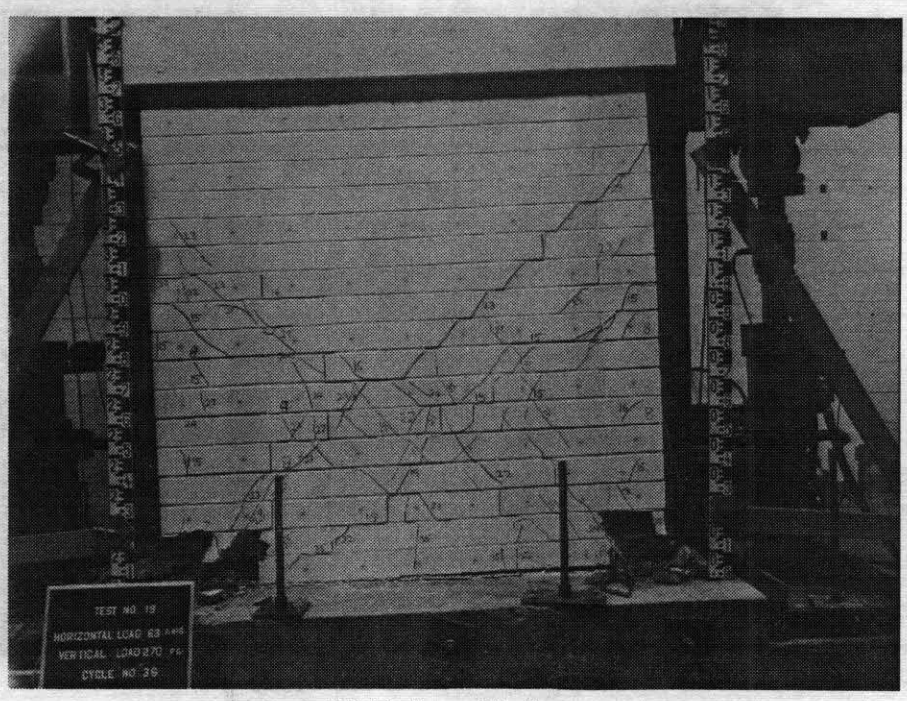

(b) Failure Mode

Figure 5.9- Hysteresis Curves and Failure Mode of Specimen 19

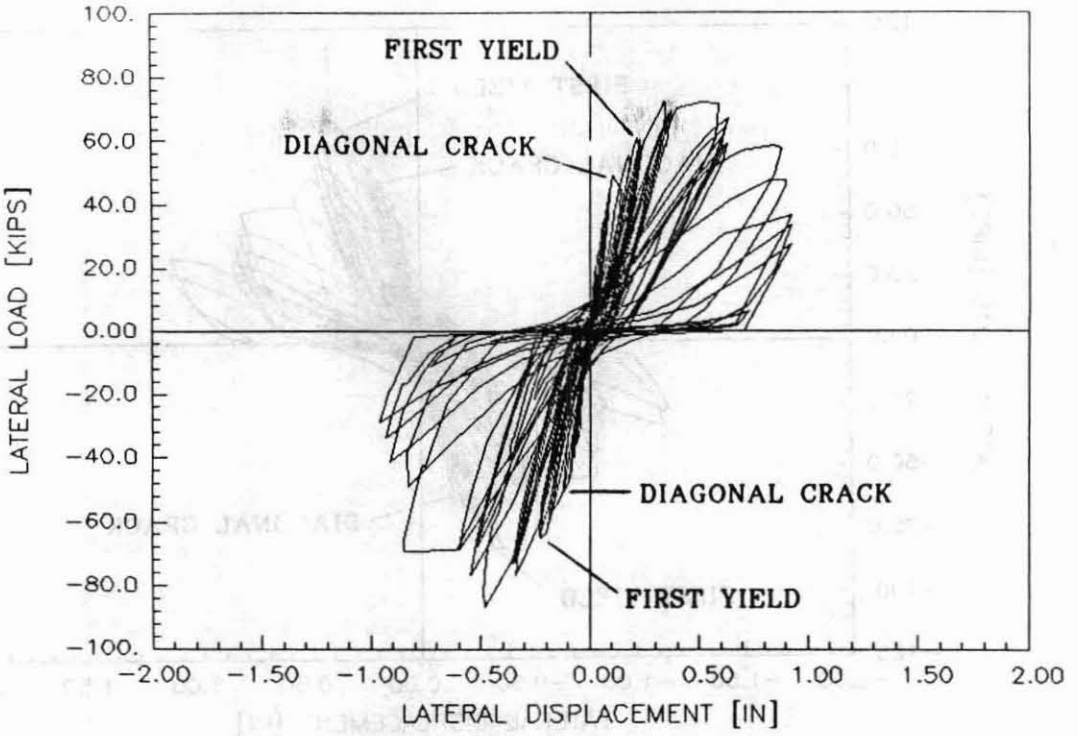

(a) Lateral Load Versus Lateral Displacement

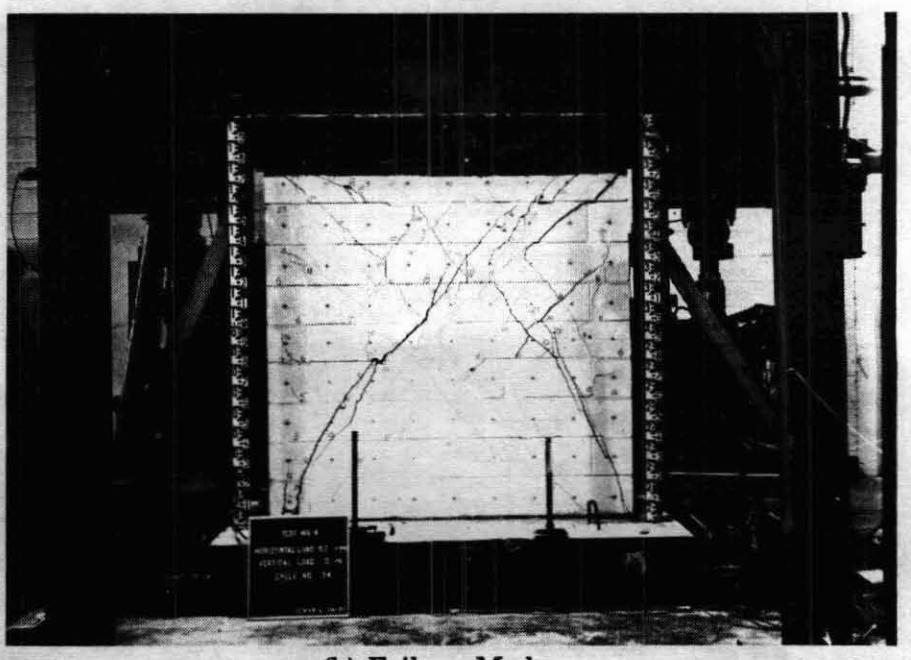

(b) Failure Mode

Figure 5.10 - Hysteresis Curves and Failure Mode of Specimen 4

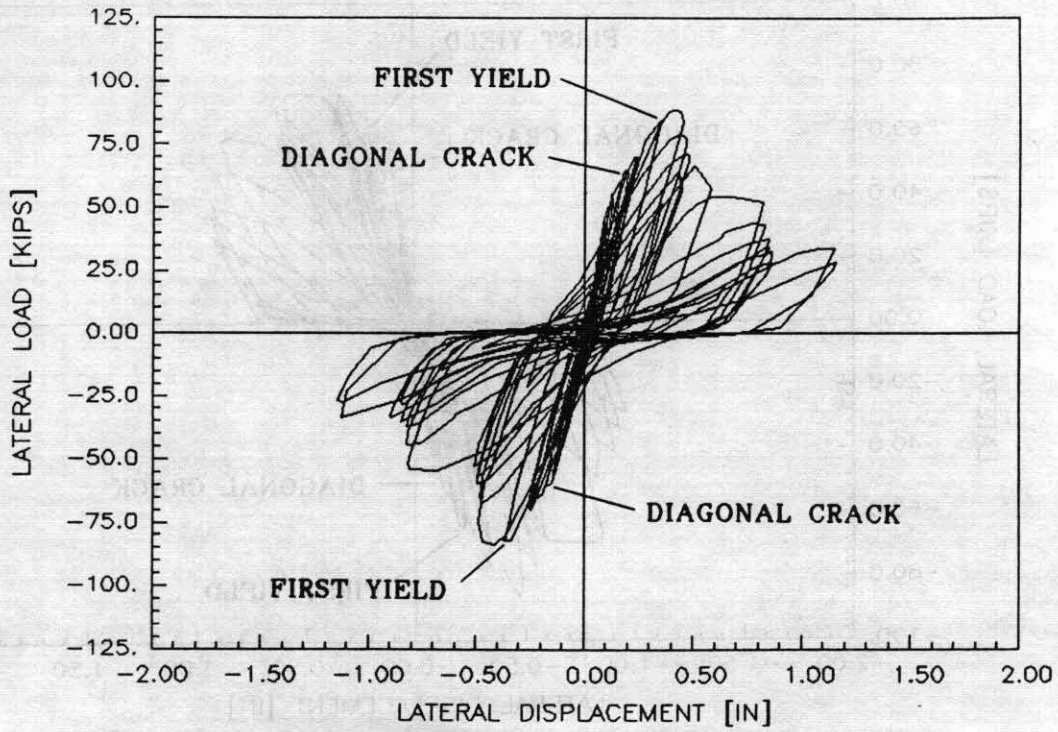

(a) Lateral Load Versus Lateral Displacement

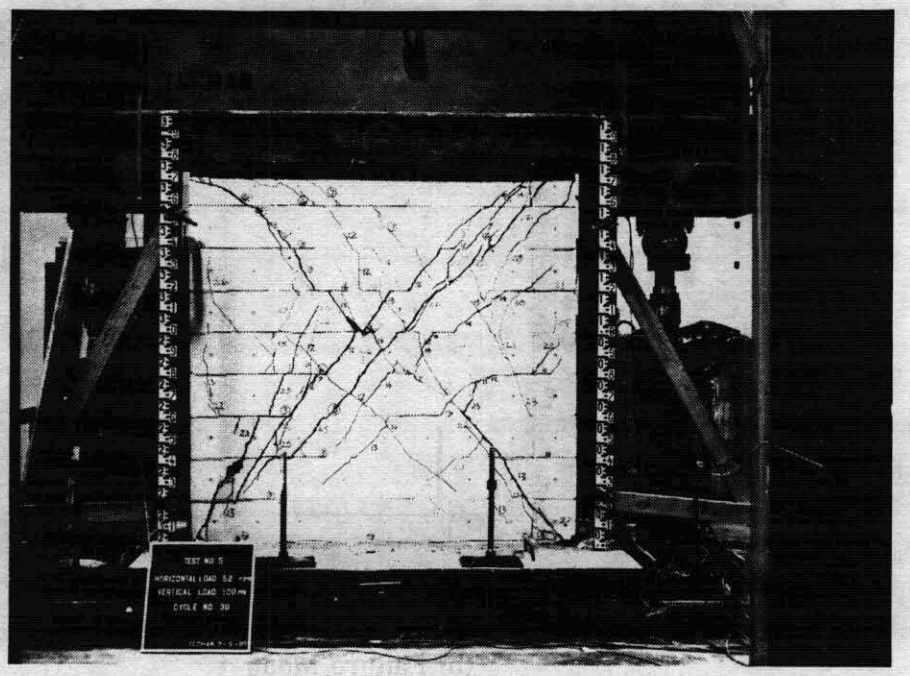

(b) Failure Mode

Figure 5.11 - Hysteresis Curves and Failure Mode of Specimen 5

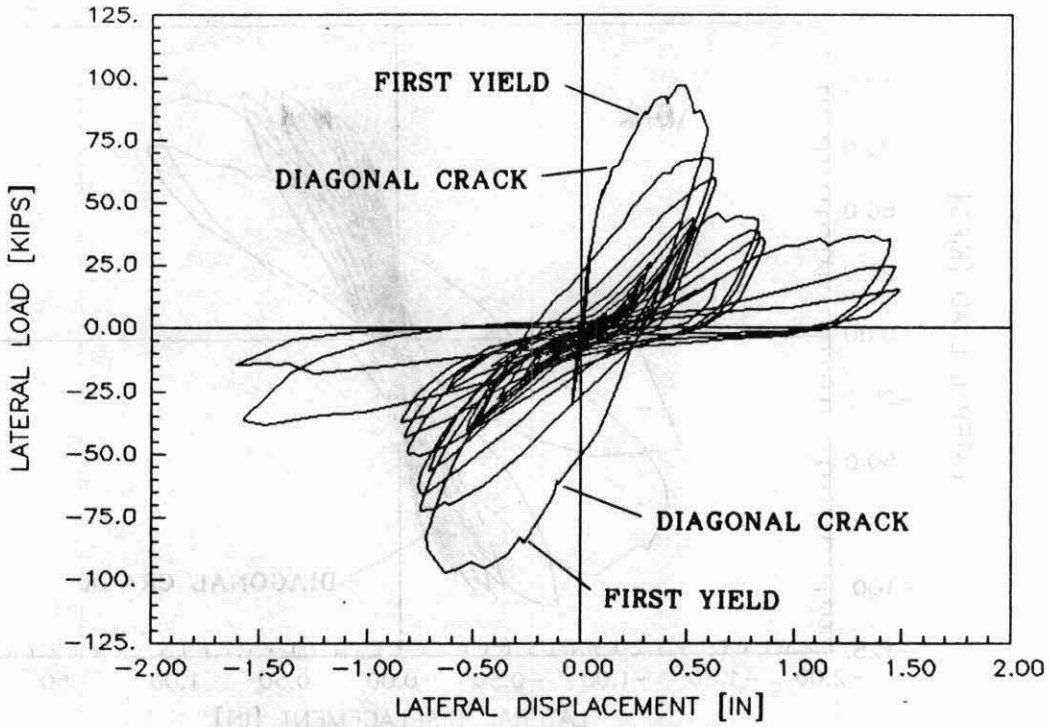

(a) Lateral Load Versus Lateral Displacement

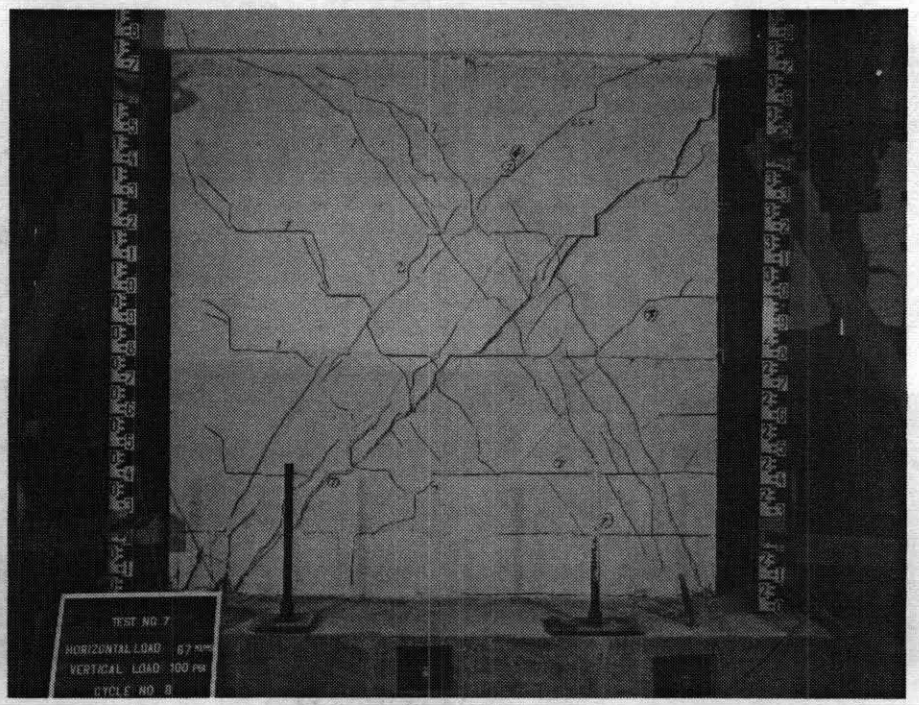

(b) Failure Mode

Figure 5.12 - Hysteresis Curves and Failure Mode of Specimen 7

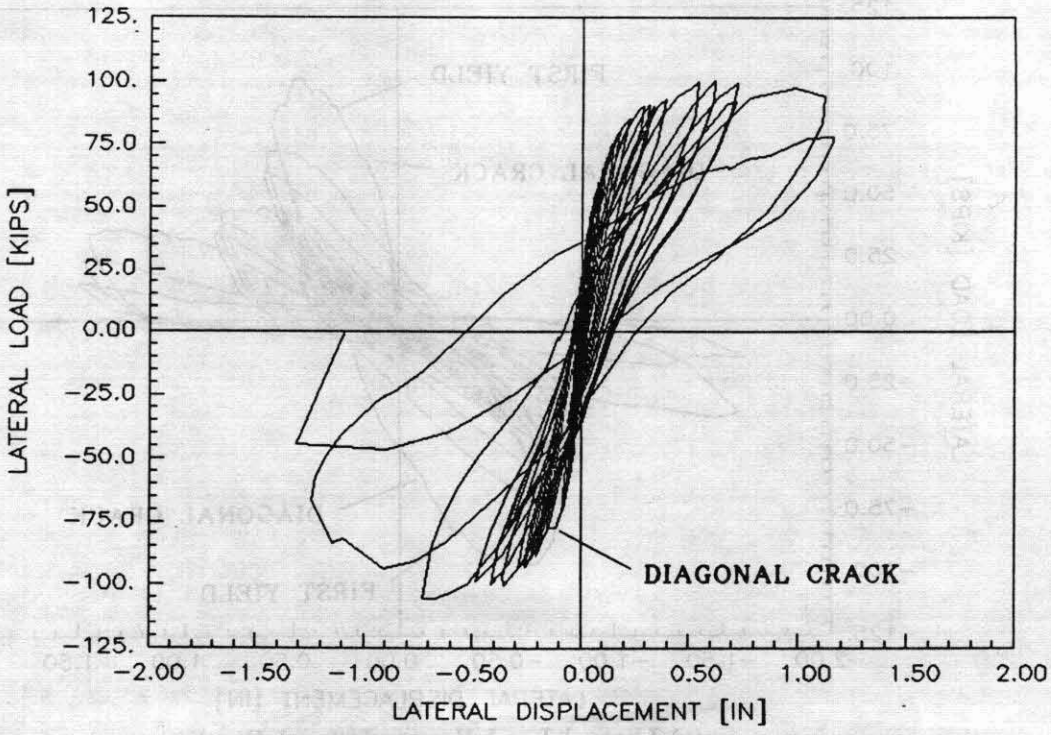

(a) Lateral Load Versus Lateral Displacement

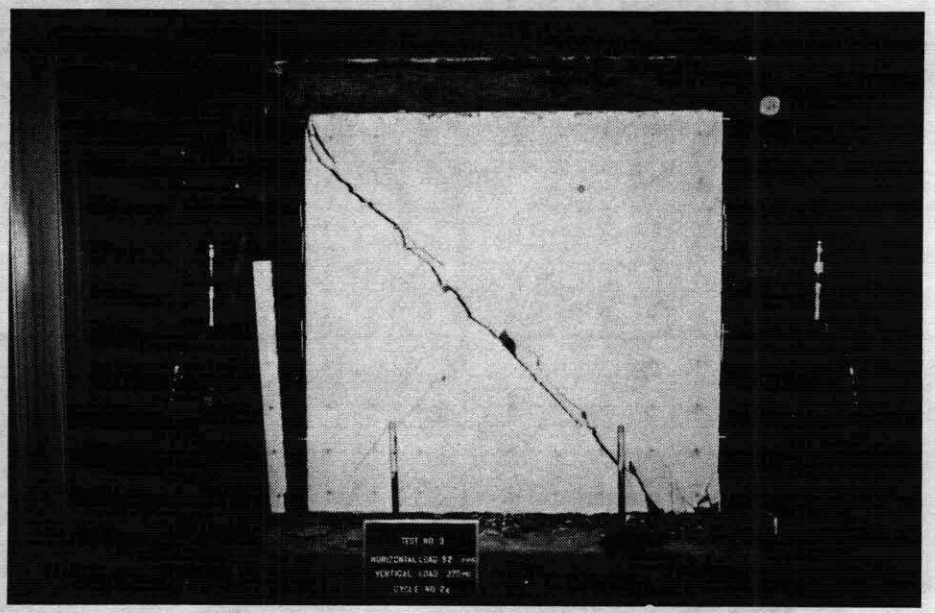

(b) Failure Mode

Figure 5.13 - Hysteresis Curves and Failure Mode of Specimen 3

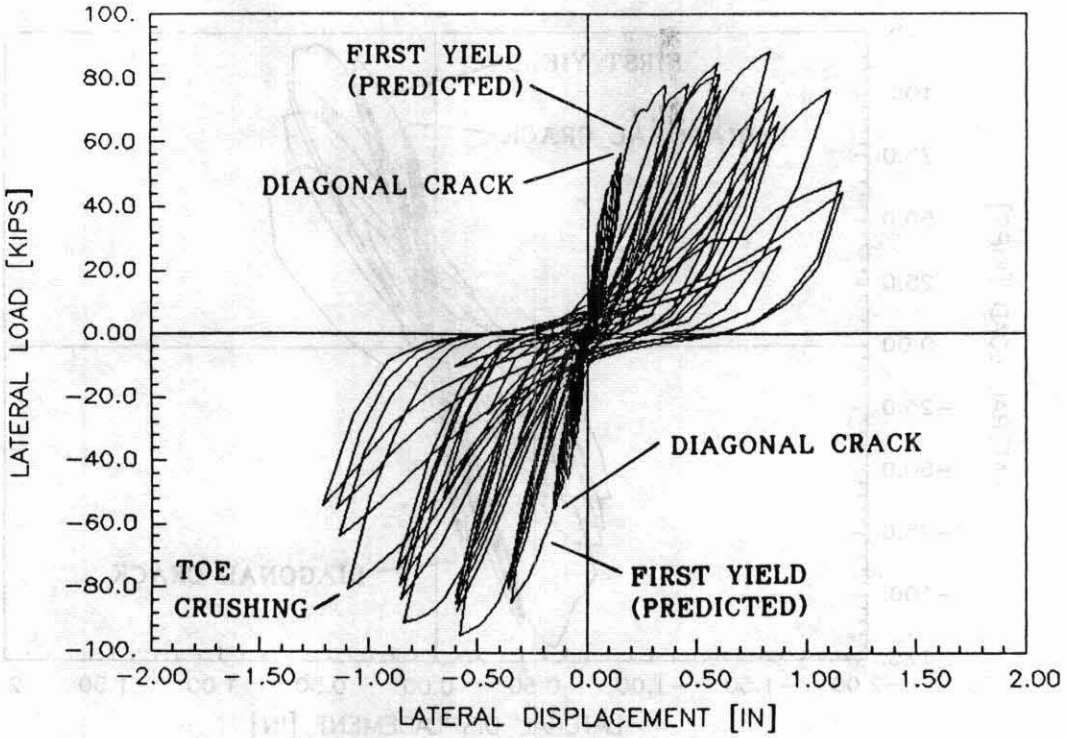

(a) Lateral Load Versus Lateral Displacement

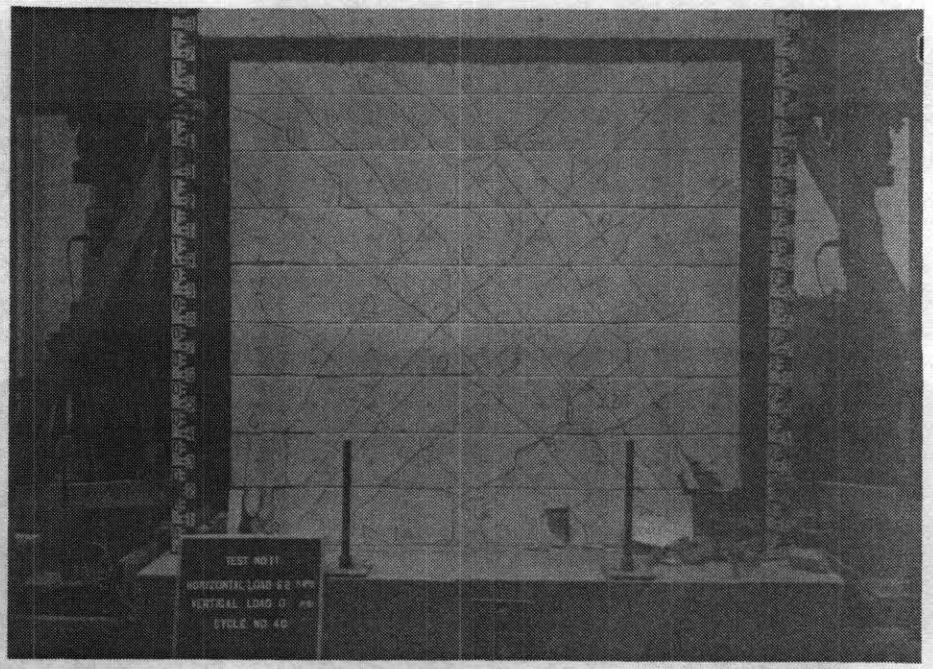

(b) Failure Mode

Figure 5.14 - Hysteresis Curves and Failure Mode of Specimen 11

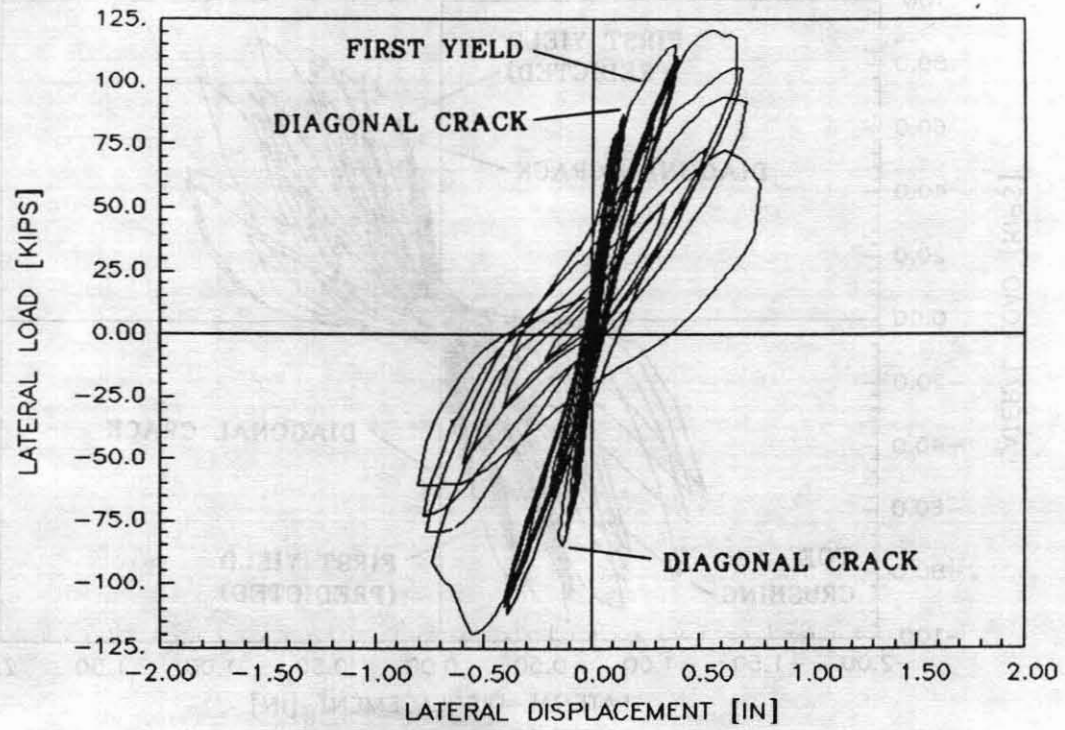

(a) Lateral Load Versus Lateral Displacement

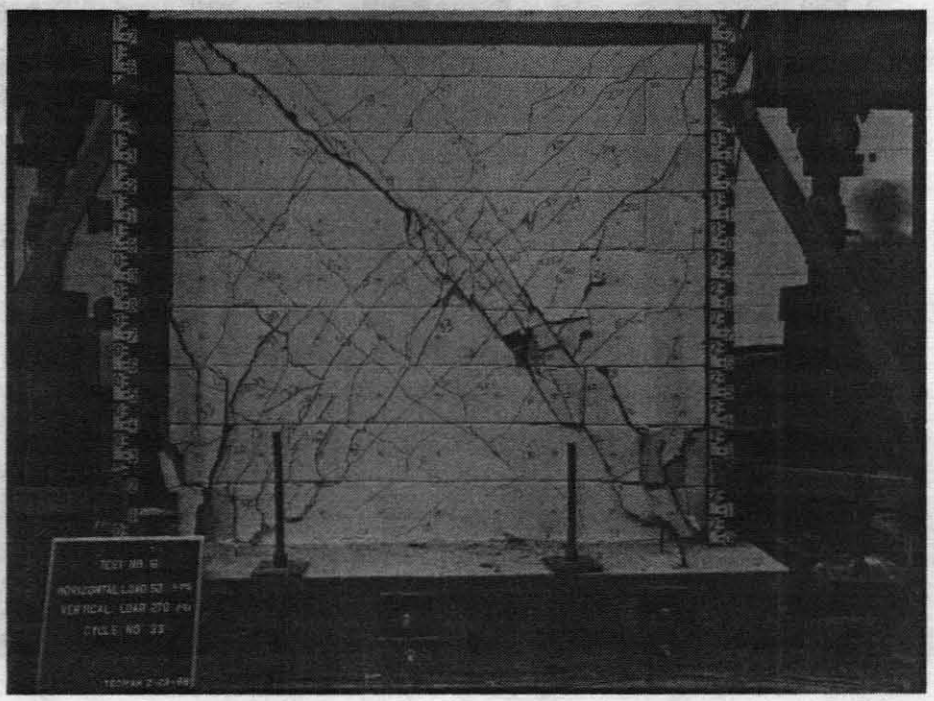

(b) Failure Mode

Figure 5.15 - Hysteresis Curves and Failure Mode of Specimen 16

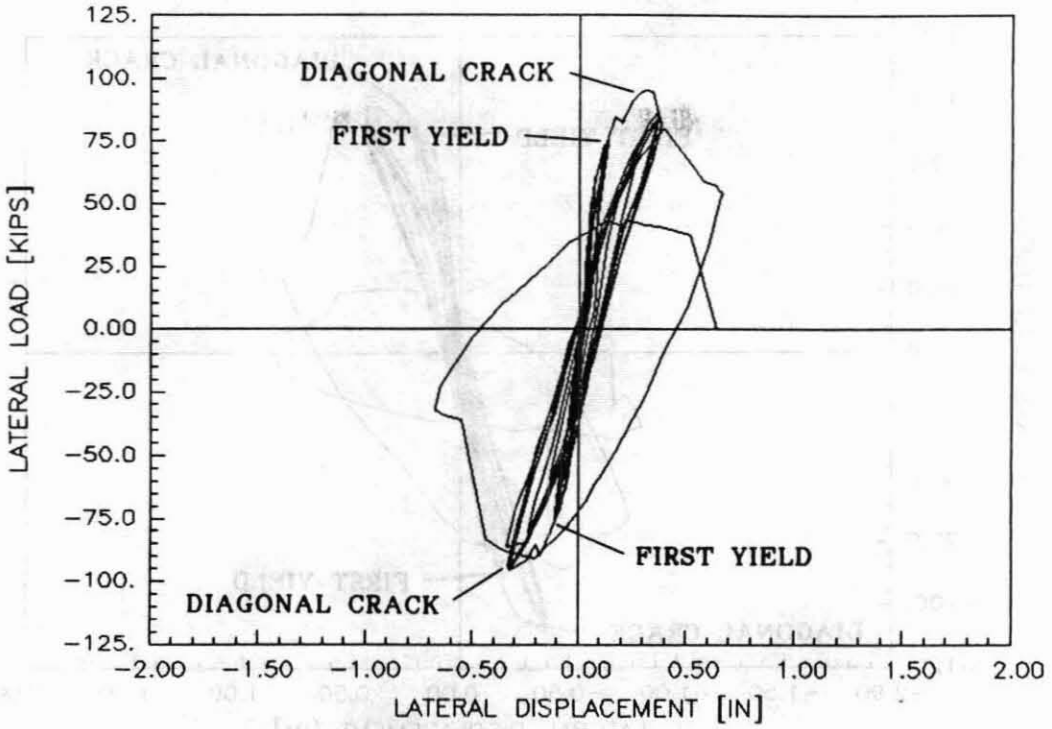

(a) Lateral Load Versus Lateral Displacement

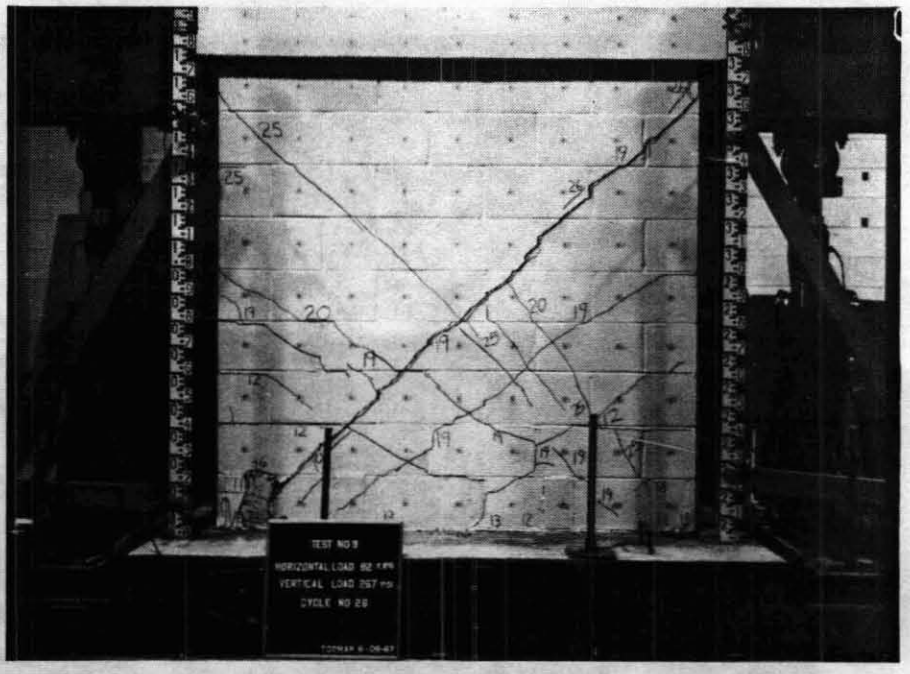

(b) Failure Mode

Figure 5.16 - Hysteresis Curves and Failure Mode of Specimen 9

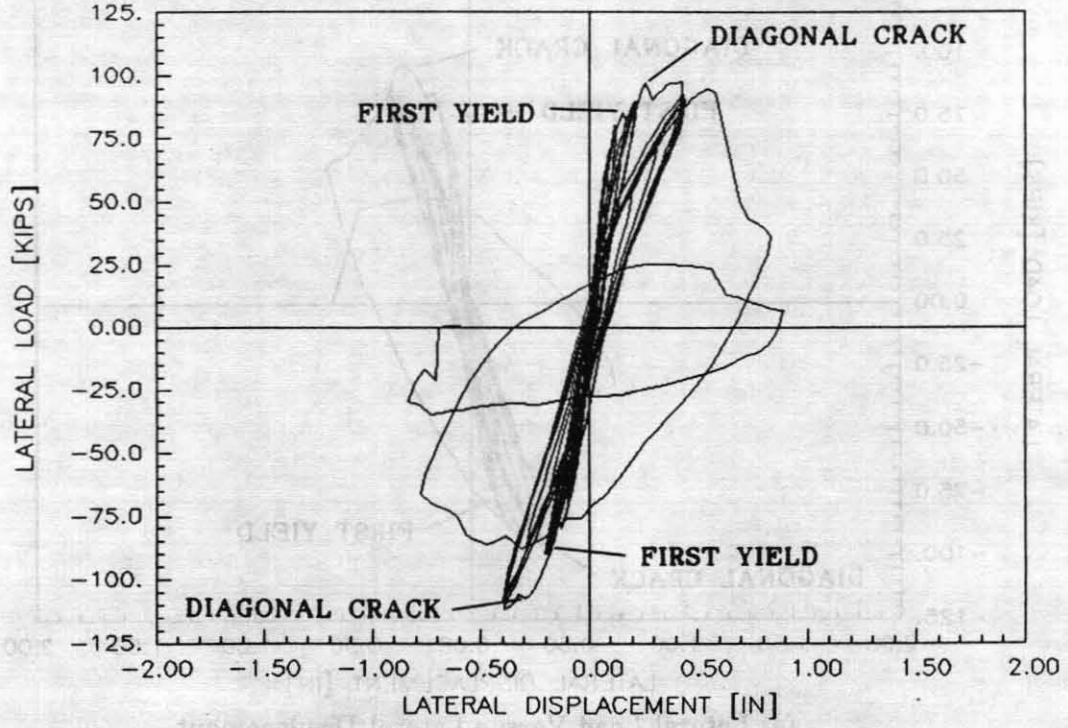

(a) Lateral Load Versus Lateral Displacement

(b) Failure Mode

Figure 5.17 - Hysteresis Curves and Failure Mode of Specimen 14

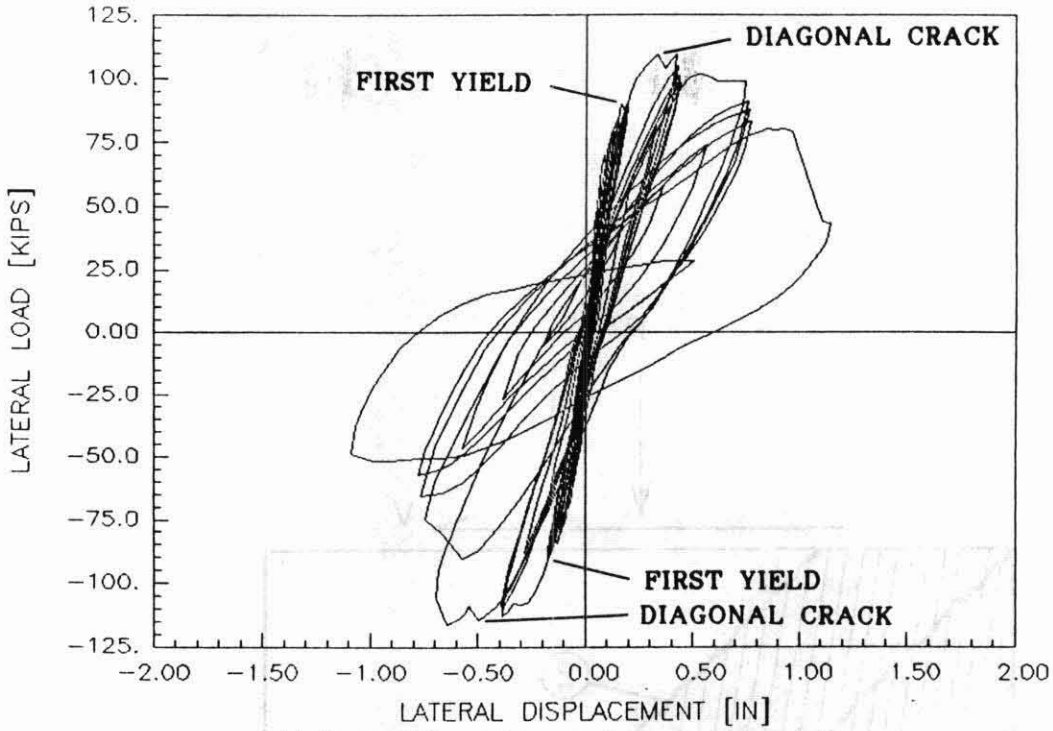

(a) Lateral Load Versus Lateral Displacement

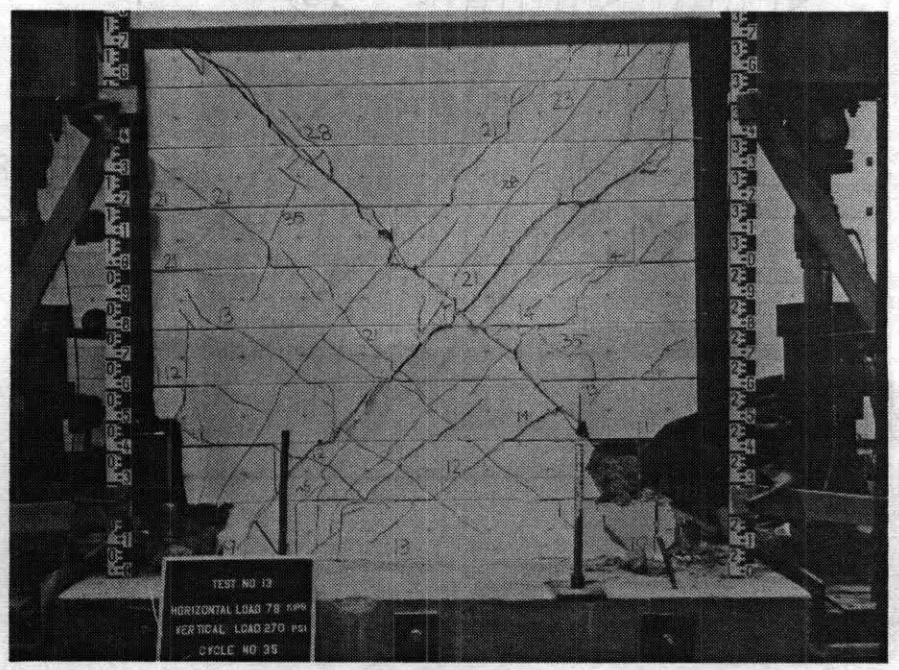

(b) Failure Mode

Figure 5.18 - Hysteresis Curves and Failure Mode of Specimen 13

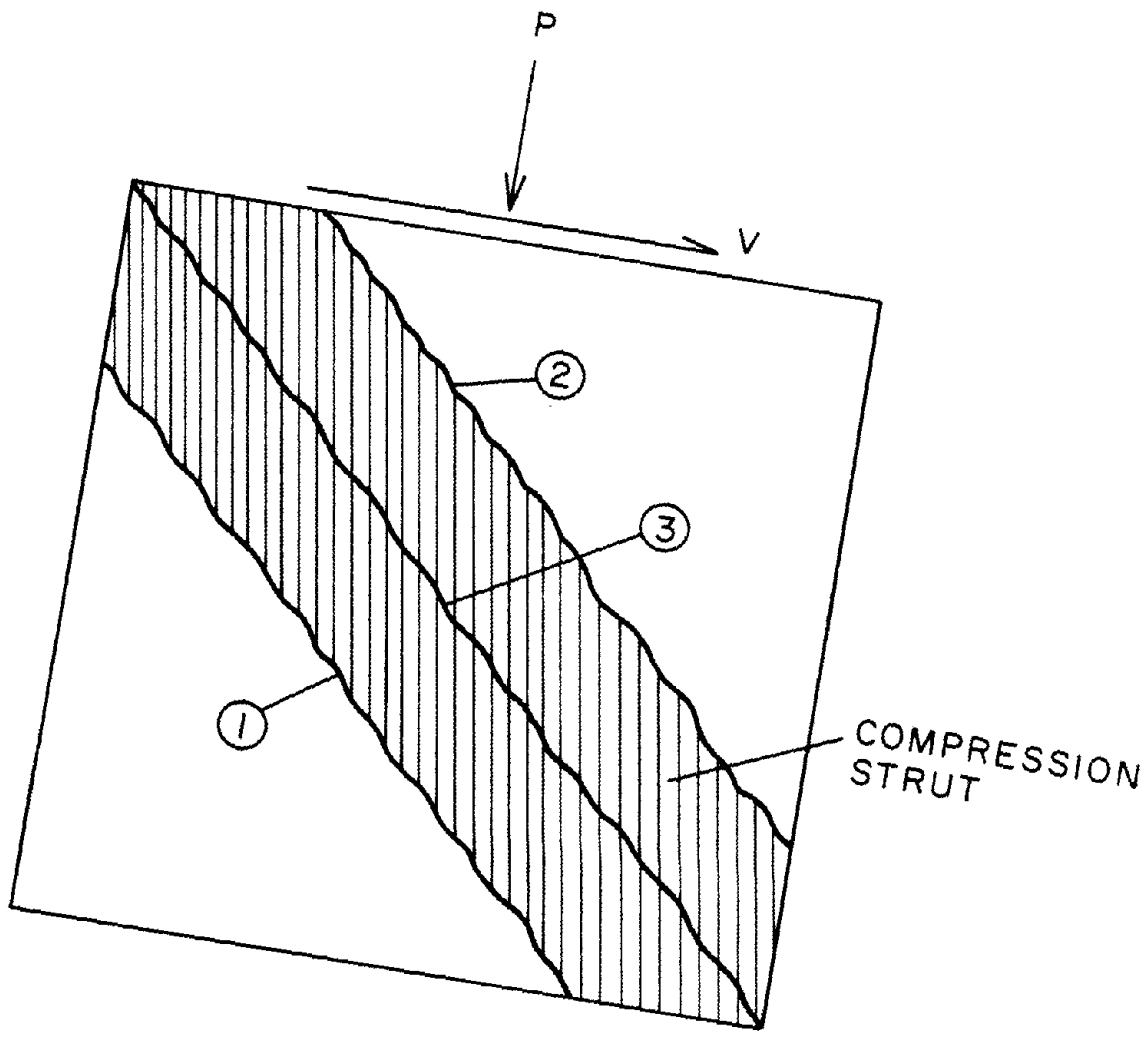

Figure 5.19 - Sequence of Diagonal Cracking

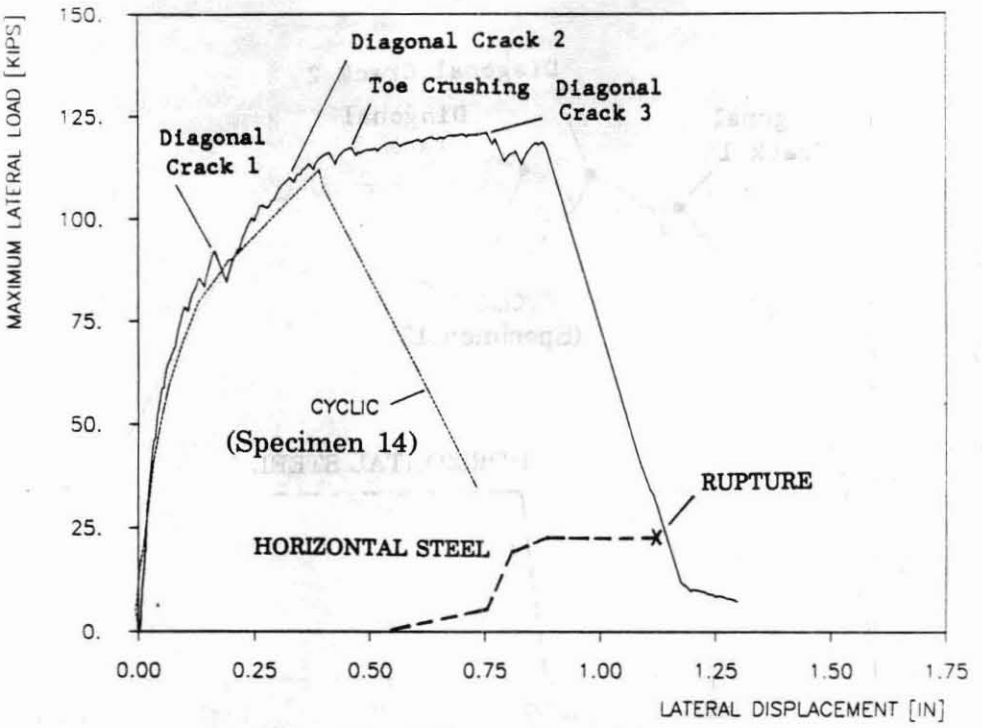

(a) Lateral Load Versus Lateral Displacement

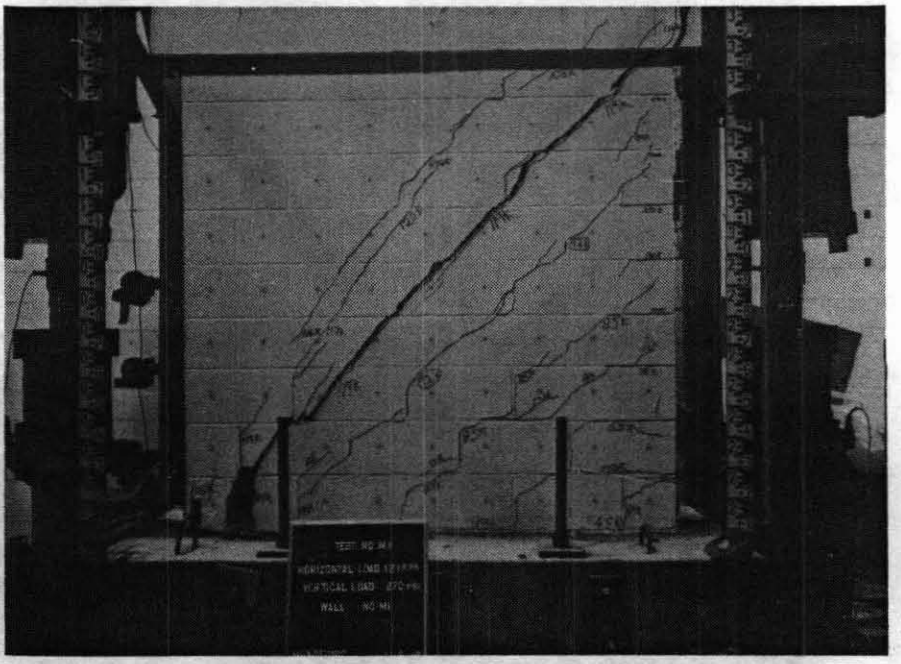

(b) Failure Mode

Figure 5.20 - Load-Displacement Curve and Failure Mode of Specimen 23

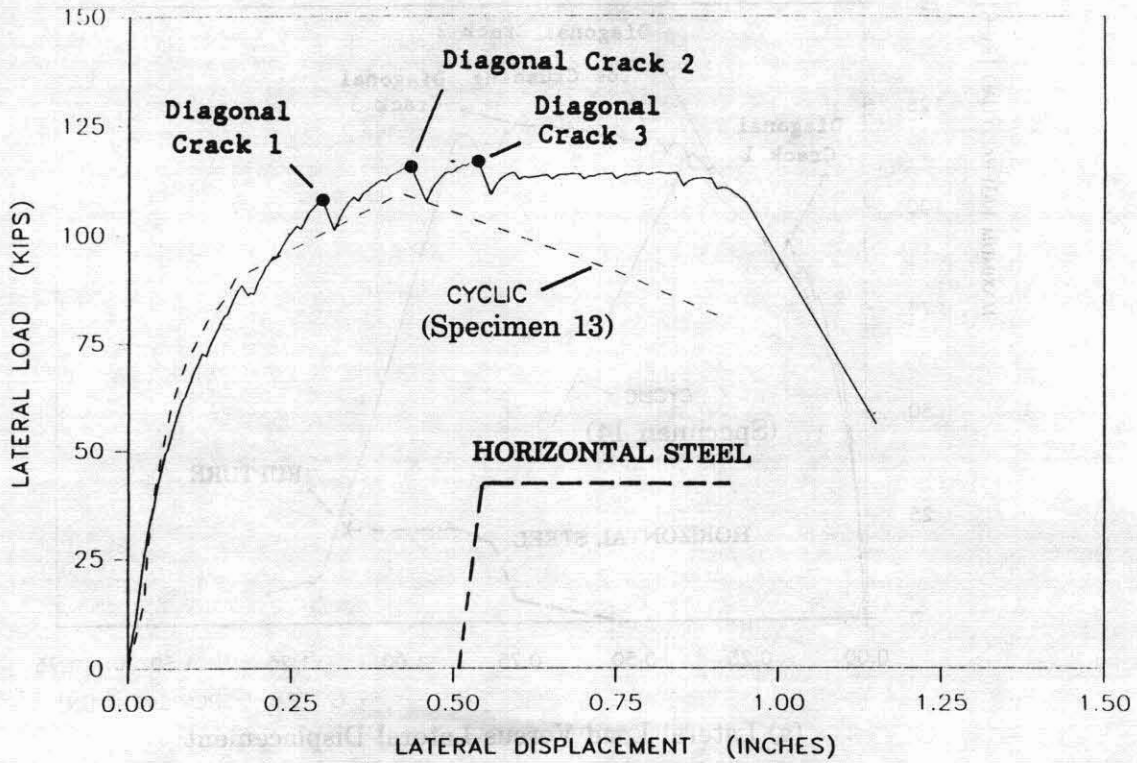

(a) Lateral Load Versus Lateral Displacement

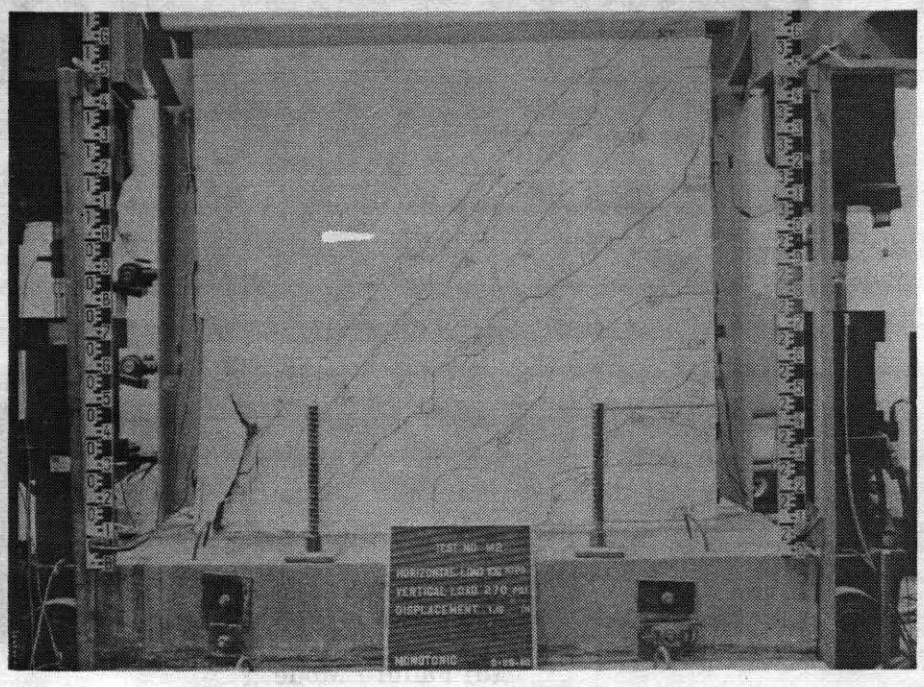

(b) Failure Mode

Figure 5.21 - Load-Displacement Curve and Failure Mode of Specimen 24

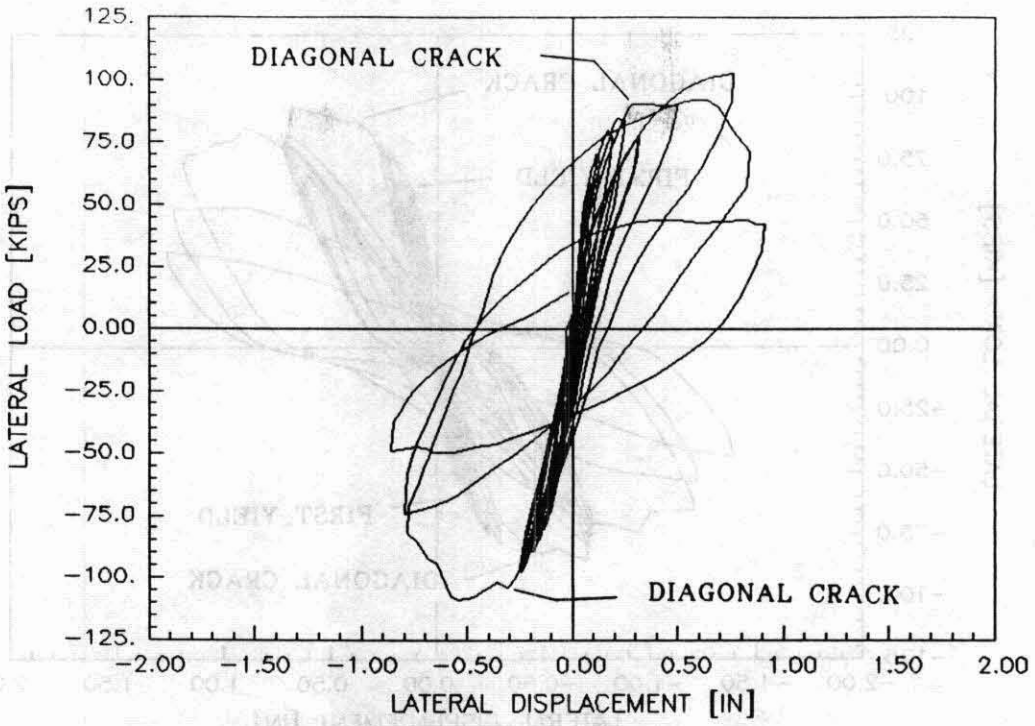

(a) Lateral Load Versus Lateral Displacement

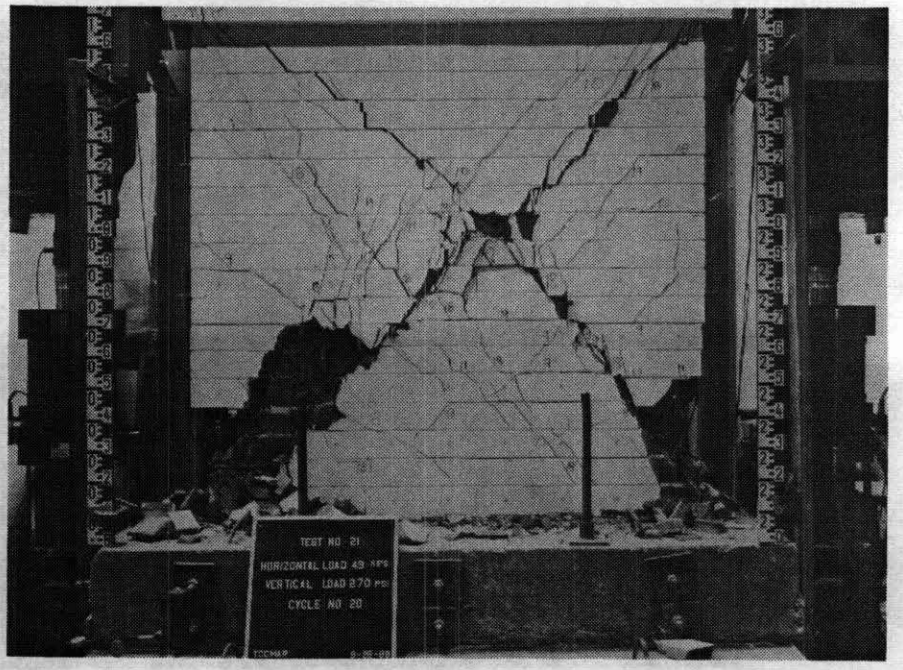

(b) Failure Mode

Figure 5.22 - Hysteresis Curves and Failure Mode of Specimen 21

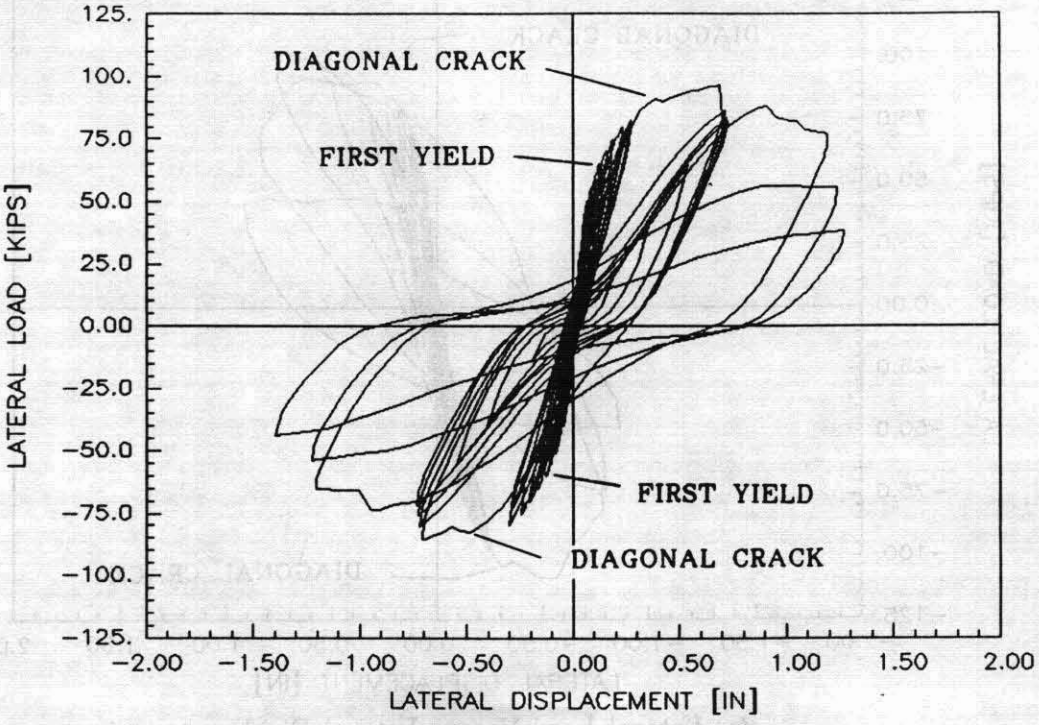

(a) Lateral Load Versus Lateral Displacement

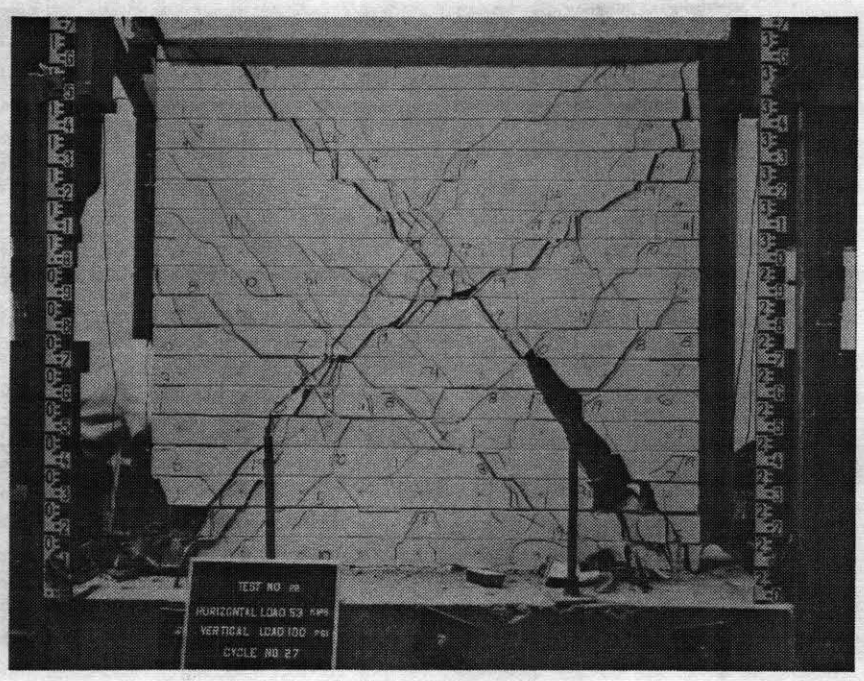

(b) Failure Mode

Figure 5.23 - Hysteresis Curves and Failure Mode of Specimen 22

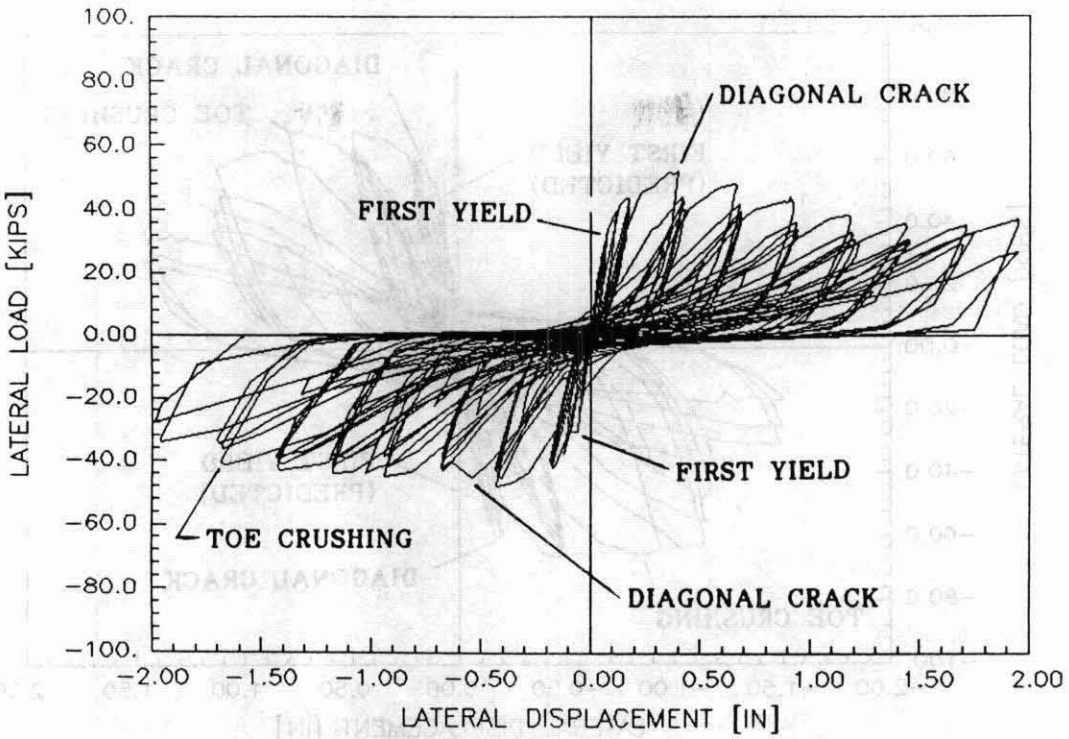

(a) Lateral Load Versus Lateral Displacement

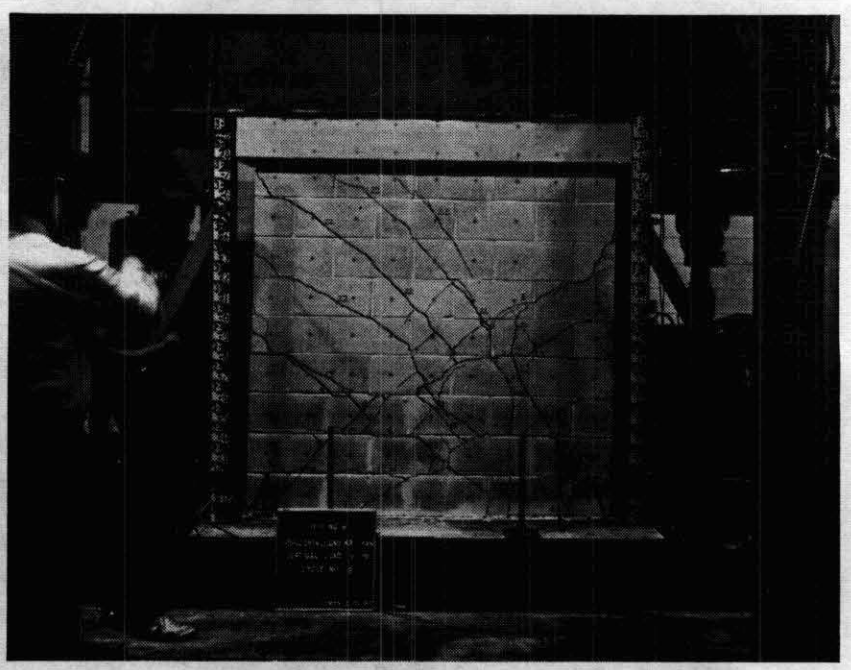

(b) Failure Mode

Figure 5.24 - Hysteresis Curves and Failure Mode of Specimen 6

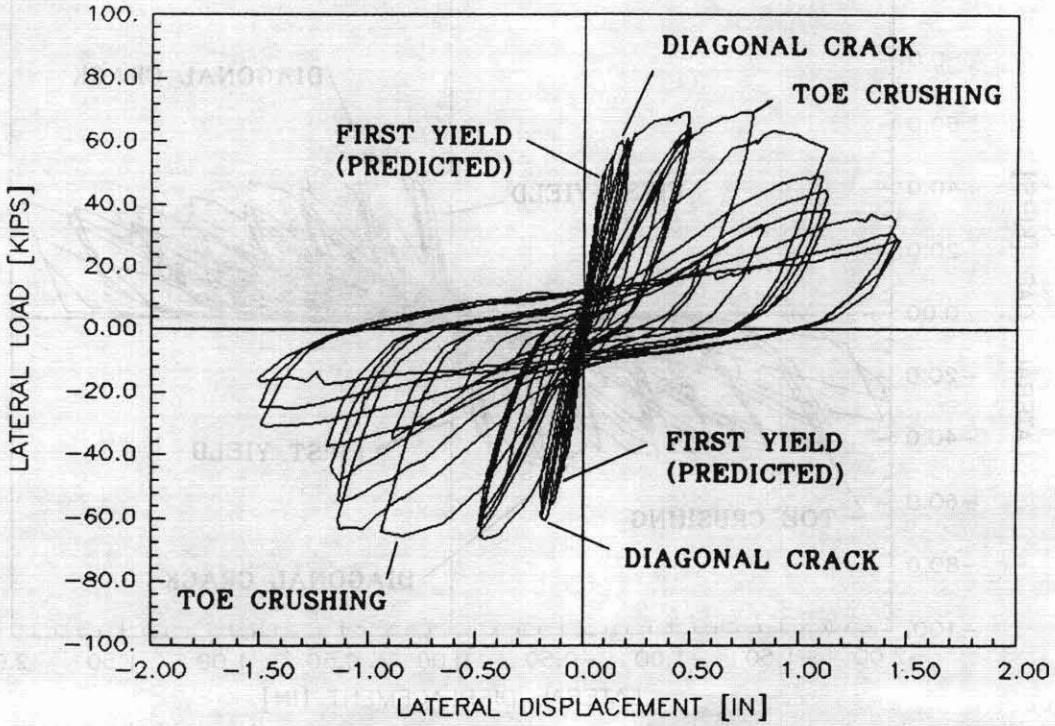

(a) Lateral Load Versus Lateral Displacement

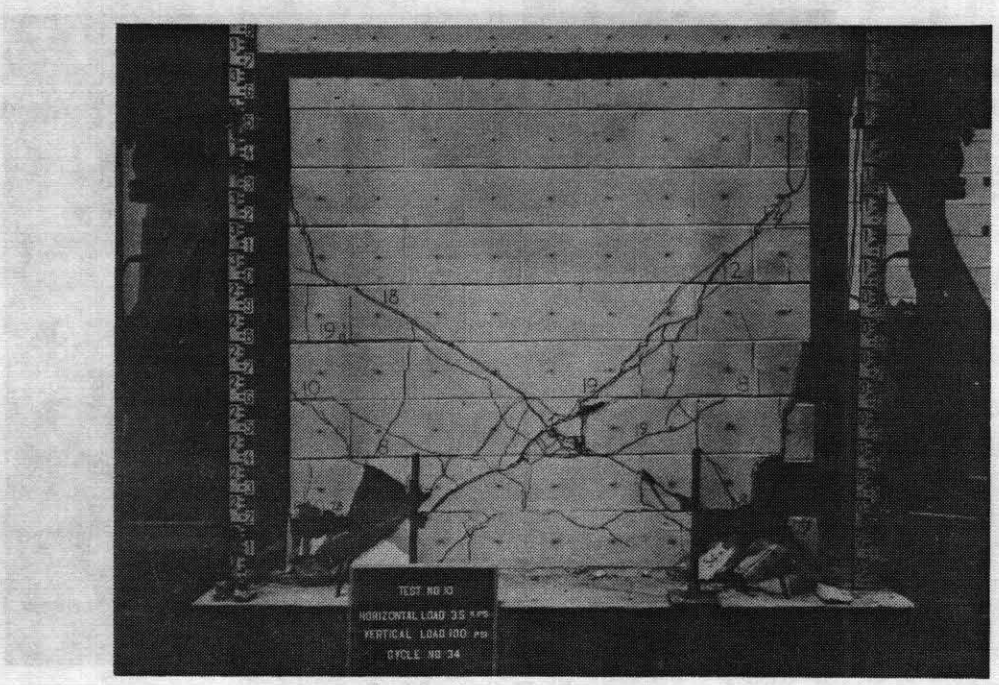

(b) Failure Mode

Figure 5.25 - Hysteresis Curves and Failure Mode of Specimen 10

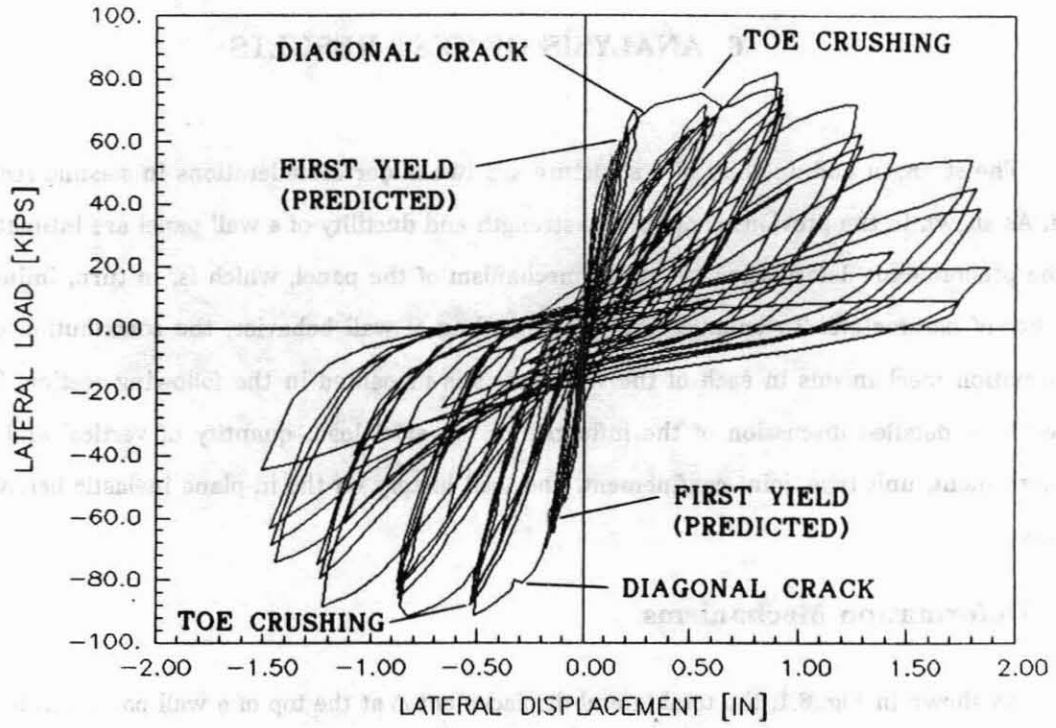

(a) Lateral Load Versus Lateral Displacement

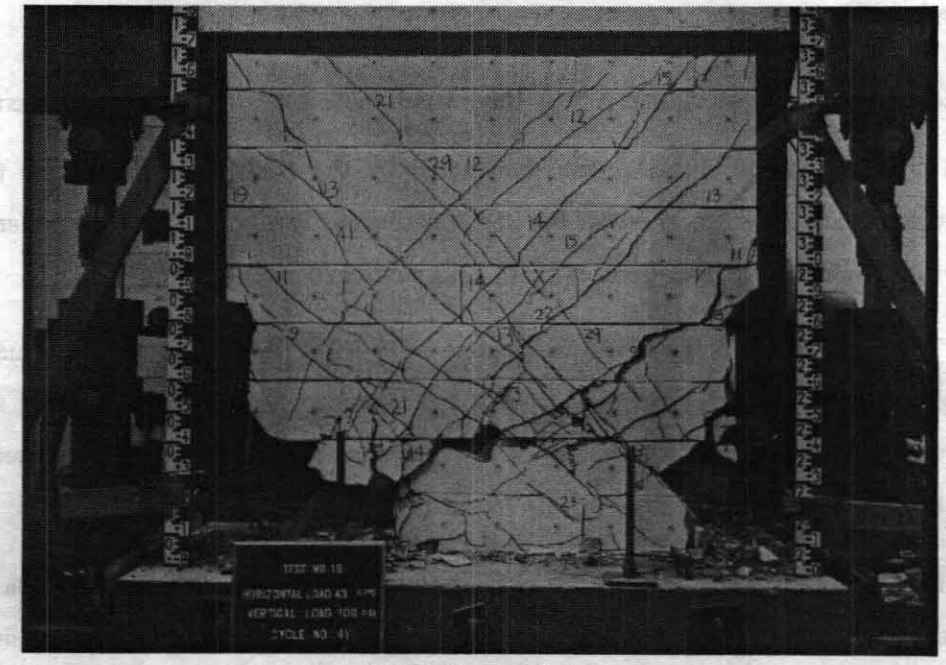

(b) Failure Mode

Figure 5.26 - Hysteresis Curves and Failure Mode of Specimen 15

6 ANALYSIS OF TEST RESULTS

The strength and ductility of a structure are two major considerations in seismic resistance design. As shown in the previous chapter, the strength and ductility of a wall panel are intimately related to the predominant deformation or failure mechanism of the panel, which is, in turn, influenced by a number of parameters. To enhance the understanding of wall behavior, the contribution of different deformation mechanisms in each of the wall panels is presented in the following section. This is followed by a detailed discussion of the influence of the axial load, quantity of vertical and horizontal reinforcement, unit type, joint confinement, and load history on the in-plane inelastic behavior of wall panels.

6.1 Deformation Mechanisms

As shown in Fig. 6.1, the total lateral displacement Δ at the top of a wall panel can be attributed to four distinct mechanisms:

$$\Delta = \Delta^{SL} + \Delta^{SH} + \Delta^{FL} + \Delta^{UP} \tag{6.1}$$

in which Δ^{SL} is the base sliding, Δ^{SH} is the overall shear distortion, Δ^{FL} is the flexural deformation, and Δ^{UP} is the lateral displacement contributed by the base uplift caused by the slippage and elongation of the vertical steel embedded in the base slab. The instrumentation scheme shown in Fig. 3.3a was intended to measure each of these deformation components.

There are several approaches to calculate each of the aforementioned deformation components from experimental data. A great deal of effort has been devoted here to identifying a reliable method of calculating the deformation components. Part of these considerations are discussed in Appendix A, and a brief summary is presented in this section.

Base sliding was measured with transducers L17 and L18 shown in Fig. 3.3a. It was observed that base sliding was only significant in specimens that did not have axial compressive load.

The flexural deformation of a wall can be calculated either directly or indirectly. To facilitate our following discussions, the notation $\overline{\Delta}^{FL}$ is used to represent the sum of Δ^{FL} and Δ^{UP} . The most direct approach is to calculate $\overline{\Delta}^{FL}$ from wall curvatures measured with displacement transducers L1 through L12 by means of the following kinematic relation:

$$\overline{\Delta}^{FL} = \Delta^{FL} + \Delta^{UP} = \int_0^h (h - x)\phi dx \tag{6.2}$$

in which h is the height of the wall, ϕ is the wall curvature, and x is the vertical distance from the base. Ideally, the deflection due to base uplift, Δ^{UP}, can be isolated from the above measurement by using the base rotation θ_b obtained with transducers L19 through L22 shown in Fig. 3.3a as follows.

$$\Delta^{UP} = \theta_b h \tag{6.3}$$

However, because of toe crushing, base rotation could not be measured reliably. As a result, one cannot easily distinguish base uplift from flexural deformation, and, therefore, the flexural deformation discussed herein refers to the combined deformations $\overline{\Delta}^{FL}$. Furthermore, the evaluation of $\overline{\Delta}^{FL}$ via Eq. (6.2) is not very reliable because the flexural curvature at the upper portion of a cantilever wall is generally too small to measure accurately and the curvature near the base is not measurable once toe crushing occurred. Hence, it is better to calculate $\overline{\Delta}^{FL}$ indirectly by subtracting other deformation components from the total measured lateral displacement.

The overall shear distortion can be measured with the diagonal transducers, L23 and L24, shown in Fig. 3.3a by using the following geometric relation [Hidalgo et Al. 1979; Bertero et al. 1974]:

$$\Delta^{SH} = \frac{\Delta_1 - \Delta_2}{2} \frac{\sqrt{h^2 + l^2}}{l} \tag{6.4}$$

in which Δ_1 and Δ_2 are the diagonal deformations monitored by L23 and L24, respectively, with extension being defined as positive, and l is the length of a wall specimen. However, the effect of flexural deformation on diagonal elongation is neglected in the above formula. In addition, the above formula is intended for an uncracked panel and does not accurately account for the additional

deformation caused by diagonal cracks. The assessment of errors introduced by flexural deformation is presented in Appendix A. It has been found that the influence of flexural deformation on diagonal elongation depends very much on the curvature variation along the height of a wall. Based on the results in Appendix A, the actual shear deformation Δ_a^{SH} could be obtained with the following correction:

$$\Delta_a^{SH} = \Delta^{SH} - \alpha \overline{\Delta}^{FL} \tag{6.5}$$

in which α is a parameter that depends on the curvature variation. It is shown in Appendix A that $\alpha = 0$ for a uniform curvature, $\alpha = 0.25$ for a triangular curvature variation, and $\alpha = 0.5$ for the extreme case that the entire flexural rotation is concentrated at the base. The second case represents the condition of an elastic cantilever wall subjected to a point load at the top, whereas the third case represents the limiting condition that a severe plastic zone occurs at the wall base. Hence, for a typical wall specimen, it is expected that α varies between 0.25 and 0.5.

Based on the above considerations, $\overline{\Delta}^{FL}$ could be alternatively calculated with the following equation:

$$\overline{\Delta}^{FL} = \frac{1}{1-\alpha}(\Delta - \Delta^{SL} - \Delta^{SH} - ER) \tag{6.6}$$

in which ER represents additional errors that might be introduced by the deformation of the base slab as discussed in Appendix A. Since base deformation contributes to the overall flexural deflection measured but not to the diagonal elongation, ER is expected to offset part of the errors caused by flexural deformation. Hence, based on the experimental data obtained, it is shown in Appendix A that unless the value of ER is known, a partial correction could be worse than no correction. Unfortunately, the value of ER is generally not known. Therefore, it is recommended that $\overline{\Delta}^{FL}$ be simply calculated as follows.

$$\overline{\Delta}^{FL} = \Delta - \Delta^{SH} - \Delta^{SL} \tag{6.7}$$

which is a direct application of Eq. (6.1). Hence, the overall flexural deformation $\overline{\Delta}^{FL}$ and shear deformation Δ^{SH} presented in the following are calculated with Eqs. (6.7) and (6.4), respectively. To examine the effect of steel reinforcement and of the applied axial stress on the deformation mechanism, the percentage of each deformation component is plotted against the axial compressive stress for each type of reinforcement content at a stage where the total lateral deflection reached one inch. As shown in Figs. 6.2 through 6.6, base sliding is significant only when the axial compressive stress is small and the behavior is dominated by flexure. Furthermore, for specimens with 0.24% horizontal steel (Figs. 6.2, 6.5, and 6.6), the flexural and shear deformations are almost equal. On the other hand, for specimens with 0.14% horizontal steel (Figs. 6.3 and 6.4), which were dominated by either the shear or flexural/shear mode, shear deformation is a lot larger than flexural deformation.

6.2 Shear Stiffness

For the design and analysis of masonry structures, it is important to estimate the overall shear stiffness of a wall panel under service load conditions. Because of the possible occurrence of flexural and shear cracks at moderate load levels, a simple theoretical solution is not possible. However, before any cracking has occurred, a wall panel can be considered linearly elastic and homogeneous. In this respect, the shear stiffness of an elastic cantilever wall with a rectangular section can be expressed as

$$K_s = \frac{A E_m}{2.4h(1+\nu)} \tag{6.8}$$

in which A is the horizontal cross-sectional area of the wall and h is the height of the wall, E_m is the elastic modulus of masonry, and ν is the Poisson's ratio. At an uncracked state, the influence of steel reinforcement on the shear stiffness is negligible. However, once flexural cracks have occurred, the distribution of the shear stress along a cracked section changes significantly, and the determination of the shear stiffness becomes difficult. When inclined shear cracks occur, the overall shear stiffness is substantially reduced and the influence of the steel reinforcement and axial compressive stress

becomes important. In general, it can be expected that increasing the quantity of vertical and horizontal steel and/or the magnitude of the axial compressive stress reduces crack opening and, thereby, increases the shear stiffness.

As shown by Specimens 23 and 24, once a major crack away from the main diagonal has occurred, the load resistance is taken over by a diagonal strut mechanism and the shear stiffness can be estimated with an appropriate strut model. However, in the case of the square wall panels, the monotonic load-displacement curves shown in Figs. 5.20a and 5.21a indicate that after the development of the strut mechanism, the stiffness can be assumed zero for most practical purposes. After the crack along the main diagonal has occurred, the resistance could drop rapidly and softening might occur, depending on the amount of horizontal steel present.

In reality, the elastic shear stiffness represented by Eq. (6.8) will only occur within a very small lateral load. To illustrate this, the shear stiffnesses K of the wall specimens measured at various lateral loads are normalized by the elastic stiffness K_s and plotted against the applied axial compressive stress in Fig. 6.7. The measured stiffnesses are the secant stiffnesses obtained at 10% and 50% of the maximum shear strength, as well as those measured at the first major diagonal cracking (which occurred at loads higher than 50% of the maximum shear strength). The elastic stiffness K_s is assumed to be 3,900 kips/in. for all specimens, which is obtained by letting E_m = 2,000 ksi, based on the data of Atkinson and Kingsley (1985), where E_m is the secant modulus of masonry prisms measured at 50% of the maximum compressive strength f_{mt}, and ν = 0.2, which is assumed to be similar to that of concrete materials. As shown in Fig. 6.7, the normalized secant stiffness, K/K_s, of the wall panels tends to decrease as the lateral load increases because of the more severe flexural and shear cracks. There is also a distinct trend that the shear stiffnesses measured at lateral loads greater than or equal to 50% of the maximum load increase as the axial compressive stress increases. Nevertheless, the experimental data do not show any consistent influence of the quantity of the vertical and horizontal steel on the postcracked shear stiffness.

Based on the data in Fig. 6.7, the following empirical formula for the overall shear stiffness of a wall panel under service load conditions is suggested.

$$\overline{K}_s = (0.2 + 0.00074\sigma_c)K_s \leq K_s \tag{6.9}$$

in which K_s is given by Eq. (6.8), with E_m approximated by the secant modulus of masonry prisms measured at 50% of the maximum compressive strength, and σ_c is the axial compressive stress, in psi, on a wall. As shown in Fig. 6.7, the above formula is obtained by approximate curve fitting of the secant stiffnesses measured at the first major diagonal cracking, and is, thus, considered to be conservative for the estimation of wall deflection up to this load level. However, the validity of the formula for slender walls remains to be verified.

6.3 Flexural Strain Profile and Wall Curvature

The actual flexural strain profiles and wall curvature are needed to obtain a reliable assessment of flexural strength and ductility. It was found that even though the wall panels had a relatively low aspect ratio, the flexural strains measured along the base of the panels essentially have a linear variation. The strain profiles along the base of Specimen 1, measured by the strain gages attached to the vertical reinforcing bars and by the displacement transducers attached to the surface of the wall, under a pure axial compressive load (200 psi) as well as at the first tensile yielding of the extreme vertical steel are shown in Fig. 6.8. It is shown in Fig. 6.8b that the strains at the first yield measured by the displacement transducers are a lot larger than those by the strain gages. The discrepancy is small when the lateral load is small (see Fig. 6.8a) and gradually increases as the lateral load increases. It is mainly due to the slippage and elongation of the reinforcing steel embedded in the concrete base slab. Based on the strain measured by the transducers from wall panels under a pure axial compression, the average elastic modulus of masonry is between 4,500 and 5,000 psi. However, this is obtained with a maximum compression of 270 psi, which is less than 10% of the compressive strength of masonry.

Because of the large number of cyclic displacement reversals, the integrity of the strain gages and of the supports of the displacement transducers was jeopardized and their readings became unreliable even before the maximum load was reached. In general, the maximum compressive strain measured by a displacement transducer at the maximum load of a typical flexure-dominated specimen appeared to be more than ten times the recommended maximum allowable value of 0.003 (1988 UBC).

The curvature variation along the height of Specimen 1 is shown in Fig. 6.9. The curvatures were measured by the displacement transducers along the two edges of the wall specimen. It is evident that crushing and inelastic deformation were concentrated at the bottom 11 in. of the specimen, which can be taken to be the length of the plastic hinge. Similar observations were obtained from other flexure-dominated specimens.

6.4 Influence of Axial Load and Steel Reinforcement

The effects of the applied axial compressive load and the quantity of vertical and horizontal reinforcement on the flexural and shear strengths, ductilities, and energy-dissipation capabilities are observed from the first sixteen concrete masonry wall specimens listed in Table 2.1. These are summarized in this section.

6.4.1 Flexural Strength

It is apparent from the experimental results that the flexural strength of a reinforced masonry wall panel increases with the magnitude of the applied axial load and the quantity of vertical reinforcement present. To assist the evaluation of test results, the flexural strengths of the sixteen concrete masonry wall specimens were calculated with the computer program UNCOLA (Kaba and Mahin 1983), which has been developed for evaluating the inelastic moment-curvature relations of reinforced concrete sections. The calculations were based upon the plane-section assumption, and the uniaxial stress-strain relation of concrete proposed by Shiekh and Uzumeri (1982). In the analyses, the model was calibrated with the uniaxial material constants obtained from prior masonry prism tests (Atkinson and Kingsley 1985). The compressive strengths of masonry and the tensile strengths of steel used in the analyses were obtained from the average values listed in Tables 4.4 and 4.5, respectively. The analytical results are compared with the experimental data in Figs. 6.10, 6.11, and 6.12. To minimize the influence of grout flaws, only the maximum strength measured in the stronger direction is used for comparison.

As shown in Fig. 6.10, for the wall panels with 0.38% vertical steel, the analytically obtained yield and maximum loads show a good correlation with the experimental data. In fact, the measured

strain profile at the first yield of the extreme vertical steel is close to the plane-section assumption used in the analyses (see previous section). The maximum strengths of Specimens 6 and 8, which had zero axial compressive tress and significant base sliding, are slightly lower than the calculated strength. The maximum strengths of Specimens 1, 2, and 12, which were dominated by the flexural mode, are 10 to 15% higher than the analytical results. The maximum strengths of Specimens 9 and 10 were governed by diagonal cracking. However, their actual strengths appear to be slightly higher than the calculated flexural strengths.

The results for the wall panels with 0.54% vertical steel are shown in Fig. 6.11. Similar to Specimens 9 and 10, the maximum strengths of Specimens 13, 14, and 15 are slightly higher than the calculated flexural strengths, even though their failure mechanisms were dominated by the shear mode.

Finally, based on the results shown in Fig. 6.12, it is evident that the failure mechanisms of Specimens 3, 4, 5, 7, 11, and 16, which had 0.74% vertical steel, were dominated by the shear mode. The flexural strengths calculated for these specimens are substantially higher than the actual strengths.

6.4.2 Shear Strength

The shear cracking mechanism of a reinforced masonry wall panel is very complex. Before diagonal cracking occurs, the horizontal reinforcement carries almost no force, and, thus, has little influence on the stress field of a wall panel. Therefore, the first occurrence of a diagonal crack is influenced to a large extent by the tensile strength of masonry as well as the applied axial load. However, once diagonal cracks have occurred, the shear resistance is redistributed among the horizontal steel, the aggregate-interlock mechanism, the uncracked zone at the compression toe, and the dowel action of the vertical steel. The resistance provided by the aggregate interlock depends in turn on the applied axial stress, and the truss action of the vertical and horizontal steel. Because of the complexity of these mechanisms, a reliable assessment of the shear strength of a wall panel is difficult.

In most design codes, the nominal shear strength of a reinforced masonry shear wall is specified as the sum of V_s and V_m, where V_s is the strength provided by the horizontal steel and V_m is the residual strength of masonry due to the various contributions, including the effects of the dowel action of the vertical steel. Evidently, it is assumed in the building codes that the shear strength is governed by the cracked state. Otherwise, V_s and V_m will not be additive. In general, the formulas for V_m have to be derived empirically based on available experimental data. Physical models based on the analogy of combined truss and arch mechanisms have also been proposed (Wakabayashi and Nakamura 1984). However, the validity of these models for walls with effective aspect ratios larger than or equal to one remains to be studied.

To provide further insight, the influence of the various design factors on the shear resistance is discussed here. As can be seen from Fig. 6.13, the load at first major diagonal crack increases with the applied axial compressive load; however, there is no direct correlation between the cracking strength and the amount of vertical and horizontal reinforcement present. The scatter of the data points can be partly attributed to the variation of the material properties of masonry. In particular, it can be observed from Fig. 6.13 that the upper and lower bounds of the data points correspond to the specimens having measured masonry compressive strengths, f_{mt}, of 3300 and 2600 psi, respectively.

The ratio of τ_{cr} to $\sqrt{f_{mt}}$, where τ_{cr} is the shear stress at the first diagonal crack and f_{mt} is the compressive strength of masonry (both expressed in psi), is plotted in Fig. 6.14. As can be seen from the figure, the scatter is slightly reduced, and the normalized values vary from 2.2 for zero axial compressive stress to 4.7 for 270-psi axial compressive stress.

Elastic finite-element analyses, using four-node quadrilateral elements, were conducted to examine the maximum diagonal tensile stress that could have been developed in Specimens 3, 4, 5, and 7 at the observed diagonal cracking loads. From the analysis results, it has been speculated that the tensile strength f_t of the specimens should be about 200 psi, which results in a $f_t/\sqrt{f_{mt}}$ ratio of 4 (for stresses expressed in psi). Using the 200-psi tensile strength, the cracking strengths of all wall specimens are calculated with the finite-element model and plotted as solid line in Fig. 6.13. Consistent

with the experimental observations, the analytical results show little variation with respect to the amount of reinforcement present. Furthermore, the results almost coincide with the lower bound of the experimental data.

The normalized shear strength, $\tau_u/\sqrt{f_{mt}}$, is plotted in Fig. 6.15, where τ_u is the maximum shear stress (in psi) in the stronger direction of a specimen. As shown in the figure, the shear strength increases with the magnitude of the applied axial compressive load.

Moreover, by comparing the behavior of Specimens 9 with that of Specimen 10, and Specimens 13 with 15, it can be observed that the axial load can change the wall response from a relatively ductile flexural/shear mode to a brittle shear mode. This indicates that the higher the axial load is, the larger is the tendency to fail in shear. Hence, the axial load must have a more significant influence on the flexural strength than on the shear strength of a specimen.

The ratio of τ_u to $\sqrt{f_{mt}}$ is 4.2 for zero axial compressive stress, and varies from 3.0 to 4.4 for 100-psi axial compressive stress and from 4.3 to 6.0 for 270-psi axial compressive stress. The range of these values is mainly due to the different amounts of reinforcement present. The shear strength tends to increase with the amount of vertical steel, as demonstrated by Specimens 3 and 9, and Specimens 13 and 16. This is partly attributed to the dowel action, and partly to the truss action of the vertical steel which can reduce crack opening and can, consequently, enhance the aggregate-interlock forces. However, this trend does not appear to be consistent, as the maximum strength of Specimen 3 is slightly lower than that of Specimen 14. This is probably due to the high cracking strength of Specimen 14, as shown in Fig 6.13. Furthermore, it can be observed from Table 5.1 that specimens with 0.74% vertical steel (Specimens 3, 4, 5, 7, and 16) sustained a fair amount of additional load after the occurrence of the first major diagonal crack, while specimens with 0.38% and 0.54% vertical steel and high axial stress (Specimens 9, 13, 14) reached their maximum strengths almost instantaneously right after the first crack, even though the amounts of horizontal steel in both cases were identical. Moreover, the comparison of Specimens 3 and 9 (Figs. 5.13a and 5.16a) indicates that the influence of the vertical steel on the postcracked hysteretic behavior can be significant.

The influence of the amount of horizontal steel on the shear strength appears to be inconsistent. Specimens 13 and 14 indicate that increasing the horizontal steel ratio from 0.14% to 0.24% leads to a small increase of the shear strength. On the other hand, the strength of Specimen 16 is 20% higher than that of Specimen 3, even though the difference in the amount of horizontal reinforcement is the same as in the previous case. This is mainly because the maximum shear strength of Specimen 16 is governed by the diagonal cracking strength, which was most likely greater than the total resistance provided by the horizontal steel and the postcracked residual strength of masonry. However, it is interesting to note from Specimens 13 and 14 that increasing the amount of horizontal steel can significantly improve the postcracked hysteretic behavior of a wall panel, while this phenomenon could not be observed from Specimens 3 and 16 due to the fact that Specimen 3 had a larger compression toe than Specimen 16 as pointed out in Section 5.3.1. Furthermore, it has been observed from Specimens 2 and 9 that increasing the amount of horizontal steel from 0.14% to 0.24% changed the behavior from a brittle shear mode to a flexural mode.

As mentioned in Section 5.3.1, in Specimens 23 and 24, the strain in the horizontal steel measured by the strain gages along a wall diagonal (shown in Fig. 3.3b) indicates compression before diagonal cracking and tension after diagonal cracking. This is illustrated in Fig. 6.16 by gages H3, H4, and H5 of Specimen 23. The compressive strain indicates the development of a diagonal strut mechanism. The resistance provided by the horizontal steel, assessed from the strain measurement, in Specimens 23 and 24 is shown in Figs. 5.20a and 5.21a. Hence, the importance of horizontal steel in improving the postcracked behavior of a wall panel is evident.

6.4.3 Ductility and Energy Dissipation

Ductility and energy-dissipation capability are important considerations in seismic resistance design. According to current building code provisions, the design strength of a structure can be substantially reduced if the structure is able to provide a good deformation capability beyond the elastic limit. Furthermore, energy dissipation through hysteretic damping can reduce the amplitude of seismic response, and, thereby, reduce the ductility demand on a structure. These quantities are now defined and used as performance indices for the wall specimens.

For elastic-perfectly-plastic systems, ductility is often defined as the ratio of the maximum allowable displacement to the displacement at which the first yield occurs. However, for masonry wall panels, the yield limit is not well defined. Walls with different design details and load conditions exhibit different yield mechanisms. For example, a flexural specimen may have its first yield governed by the tensile stress in the extreme vertical steel, whereas a shear specimen may have its major inelastic deformation initiated by diagonal cracking. To make an objective evaluation of the inelastic performance of different wall specimens, the definition of ductility has to be consistent and independent of the failure mechanism. For this reason, an equivalent elastic-perfectly-plastic system is defined for each specimen, as shown in Fig. 6.17. Based on that, ductility is defined in this study as

$$\mu = \frac{\Delta_{50}}{\Delta_y^{ep}} \tag{6.10}$$

in which Δ_{50} is the displacement at which the peak lateral resistance is reduced to 50% of the maximum resistance and is intended to represent a specific damage state of a specimen, and Δ_y^{ep} is the yield displacement of the equivalent elastic-perfectly-plastic system. The yield resistance of the equivalent system is selected to be the maximum resistance V_u in the stronger direction of the specimen, and the elastic stiffness, k , is based on the average initial stiffness measured at a small-amplitude displacement cycle in which the peak load is about 50% of the maximum resistance of the specimen. These parameters are defined in Fig. 6.17.

As indicated by limited test results, the inelastic performance of a structure appears to be highly sensitive to the load or displacement history imposed. Therefore, the ductility index may be different if the structure is subjected to a different displacement history. In view of that, a more objective measure of the inelastic performance of a wall specimen is desirable. For this purpose, a normalized cumulative energy dissipation is defined as

$$\hat{U} = \frac{1}{U^e} \sum_{i=1}^{n} U_i \tag{6.11}$$

in which U^e is equal to $\frac{1}{2}k(\Delta_y^{ep})^2$, which is the total elastic energy absorption of the equivalent elastic-perfectly-plastic model, U_i is the energy dissipated in cycle i of a test, as shown in Fig. 6.17, and n is the cycle number after which the peak lateral resistance is reduced to 50% of the maximum resistance. Hence, $\hat{U}$ represents the cumulative energy dissipated at a certain damage state. Since it is normalized by the elastic energy absorption, it is more of a measure of the hysteretic behavior than the absolute strength of a specimen.

The values of Δ_y^{ep}, μ, and $\hat{U}$ of the sixteen cyclically loaded concrete masonry specimens are listed in Table 6.1, together with the drift factors, which are defined as the ratios of Δ_{50} to the height of a wall specimen. As shown in the table, Specimen 6 had the highest ductility and energy-dissipation capability. However, large portions of the lateral displacement and energy dissipation of this specimen were due to base sliding. With the exception of the slide dominated specimens, the ductilities of all specimens are plotted against the axial load in Fig. 6.18. It is evident that the flexural specimens had larger ductilities than the shear specimens, while the ductilities of the flexural/shear specimens lie between the two. As shown by Specimens 12 and 2, the increase of axial compressive load tends to reduce the ductility of a flexural specimen. Moreover, the increase of axial load can change the behavior from a relatively ductile flexural/shear mode (Specimens 10 and 15) to a more brittle shear mode (Specimens 9 and 13). On the other hand, ductility tends to increase with the axial compressive load for the shear dominated specimens (Specimens 4, 5, 7, and 3). This is probably due to the fact that the increase of the axial load enhances the aggregate-interlock forces, and, thereby, increases the postcracked shear resistance.

Similar tendency can be observed from the normalized cumulative energy dissipation plot in Fig. 6.19. Comparing Specimens 9, 14, and 3, and Specimens 13 and 14, it is apparent that the larger the amount of vertical and horizontal reinforcement is, the greater the energy-dissipation capability will be. However, as shown by Specimens 3 and 16, the energy-dissipation capability also depends on the orientation and location of the diagonal crack. Specimen 3, which had a larger compression zone at the wall toe (resulting from the orientation of the diagonal crack), had a much better energy-dissipation capability than Specimen 16.

The ductility of a specimen can also be approximately indicated by the load-deformation envelope of its hysteresis curves. The load-deformation envelopes of the twenty-two cyclically load specimens can be found in Appendix B.

6.5 Influence of Unit Types

Even though the compressive strength of hollow clay unit masonry is a lot higher than that of hollow concrete unit masonry, the performance of the concrete unit masonry specimens is very similar to that of clay unit specimens. The comparison of Specimens 14 and 21, which had the same axial load and reinforcement content, shows that the shear strengths, ductilities, and energy-dissipation capabilities of the two specimens are almost the same in spite of the different masonry materials. By taking into account that the clay unit masonry specimen had a smaller cross-sectional area and a larger compressive strength, the normalized shear strength, $\tau_u/\sqrt{f_{mt}}$, of Specimen 21 turns out to be about 4.3, which is very close to that of the concrete unit masonry specimen (Fig. 6.15). The flexural strength of Specimen 20 is slightly higher than that of Specimen 2, but their ductilities and energy-dissipation capabilities are almost the same. However, the compressive failure mode of clay unit masonry is different from that of concrete unit masonry. In Specimen 20, the compression failure of clay unit masonry was initiated by the spalling of the face shell from the grout core due to the different compressive strengths and stiffnesses of the hollow clay units and grout. On the other hand, the compression failure of concrete unit masonry in Specimen 2 involved more or less simultaneous crushing of the face shell and grout.

6.6 Influence of Joint Confinement

Comparison of Specimens 19 and 20 indicates that joint confinement improved flexural ductility, but it had no influence on the flexural strength. Specimen 19, which had wire-mesh confinement, had a ductility about 70% higher than that of Specimen 20, while its energy-dissipation capability is 150% higher.

6.7 Influence of Load History

Test results with respect to the influence of load history are only available for shear-dominated specimens. Comparison of Specimens 5 and 7, 14 and 23, and 13 and 24 indicates that load history has some influence on the strength and ductility of shear-dominated wall specimens. As shown in Figs. 5.20a and 5.21a, cyclic loads resulted in a lower shear strength and ductility than monotonic loads probably due to the more severe reduction of aggregate-interlock forces under cyclic loads.

Table 6.1 - Ductility and Energy-Dissipation Capability of Concrete Masonry Walls

Wall Specimens	Maximum Strength (kips)	Initial Stiffness (kips/in.)	Critical Displ. $\Delta_y^{@P}$ (in.)	Drift*	Ductility*	Norm. Energy Dissipat.*
1	87	500	0.17	0.022	9	16
2	98	820	0.12	0.018	11	17
3	105	1000	0.11	0.017	11	17
4	87	500	0.17	0.013	5	9
5	89	470	0.19	0.011	4	8
6	52	470	0.11	0.028	18	65
7	97	770	0.13	0.011	6	10
8	50	410	0.12	0.020	11	40
9	96	1040	0.09	0.009	7	7
10	69	540	0.13	0.020	11	26
11	95	420	0.23	0.016	5	10
12	71	760	0.09	0.020	16	55
13	116	1180	0.10	0.015	11	14
14	112	910	0.12	0.010	6	9
15	94	720	0.13	0.025	14	39
16	121	900	0.13	0.011	6	12

* Measured at 50% Load Degradation

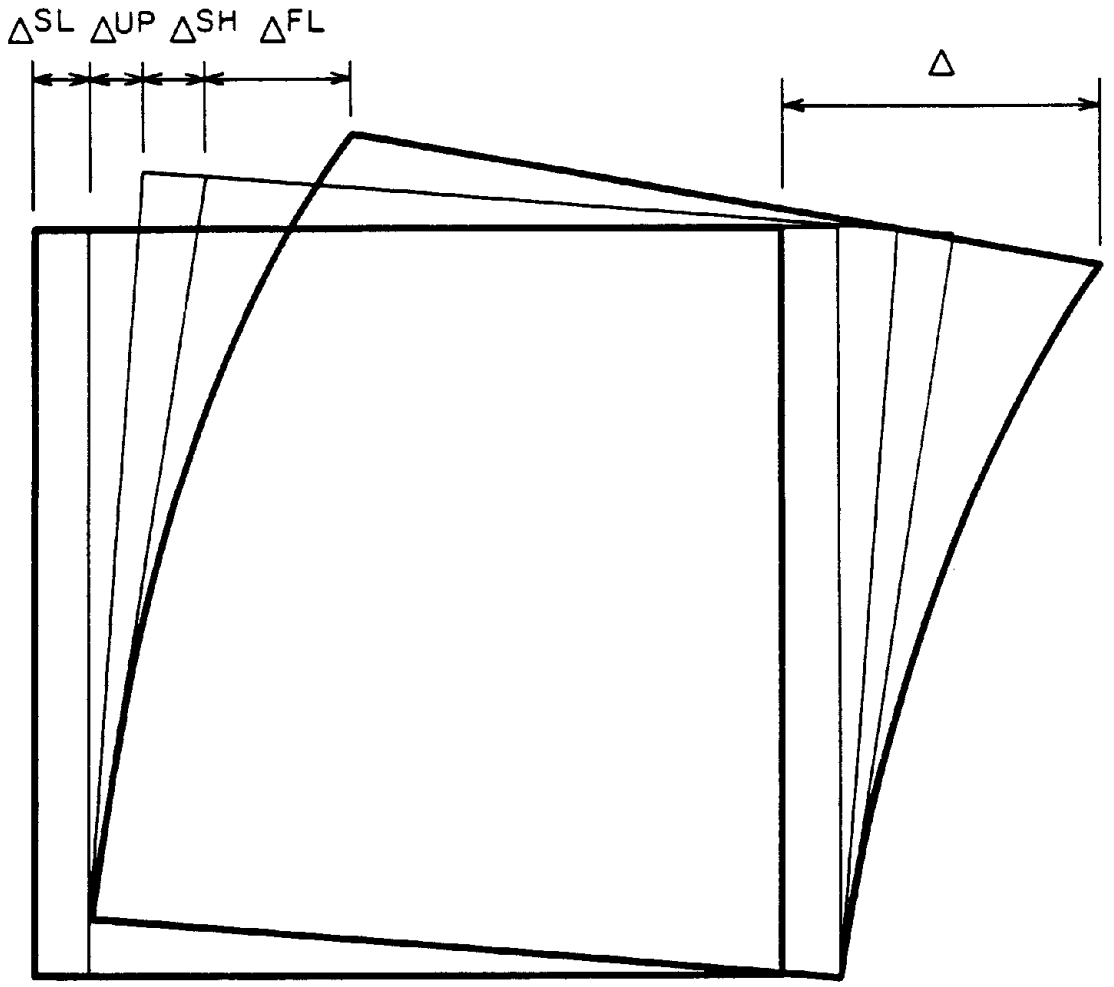

Figure 6.1 - Deformation Mechanisms of Wall Panels

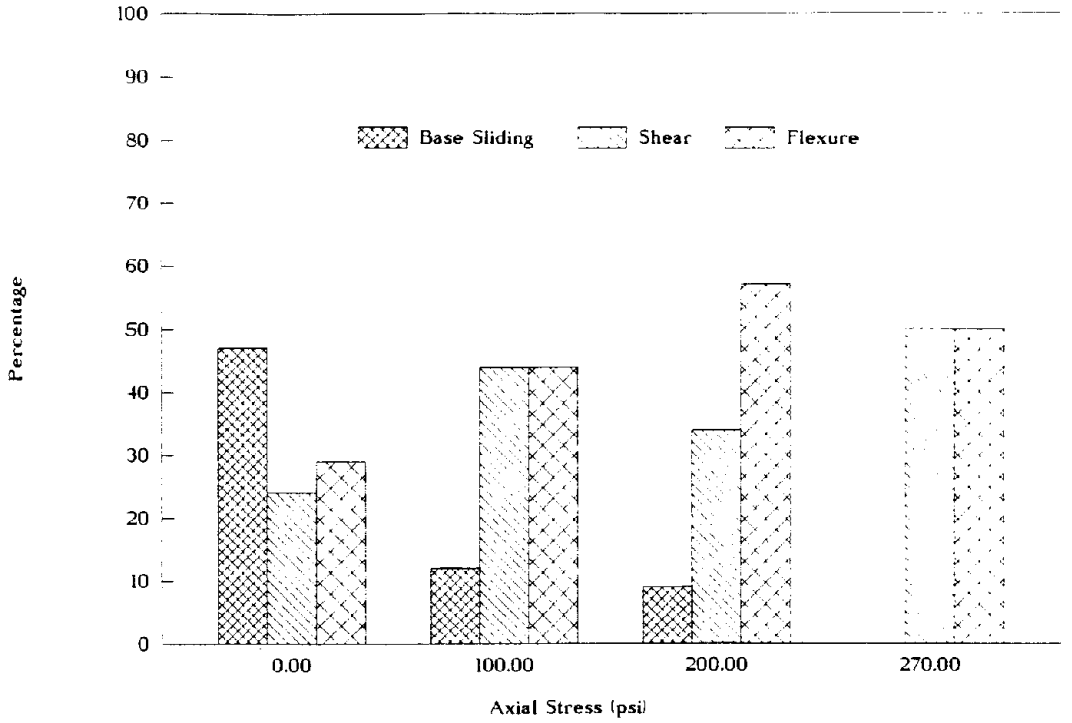

Figure 6.2 - Contribution of Different Deformation Mechanisms at about One-Inch Total Displacement (No. 5 Vertical and No. 4 Horizontal Bars)

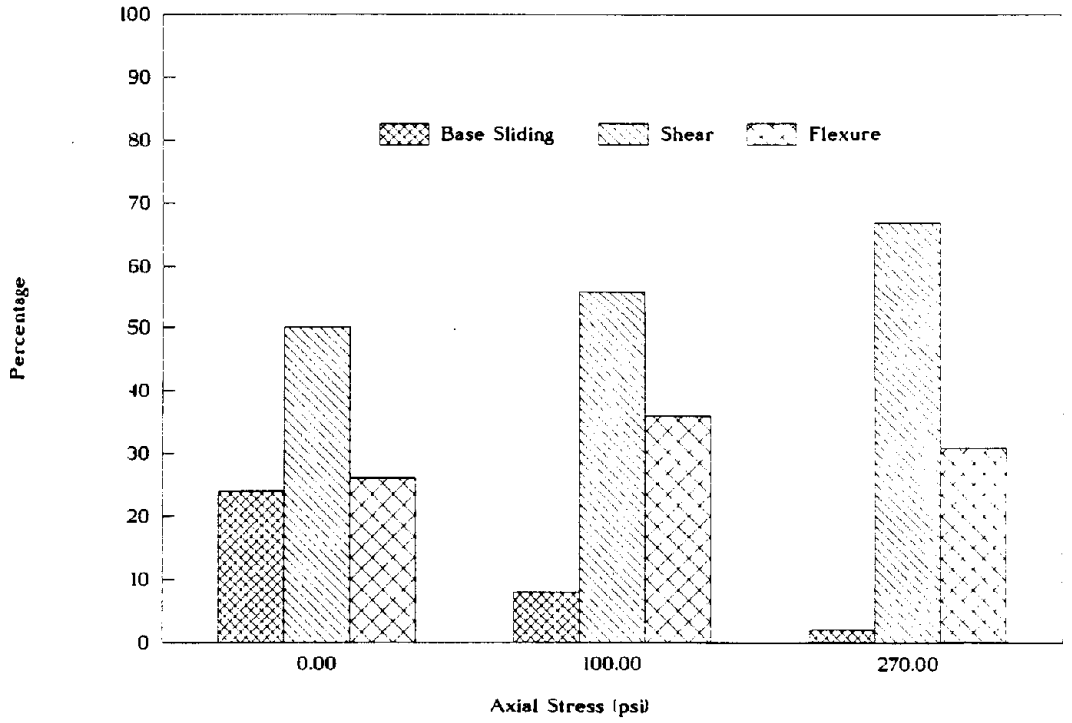

Figure 6.3 - Contribution of Different Deformation Mechanisms at about One-Inch Total Displacement (No. 5 Vertical and No. 3 Horizontal Bars)

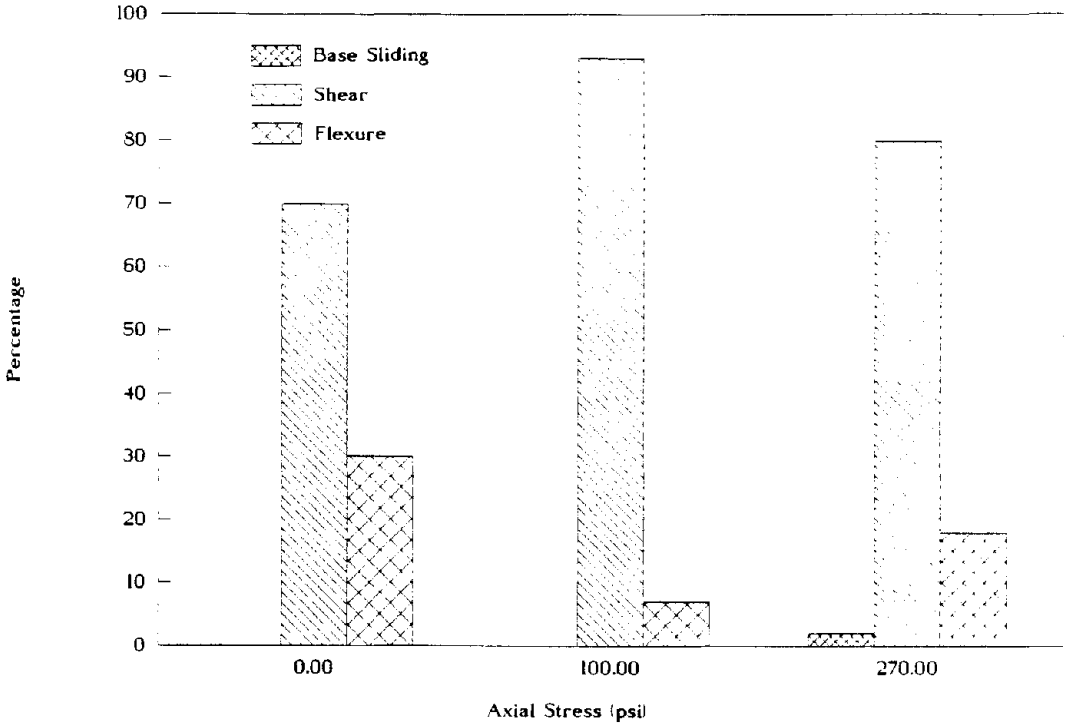

Figure 6.4 - Contribution of Different Deformation Mechanisms at about One-Inch Total Displacement (No. 7 Vertical and No. 3 Horizontal Bars)

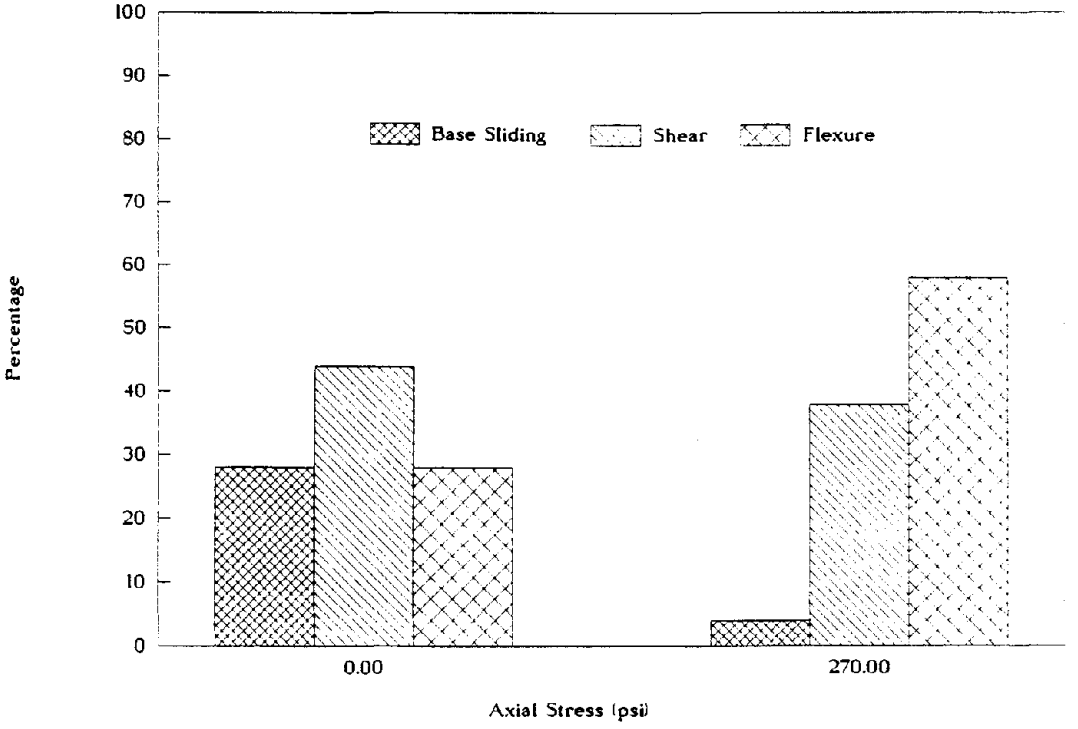

Figure 6.5 - Contribution of Different Deformation Mechanisms at about One-Inch Total Displacement (No. 7 Vertical and No. 4 Horizontal Bars)

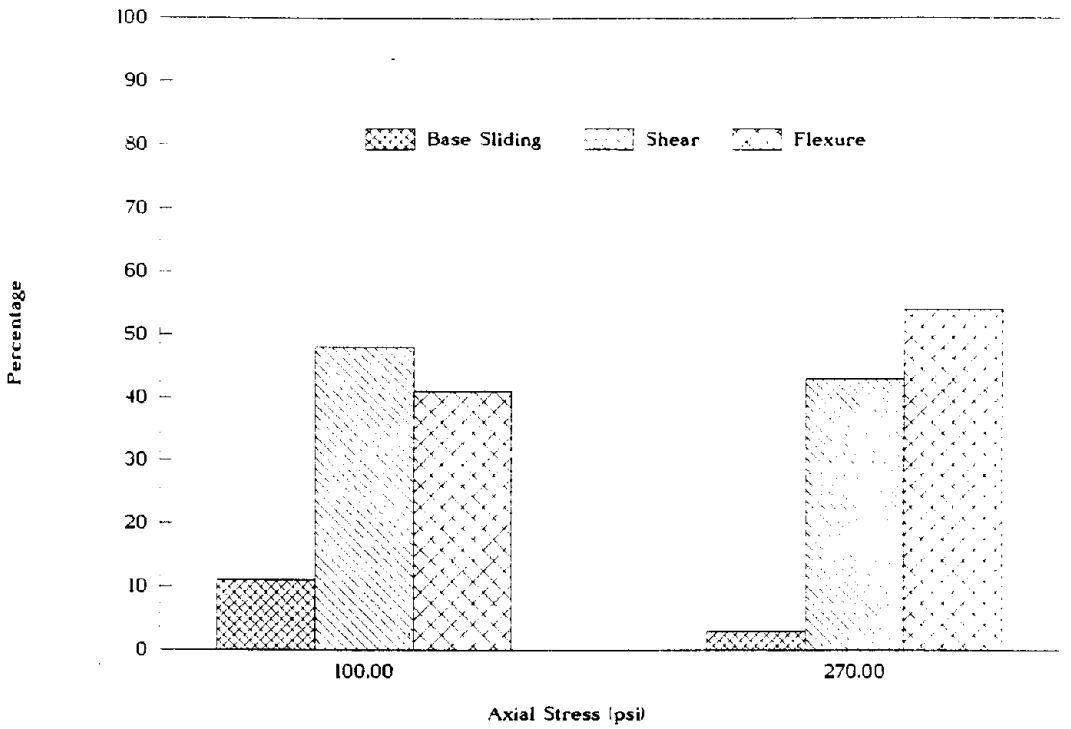

Figure 6.6 - Contribution of Different Deformation Mechanisms at about One-Inch Total Displacement (No. 6 Vertical and No. 4 Horizontal Bars)

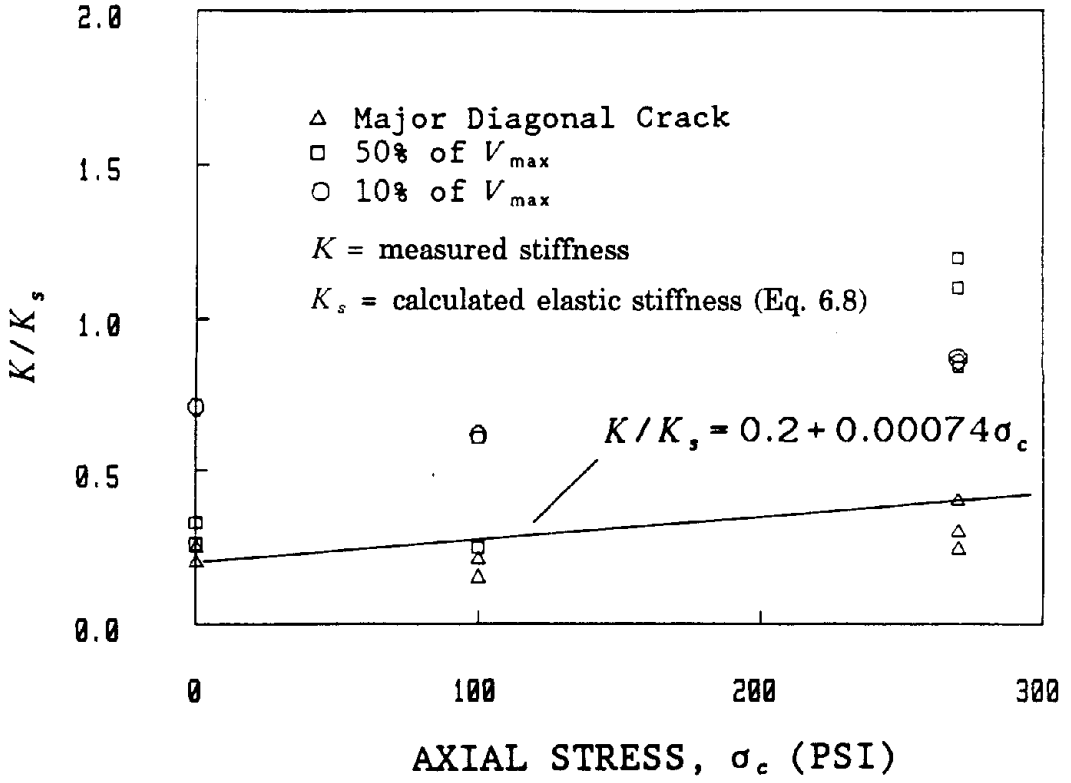

Figure 6.7 - Shear Stiffness

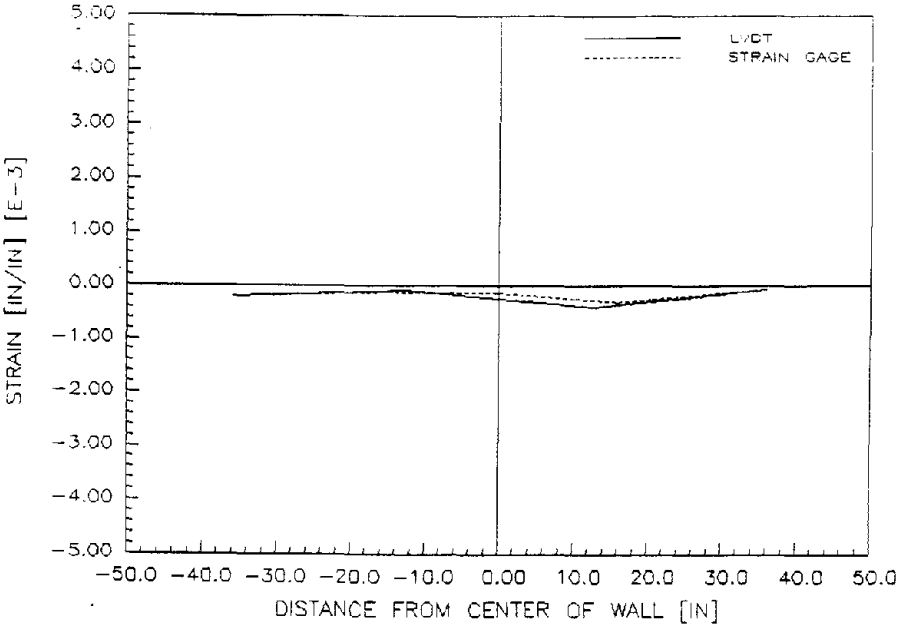

(a) Pure Axial Compression

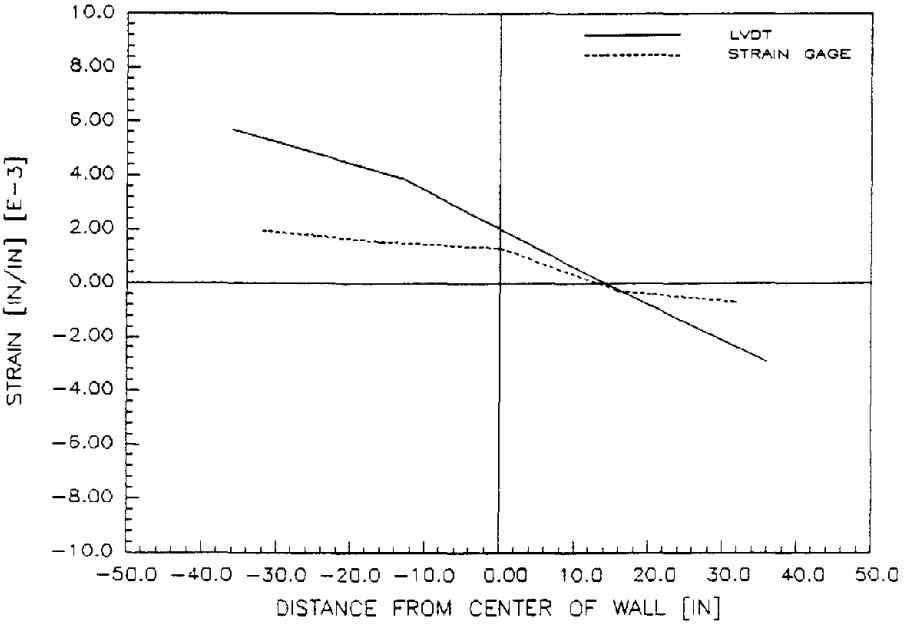

(b) At First Yield of Flexural Steel

Figure 6.8 - Flexural Strain Profiles in Specimen 1

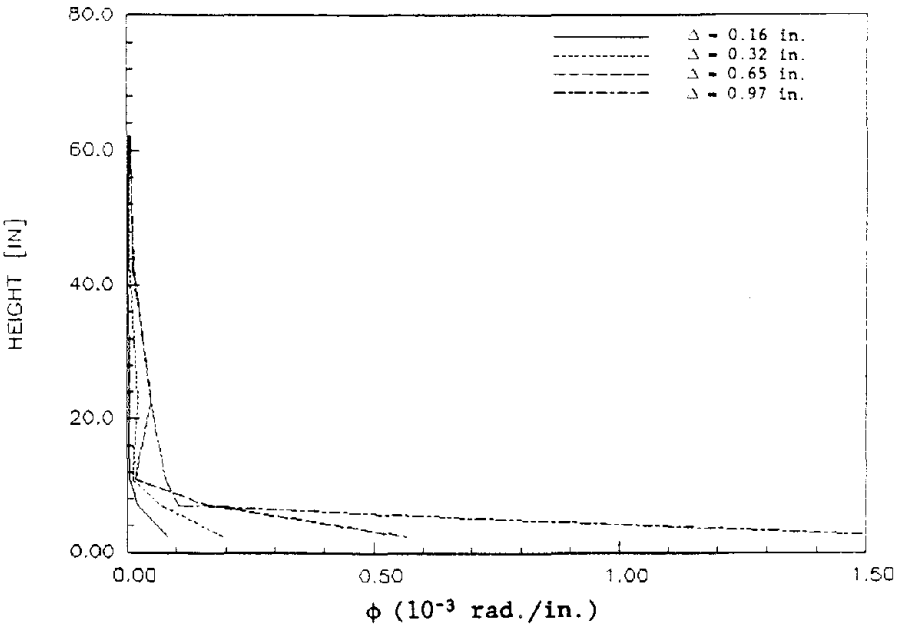

Figure 6.9 - Curvature Variation in Specimen 1

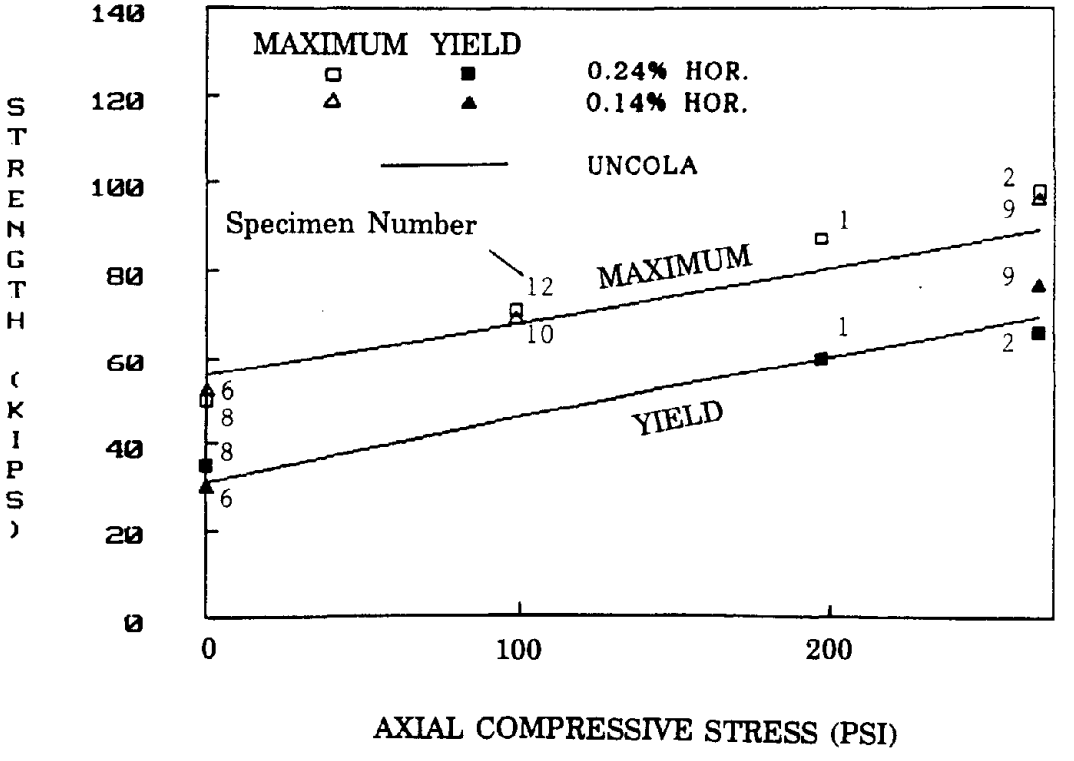

Figure 6.10 - Flexural Strength of Concrete Masonry Walls with 0.38% Vertical Steel

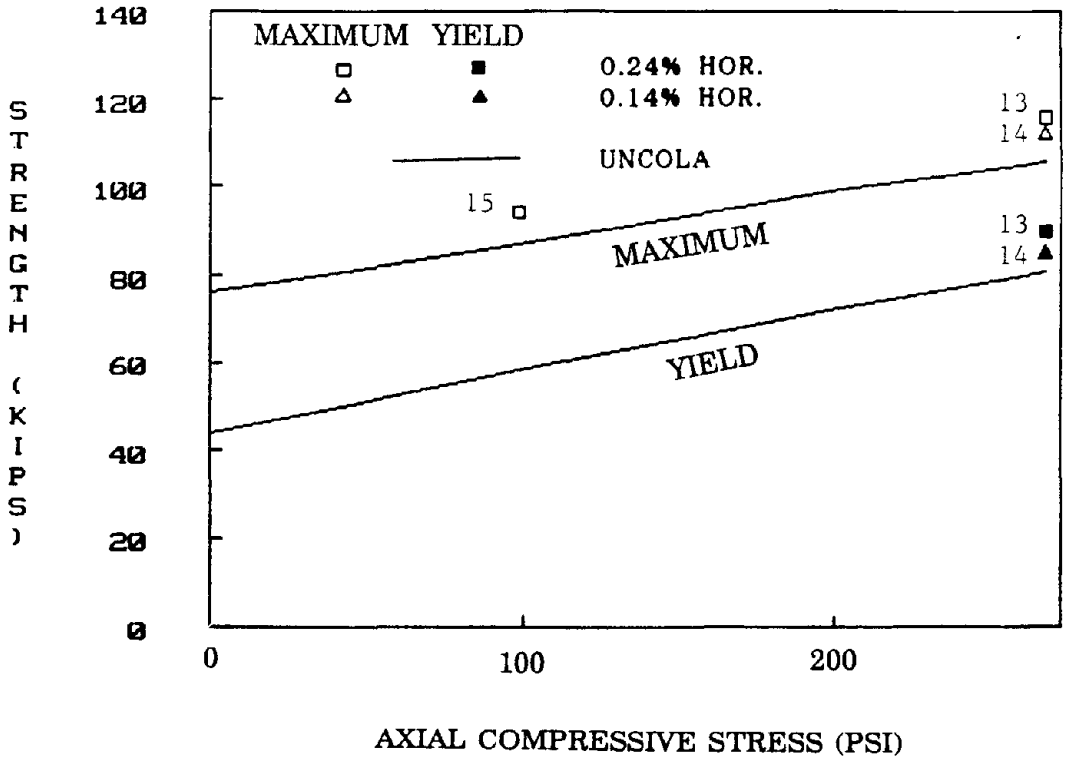

Figure 6.11 - Flexural Strength of Concrete Masonry Walls with 0.54% Vertical Steel

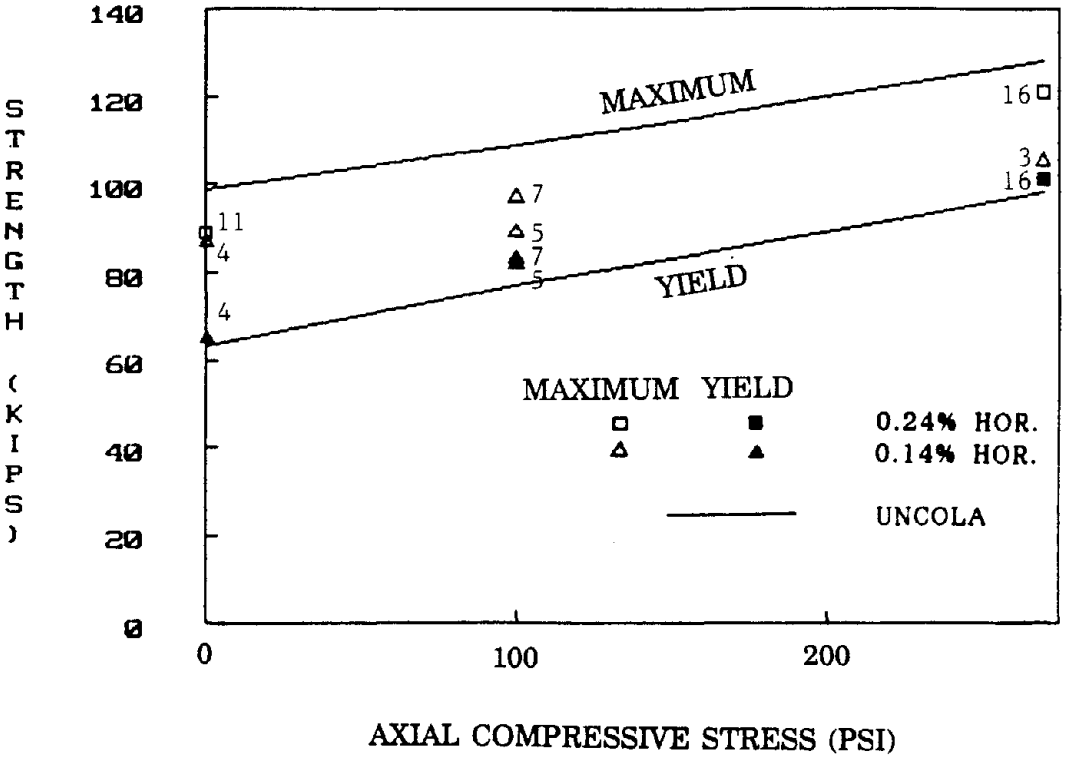

Figure 6.12 - Flexural Strength of Concrete Masonry Walls with 0.74% Vertical Steel

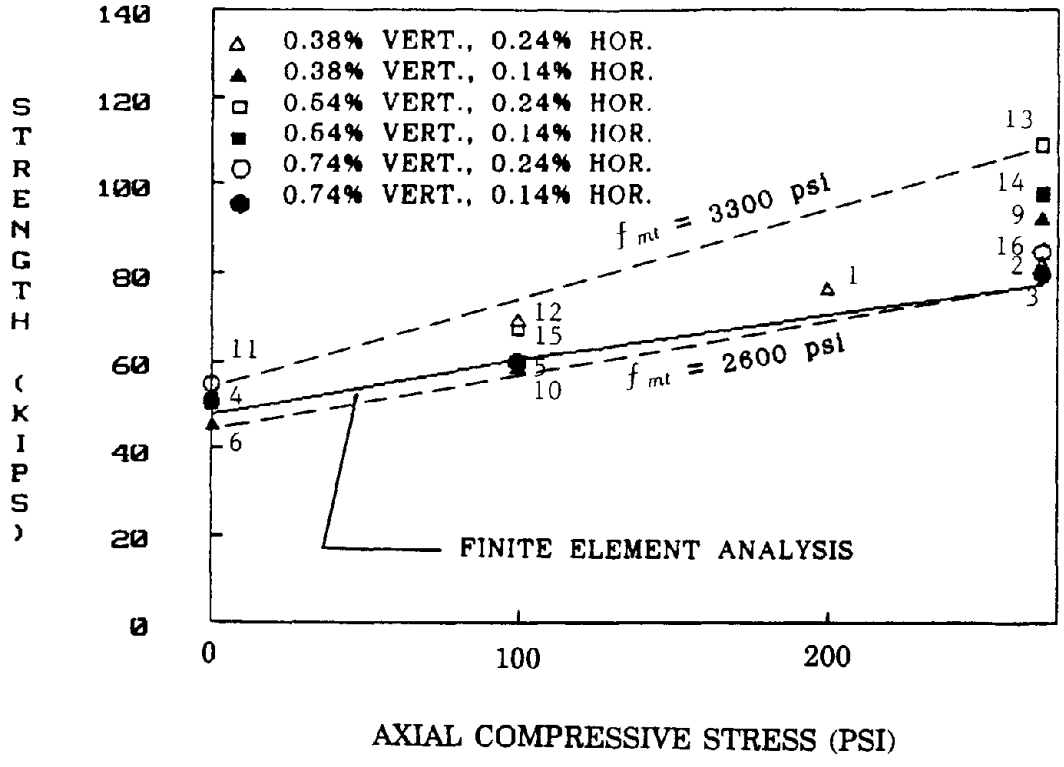

Figure 6.13 - Diagonal Cracking Strength of Concrete Masonry Specimens

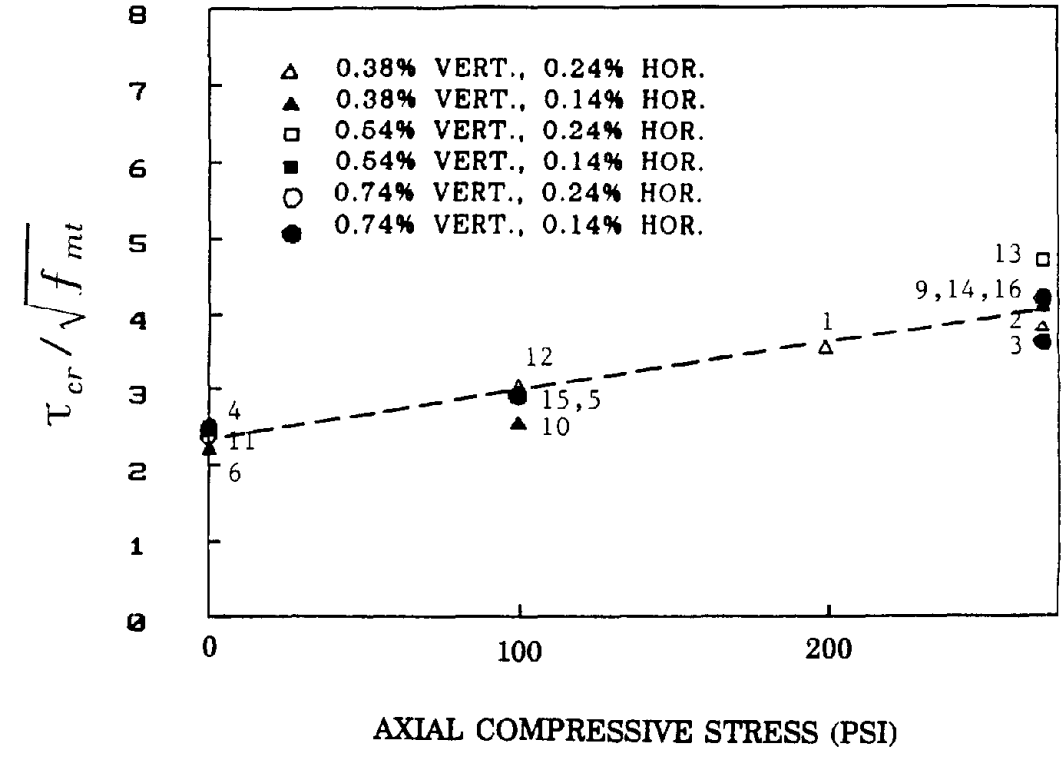

Figure 6.14 - Normalized Diagonal Cracking Strength of Concrete Masonry Specimens

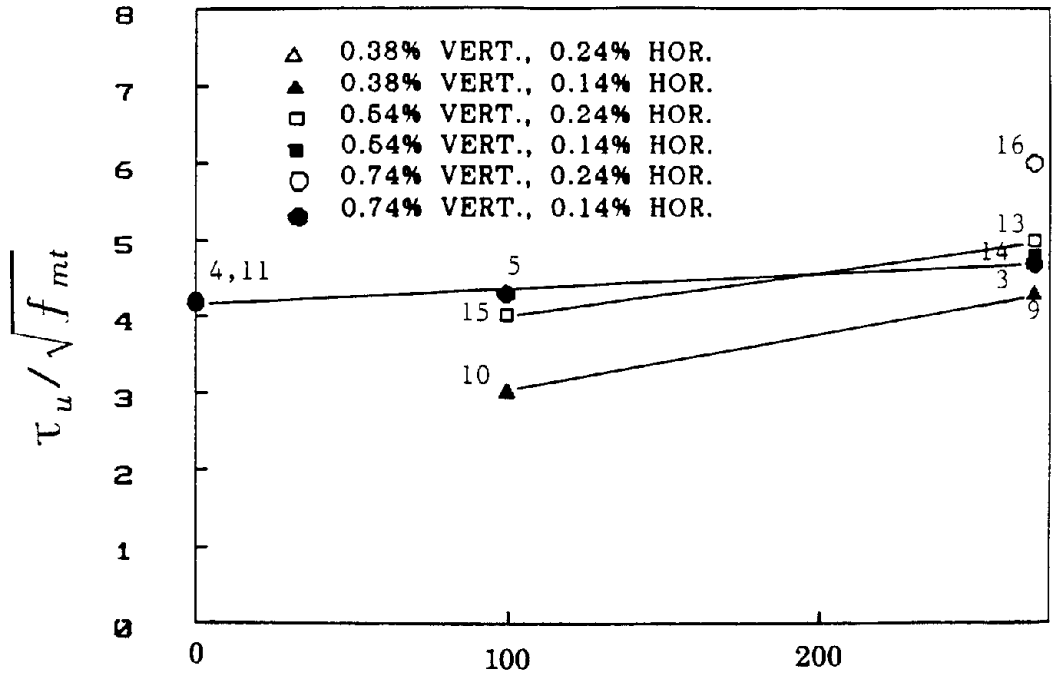

Figure 6.15 - Normalized Maximum Shear Strength of Concrete Masonry Specimens

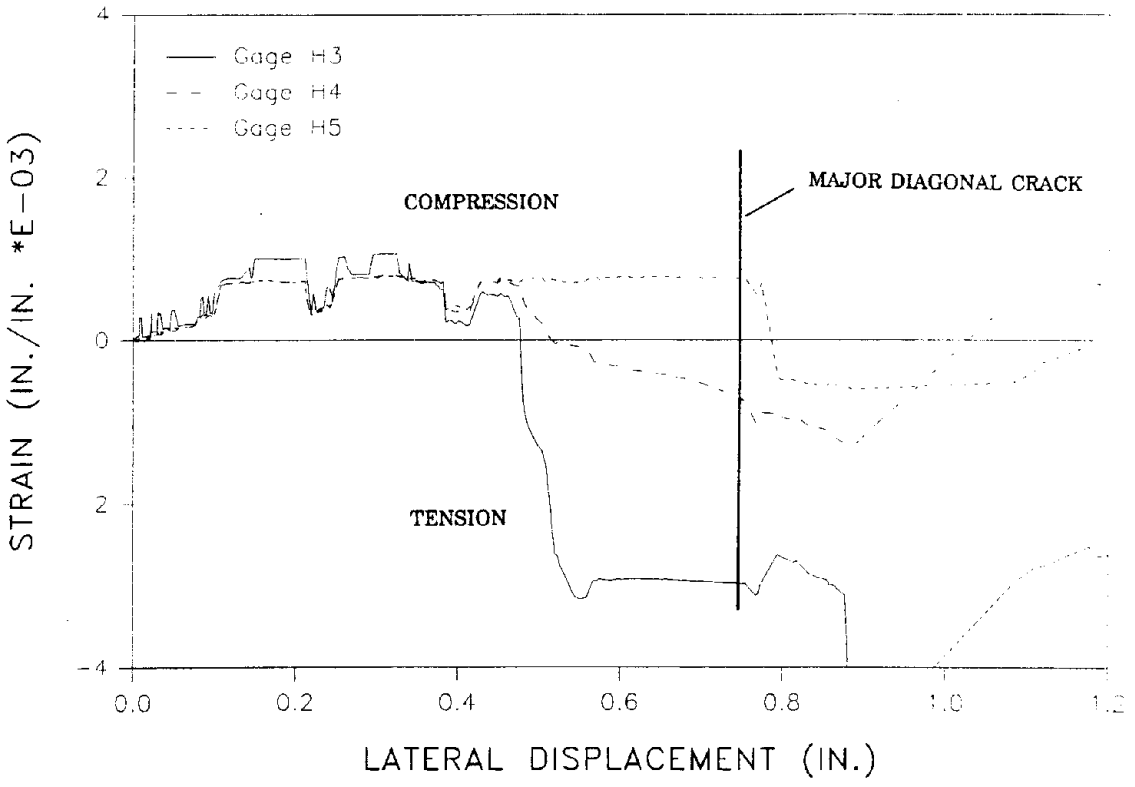

Figure 6.16 - Strain in Horizontal Steel in Specimen 23

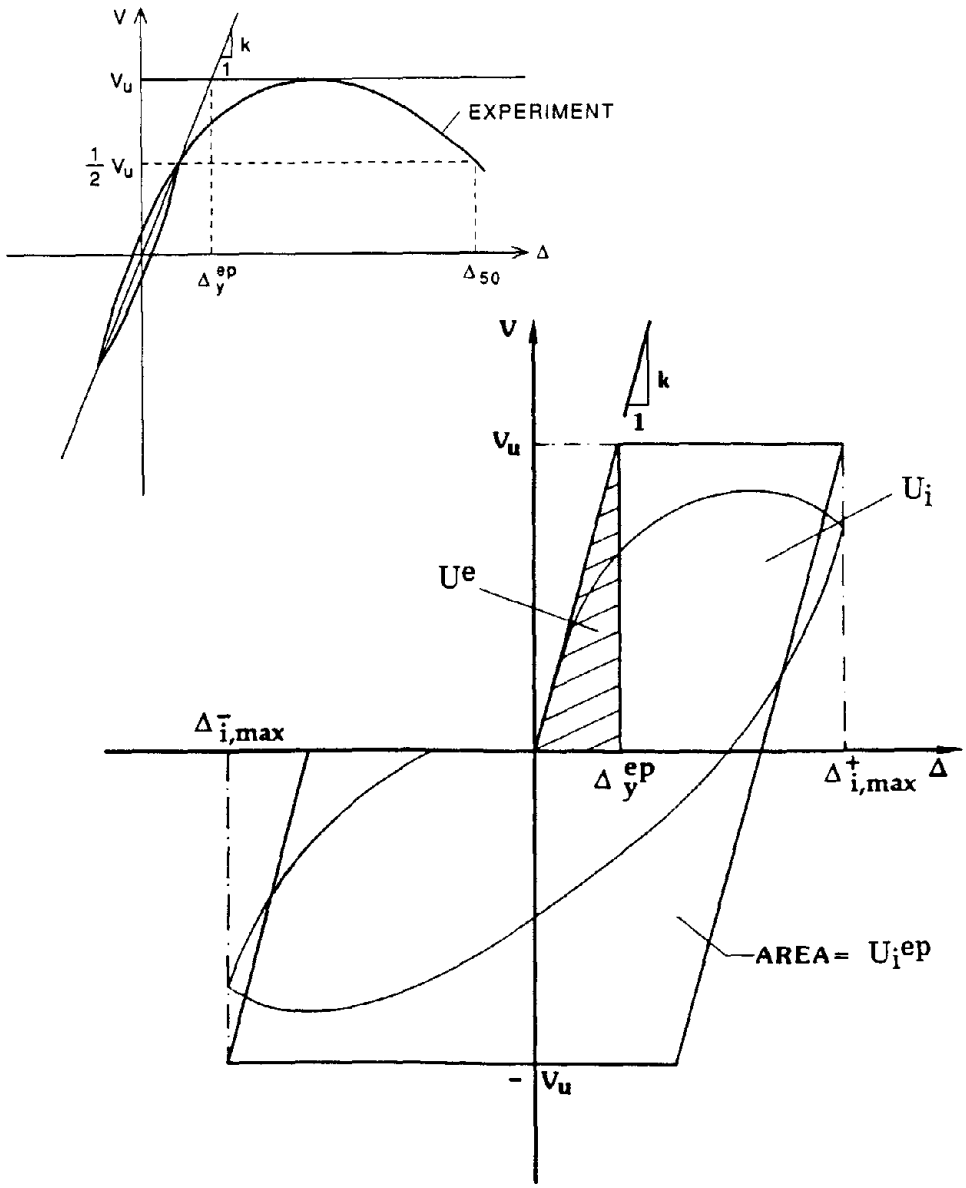

Figure 6.17 - Equivalent Elastic-Perfectly Plastic Model

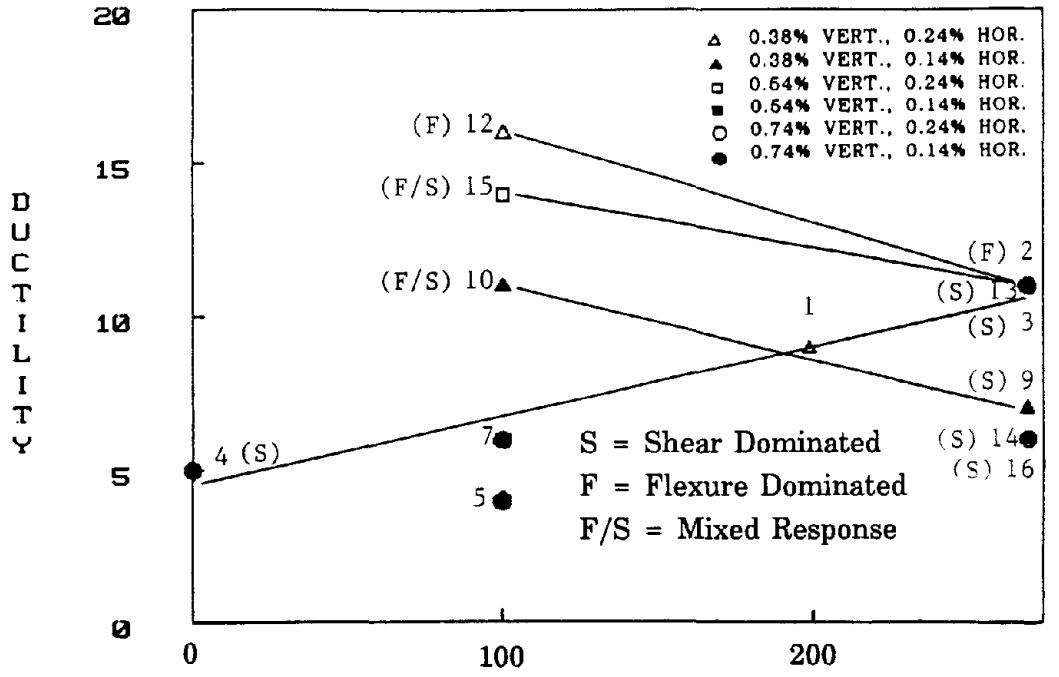

Figure 6.18 - Ductility of Concrete Masonry Wall Specimens

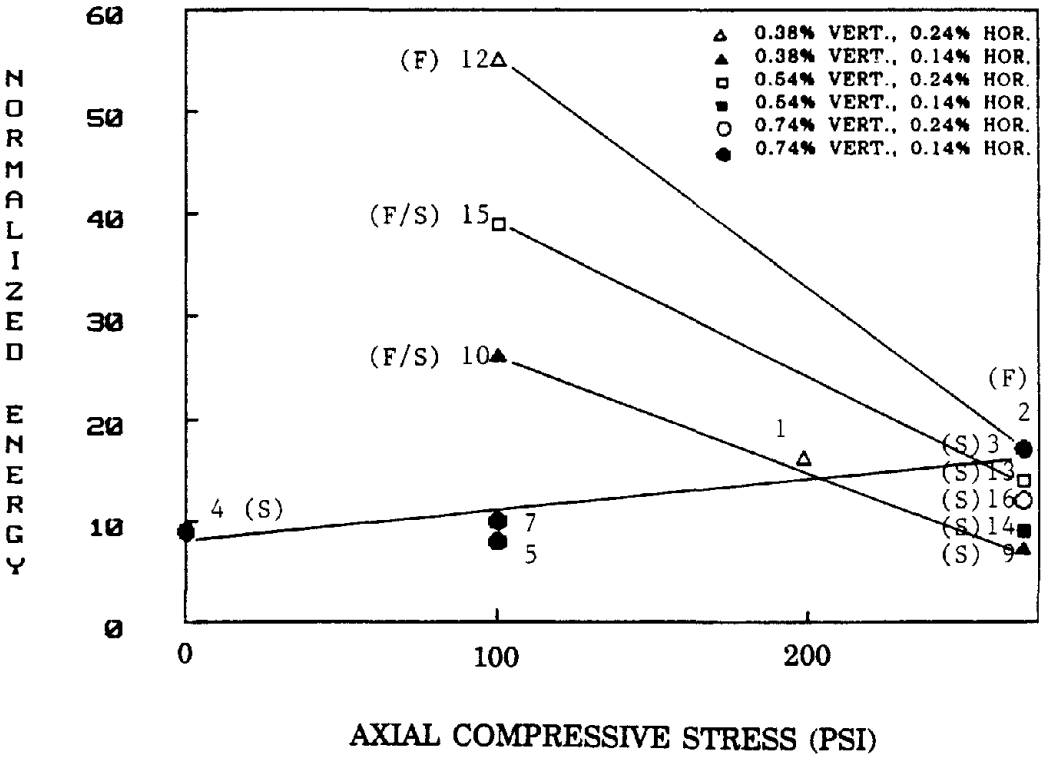

Figure 6.19 - Energy-Dissipation Capability of Concrete Masonry Wall Specimens

7 CONCLUSIONS

7.1 Summary

Twenty-four 6-ft.-by-6-ft. reinforced masonry shear wall panels were tested to examine the influence of the axial compressive load and the quantity of steel reinforcement on the failure mechanism, ductility, and inelastic load resistance capability of wall panels. Furthermore, the influence of other parameters, such as masonry units, confinement steel, and load or displacement history, was also examined in some of the wall specimens. Two major types of response modes have been identified from the wall specimens. One is flexural response and the other is shear response.

In general, specimens dominated by flexure exhibited more ductile behavior than those dominated by shear. The increase of axial compressive load and/or the quantity of vertical reinforcement tended to increase the flexural strength and change the response mode from flexure to shear. While increasing the axial compressive load and vertical steel ratio also led to an increase of the shear resistance, the effect was not as significant as that on the flexural strength. Flexural ductility appeared to be reduced by the increase of axial compressive load because of more significant toe spalling. However, as shown by one specimen, the ductility of a flexure-dominated wall can be substantially improved by wire-mesh-type joint confinement installed at wall toes. The test results indicate that the influence of horizontal steel on the shear strength is not very consistent, and that the increase of the shear strength is not proportional to the increase of horizontal steel. This is consistent with prior studies. In spite of this, it has been shown that the horizontal steel helps to improve the ductility of a wall panel dominated by diagonal shear cracks, and that shear failure can be prevented by increasing the quantity of horizontal steel. Moreover, it is shown that neither the vertical nor horizontal steel has any noticeable influence on the initiation of a diagonal crack, which is affected by the axial compressive load only.

The behavior of concrete masonry specimens was very similar to that of clay masonry. Because all the flexure-dominated specimens exhibited inelastic deformation initiated by tensile yielding, the higher compressive strength of clay masonry did not have any significant impact on the flexural strength.

The performance of the wall specimens seems to be affected by the load or displacement history applied. For example, in flexure-dominated specimens, it was observed that the maximum strength reached in the initial cycle is larger than that obtained after a number of small amplitude cycles. In shear-dominated specimens, it was observed that monotonic loads resulted in a slightly higher shear strength than cyclic loads but led to substantially larger ductility.

7.2 Conclusions

The test results have demonstrated that reinforced masonry wall panels can provide ductility and energy-dissipation capability under cyclic displacement reversals, and are, therefore, suitable for seismic resistance design provided proper reinforcement guidelines are developed and followed. In particular, the test data have indicated the important influence of toe confinement on flexural ductility. It has also been shown that brittle shear behavior dominated by diagonal cracking is undesirable and difficult to analyze. In this respect, the current UBC provisions (1988) on the shear strength of reinforced masonry shear walls appear to be simplistic. In particular, the beneficial influence of the axial compressive load and the quantity of vertical steel on the shear strength, as evident from the test results, has been neglected. Results of this study, based on a systematic variation of selected design parameters and load conditions, provide additional information for such considerations.

7.3 Recommendations for Future Studies

The limited test data indicate that the development of effective confinement details for flexure-dominated walls is an important topic for future research. Further experimental studies on this issue are desirable. It is evident that shear strength is very much influenced by the effective aspect ratio of a wall panel. However, the current study has focussed on a single aspect ratio. In this respect, further

experimental studies on the influence of the effective aspect ratio and wall geometry on the shear behavior are necessary. The effects of load or displacement history on the inelastic behavior of wall panels, in particular, with respect to the flexural behavior, also need to be further investigated.

Finally, reliable analytical models should be developed to give a better prediction of the shear strength of a wall panel, and the current code provisions should be improved by considering the influence of the axial compressive load and vertical steel content on the shear strength. Results of this study provide a useful data base for these developments.

APPENDIX A: MEASUREMENT OF SHEAR DEFORMATION

The measurement of overall shear deformation of a wall panel that is subject to combined shear and flexure is discussed here.

A.1 Pure Shear

For a wall panel subject to pure shear, the shear deformation can be calculated from the change of the diagonal length along any of the two diagonals, as shown in Fig. A1. However, in a test environment, some experimental errors could be introduced into the measurement of diagonal deformation. To minimize the measurement errors, the average of two diagonal measurements is usually used to find the overall shear deformation in a panel. As a result, the shear deformation Δ^{SH} can be calculated as follows:

$$\Delta^{SH} = \frac{\Delta_1 - \Delta_2}{2}\frac{\sqrt{h^2 + l^2}}{l} \tag{A1}$$

in which Δ_1 and Δ_2 are the diagonal deformations shown in Fig. A1, with extension being defined as positive, and h and l are the height and length of a panel.

A.2 Combined Flexure and Shear

Strictly speaking, under combined flexure and shear, Eq. (A1) is no longer valid, as flexural deformation introduces a change of diagonal deformation as well. To assess the amount of errors that will be introduced into Eq. (A1) by flexure, we consider the case of pure flexure as shown in Fig. A2. Assuming that the wall curvature $\phi(x)$ varies with respect to the vertical distance x from the base and that the location of the neutral axis of bending is a constant, the deformation quantities, $\overline{\Delta}^{FL}$, υ_1, υ_2, Δ_1, and Δ_2, as shown in Fig. A2, can be calculated with the following formulas:

$$\overline{\Delta}^{FL} = \int_0^h \phi(x)(h-x)dx \tag{A2}$$

$$v_1 = a\int_0^h \phi(x)dx \tag{A3}$$

$$v_2 = (l-a)\int_0^h \phi(x)dx \tag{A4}$$

$$\Delta_1 = \sqrt{(l+\overline{\Delta}^{FL})^2 + (h-v_1)^2} - \sqrt{l^2+h^2} \tag{A5}$$

$$\Delta_2 = \sqrt{(l-\overline{\Delta}^{FL})^2 + (h+v_2)^2} - \sqrt{l^2+h^2} \tag{A6}$$

in which a is the distance of the neutral axis from one end of a wall panel, as shown in Fig. A2. By substituting Eqs. (A5) and (A6) into Eq. (A1) and assuming that the deformations are small with respect to the dimensions of a panel, the amount of errors in shear deformation can be expressed as

$$\Delta_F^{SH} = \frac{1}{4l}\left[4l\overline{\Delta}^{FL} - 2h(v_1+v_2)\right] \tag{A7}$$

in which Δ_F^{SH} is the error in shear deformation caused by flexure. To assess the significance of these errors, three different curvature variations are examined in the following: (1) linear curvature of an elastic cantilever wall, (2) uniform curvature, and (3) rotation being concentrated at the wall base.

Linear Curvature

If the curvature variation is given by a linear function, i.e., $\phi(x) = \tilde{\phi}(h-x)/h$, then, according to Eqs. (A2) through (A4),

$$\overline{\Delta}^{FL} = \frac{\tilde{\phi}h^2}{3} \tag{A8}$$

$$v_1 = \frac{a\tilde{\phi}h}{2} \tag{A9}$$

$$v_2 = \frac{(l-\alpha)\hat{\phi}h}{2} \tag{A10}$$

Substituting the above equations into Eq. (A7), we obtain

$$\Delta_F^{SH} = \frac{1}{4}\bar{\Delta}^{FL} \tag{A11}$$

Uniform Curvature

If the curvature ϕ is a constant, then

$$\bar{\Delta}^{FL} = \frac{\phi h^2}{2} \tag{A12}$$

$$v_1 = \alpha\phi h \tag{A13}$$

$$v_2 = (l-\alpha)\phi h \tag{A14}$$

and

$$\Delta_F^{SH} = 0 \tag{A15}$$

Concentrated Base Rotation

If the concentrated base rotation is θ, then

$$\bar{\Delta}^{FL} = \theta h \tag{A16}$$

$$v_1 = \alpha\theta \tag{A17}$$

$$v_2 = (l-\alpha)\theta \tag{A18}$$

If the diagonal deformation is measured with transducers attached to a fixed base, as is the case in this study, then

$$\Delta_F^{SH} = \frac{1}{2}\overline{\Delta}^{FL} \tag{A19}$$

Based on the above analysis, it is evident that the errors in shear deformation can be expressed as

$$\Delta_F^{SH} = \alpha\overline{\Delta}^{FL} \tag{A20}$$

in which α varies between 0.25 and 0.50 for a cantilever wall which may have a large base rotation due to a plastic hinge. However, the exact value of α is difficult to assess because of the axial load and flexural cracks, which may lead to a variation of the location of the neutral axis along the height of a wall panel. In this case, Eq. (A7) may be used directly if υ_1 and υ_2 are known (Merryman et al. 1990).

A.3 Correction of Experimental Measurement

Based on the above formulas, one can approximately correct the errors and estimate the actual overall shear deformation as follows. First, estimate the actual flexural deformation from the measured total and shear deformations (Δ and Δ^{SH}) and base sliding (Δ^{SL}) using Eq. (6.1):

$$\overline{\Delta}^{FL} = \frac{1}{1-\alpha}(\Delta - \Delta^{SH} - \Delta^{SL}) \tag{A21}$$

Then, based on Eq. (A20), evaluate the actual shear deformation:

$$\Delta_a^{SH} = \Delta^{SH} - \alpha\overline{\Delta}^{FL} \tag{A22}$$

Alternatively, one can also estimate Δ_F^{SH} directly with Eq. (A7) provided υ_1 and υ_2 are measured. However, with respect to the setup shown in Fig. 3.3a, the readings for υ_1 and υ_2 would not be reliable once toe crushing occurred.

A.4 Evaluation of Experimental Data

Eqs. (A21) and (A22) were used to calculate flexural and shear deformations from the experimental results obtained from the cantilever wall specimens. However, by using $\alpha = 0.25$, it was found that the shear deformation appeared to be over-corrected, as Δ_a^{SH} became negative in some cases, especially when the total deflection was very small.

Moreover, for Specimens 1, 2, and 3, the shear and flexural deformations were independently calculated by means of Eqs. (A1) and (A2), respectively, and were substituted, together with the value of base sliding, into Eq. (6.1) to obtain the total deflection of a wall. The flexural deformation was calculated with the measurements obtained with transducers L1 through L12 shown in Fig. 3.3a. No corrections were applied. The results obtained are compared to the total displacements measured directly with transducer L25 in Figs. A3 through A5. It is apparent that the estimation is excellent for Specimen 1, but not for Specimens 2 and 3. While the summed deflection significantly overestimates the actual deflection of Specimen 2, it underestimates the actual deflection of Specimen 3. It is also apparent that, except for Specimen 2, any correction to shear deformation with any of the aforementioned procedures will lead to worse results.

Based on the above observations, it is believed that there are probably other experimental errors which have not been considered in the aforementioned analysis. One possible source could be the errors introduced by the deformation of the base slab, as shown in Fig. A6, which could not be picked up by the diagonal transducers but contributed to the total flexural deformation. The slab was not perfectly rigid and would most likely be deformed by the overturning moment. To account for this, Eq. (A21) should be modified as follows:

$$\overline{\Delta}^{FL} = \frac{1}{1-\alpha}(\Delta - \Delta^{SL} - \Delta^{SH} - ER) \tag{A23}$$

in which ER is the additional deflection due to base deformation. It is very likely that ER will partly offset the error $\alpha\overline{\Delta}^{FL}$, resulting in an over-correction.

Based on the above discussions and the fact that the value of ER is difficult to obtain, it is decided that the partial correction based on Eqs. (A21) and (A22) should not be applied to the experimental results. Moreover, it must be realized that Eq. (A1) presents only an approximate assessment of the overall shear deformation and is not entirely valid for wall panels which have severe diagonal cracks.

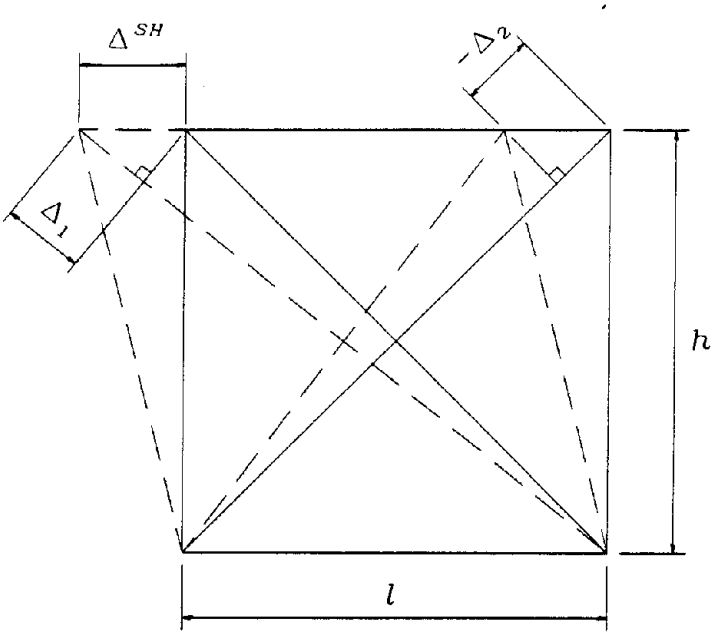

Figure A1 - Diagonal Deformation due to Pure Shear

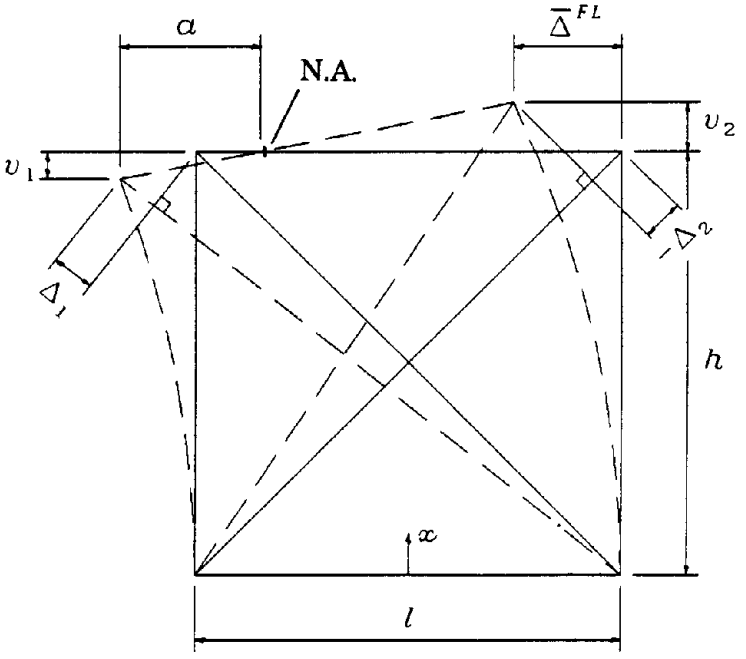

Figure A2 - Diagonal Deformation due to Pure Flexure

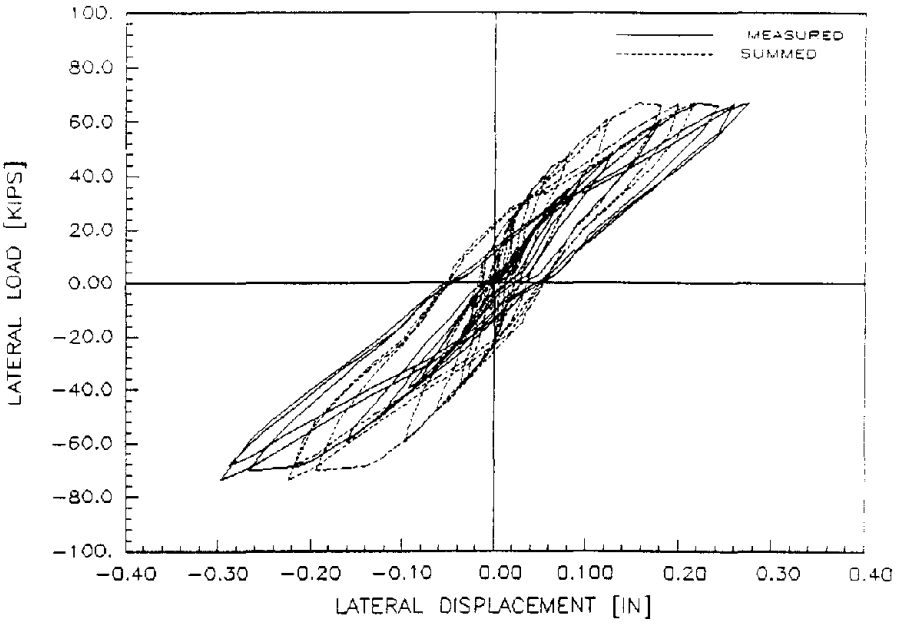

(a) First Sequence

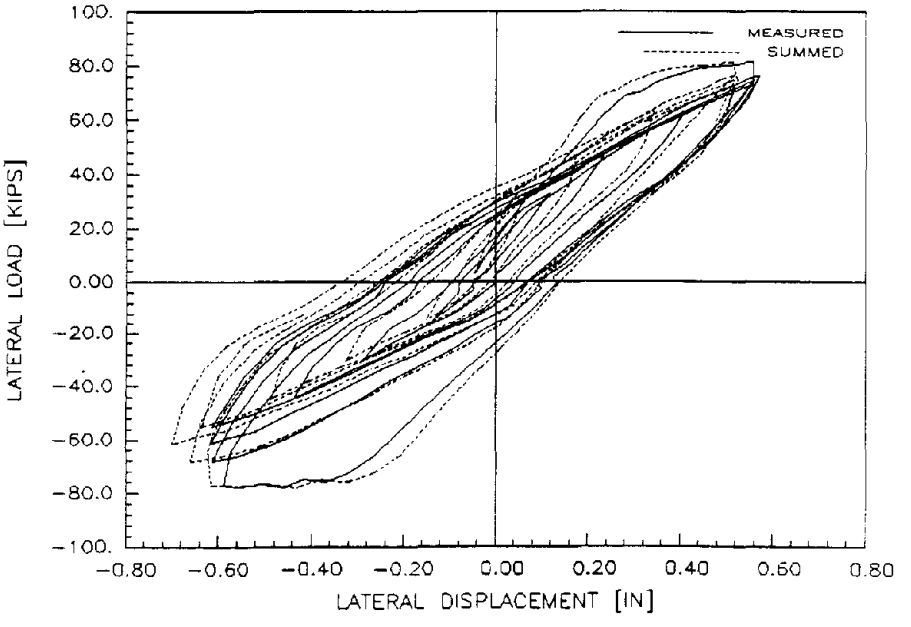

(b) Second Sequence

Figure A3 - Comparison of Actual and Summed Total Displacement Response of Specimen 1

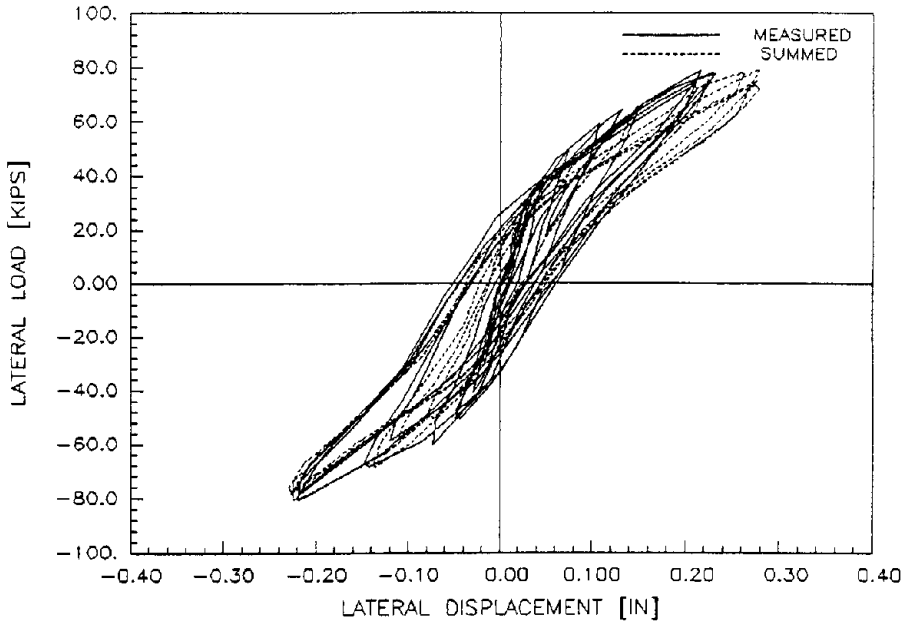

(a) First Sequence

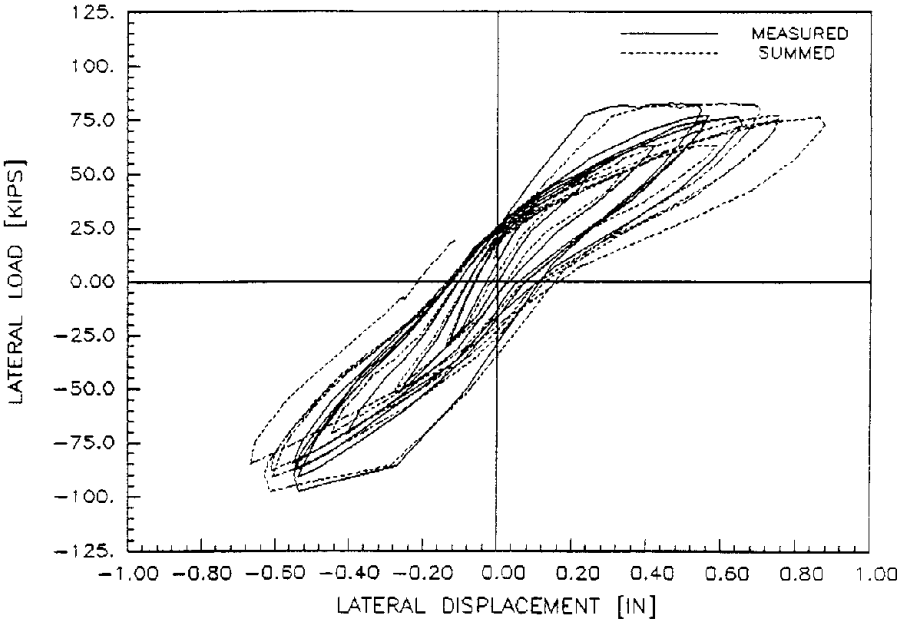

(b) Second Sequence

Figure A4 - Comparison of Actual and Summed Total Displacement Response of Specimen 2

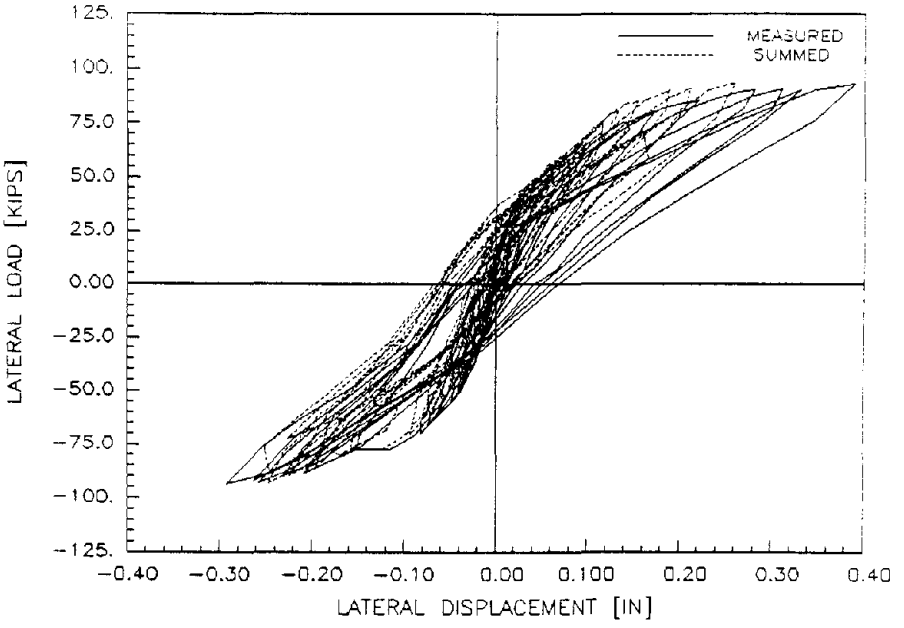

(a) First Sequence

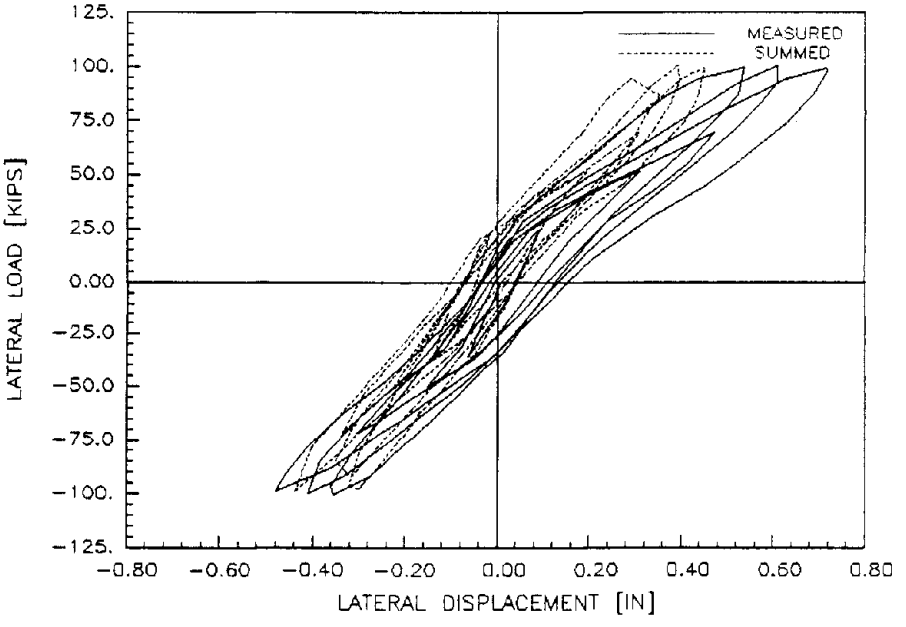

(b) Second Sequence

Figure A5 - Comparison of Actual and Summed Total Displacement Response of Specimen 3

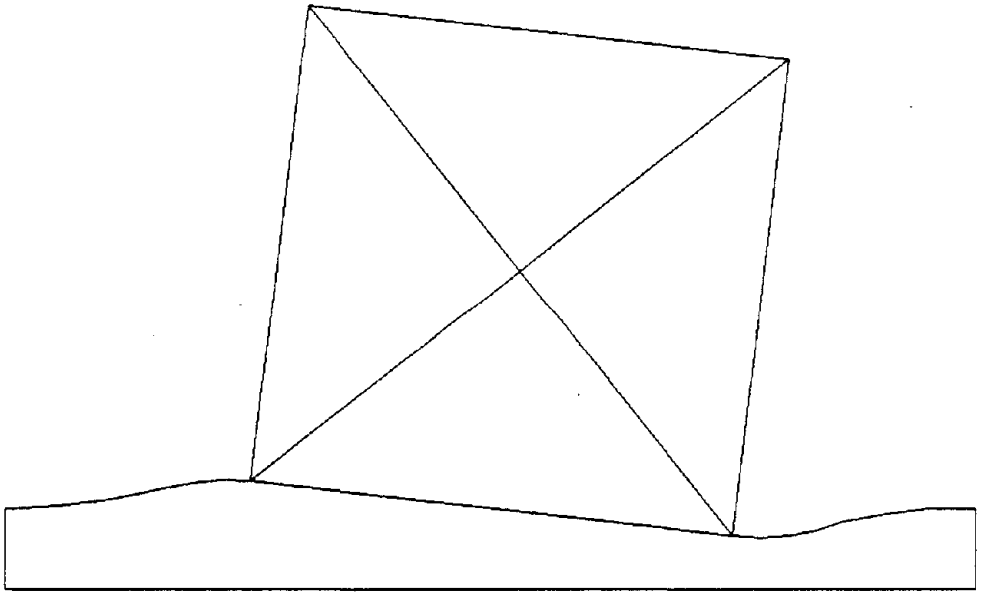

Figure A6 - Base Deformation

APPENDIX B: LOAD-VERSUS-DISPLACEMENT ENVELOPES OF CYCLICALLY LOADED SPECIMENS

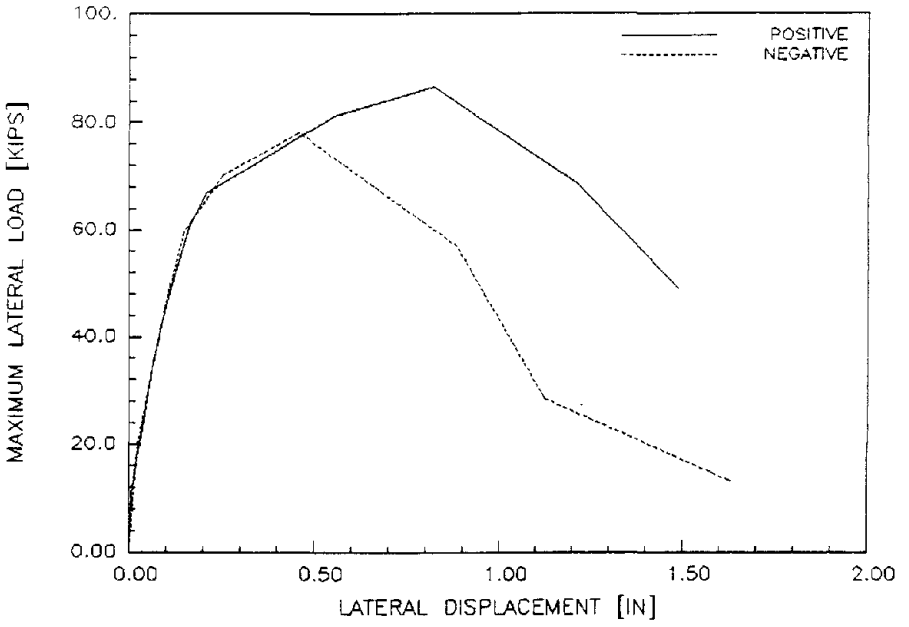

Figure B1 - Load Versus Displacement Envelopes of Specimen 1

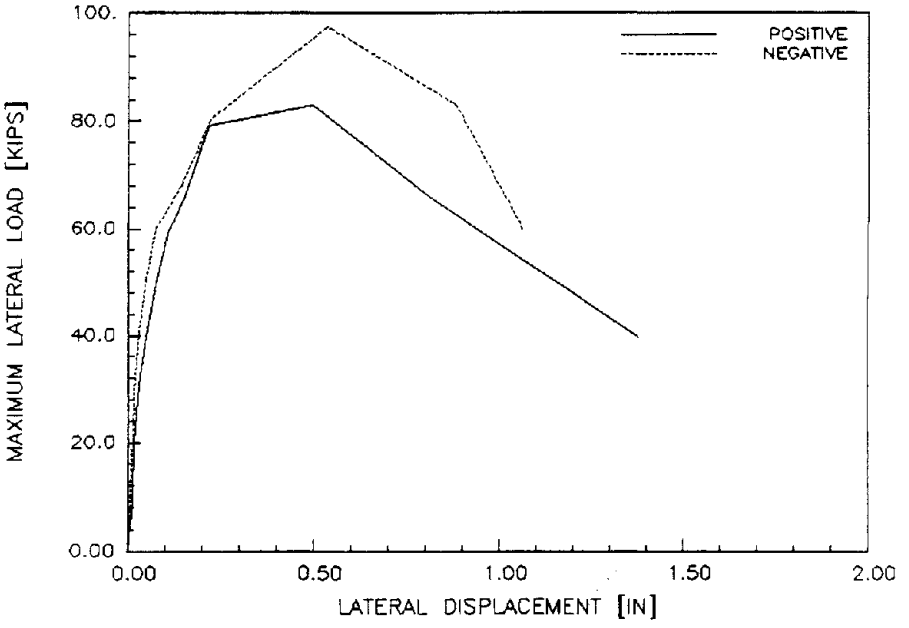

Figure B2 - Load Versus Displacement Envelopes of Specimen 2

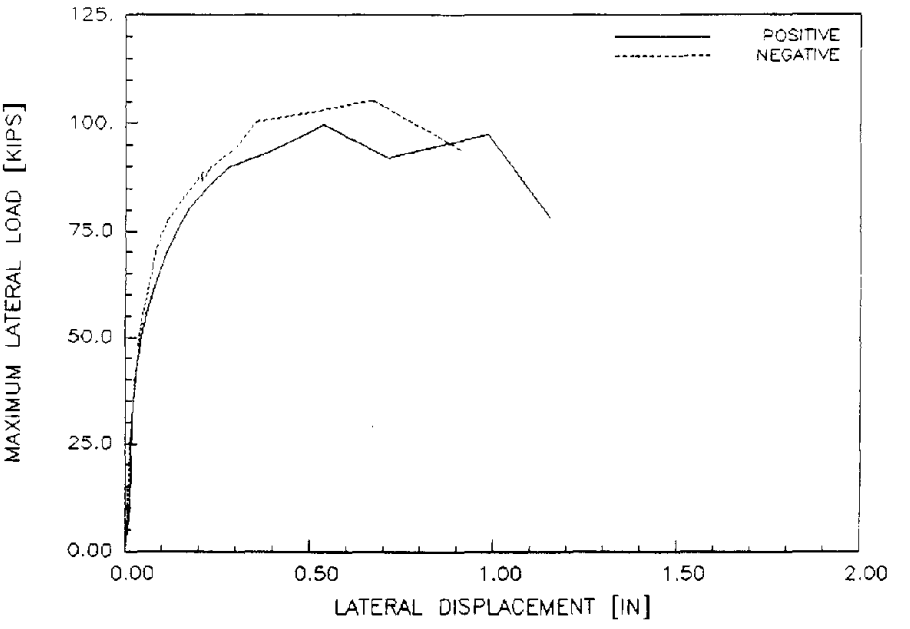

Figure B3 - Load Versus Displacement Envelopes of Specimen 3

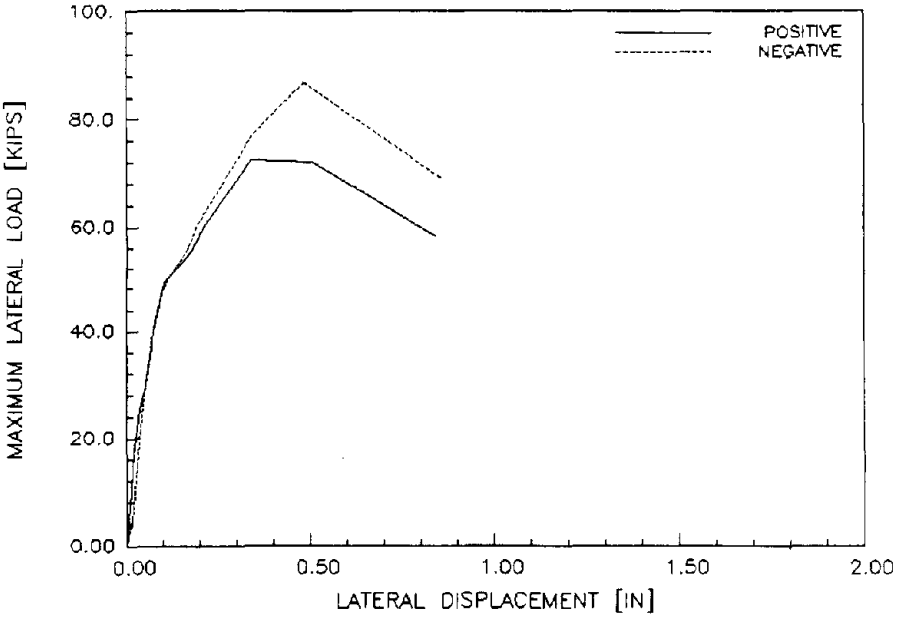

Figure B4 - Load Versus Displacement Envelopes of Specimen 4

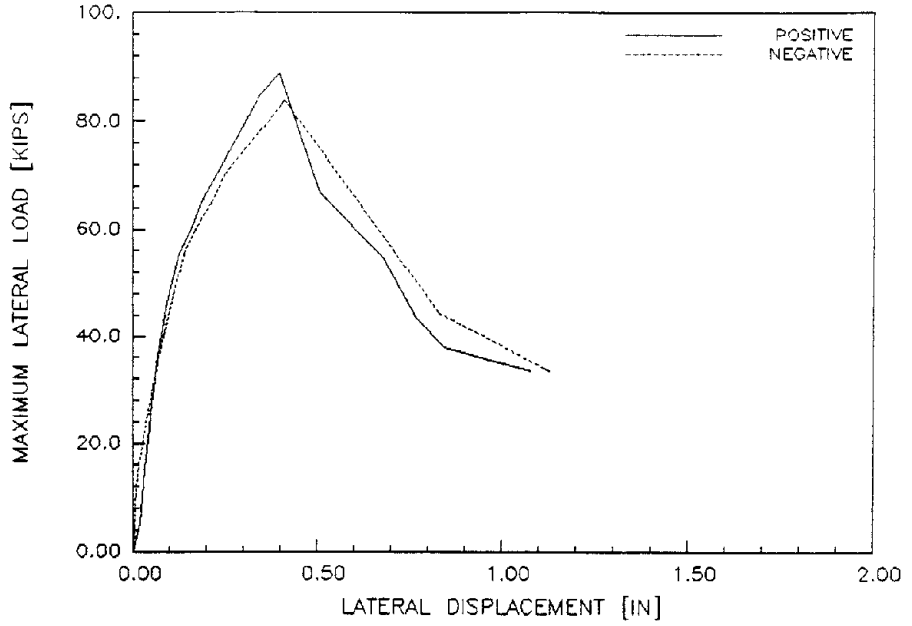

Figure B5 - Load Versus Displacement Envelopes of Specimen 5

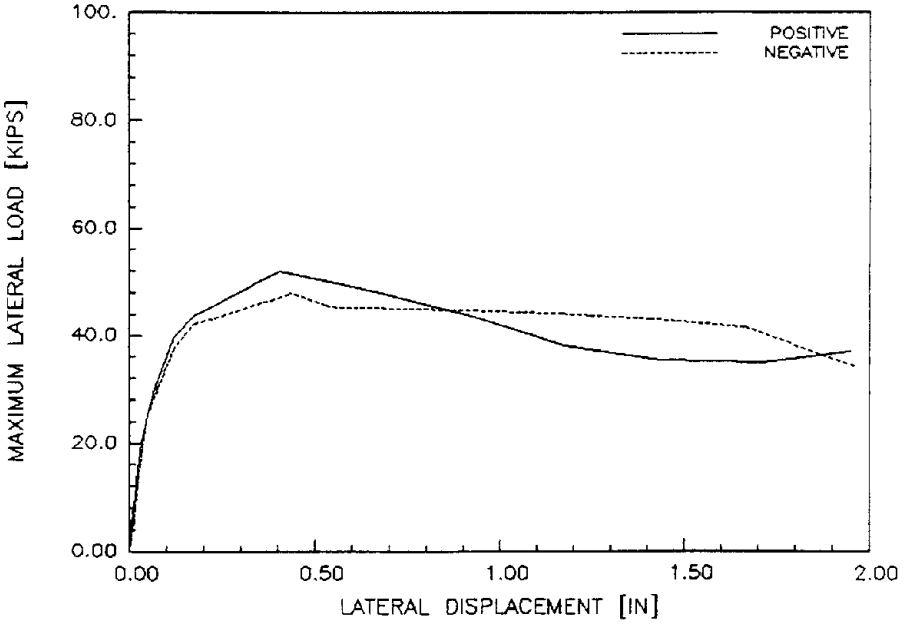

Figure B6 - Load Versus Displacement Envelopes of Specimen 6

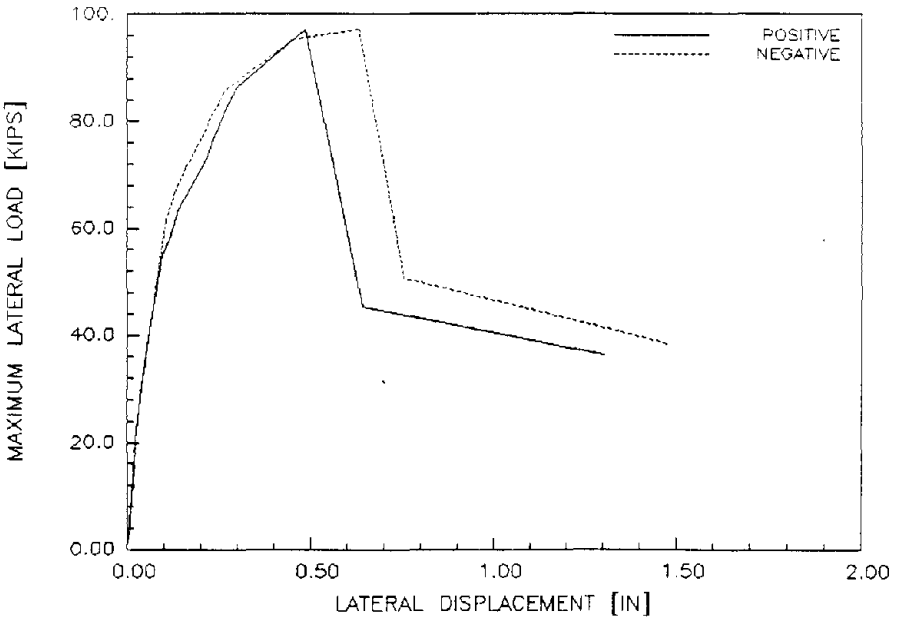

Figure B7 - Load Versus Displacement Envelopes of Specimen 7

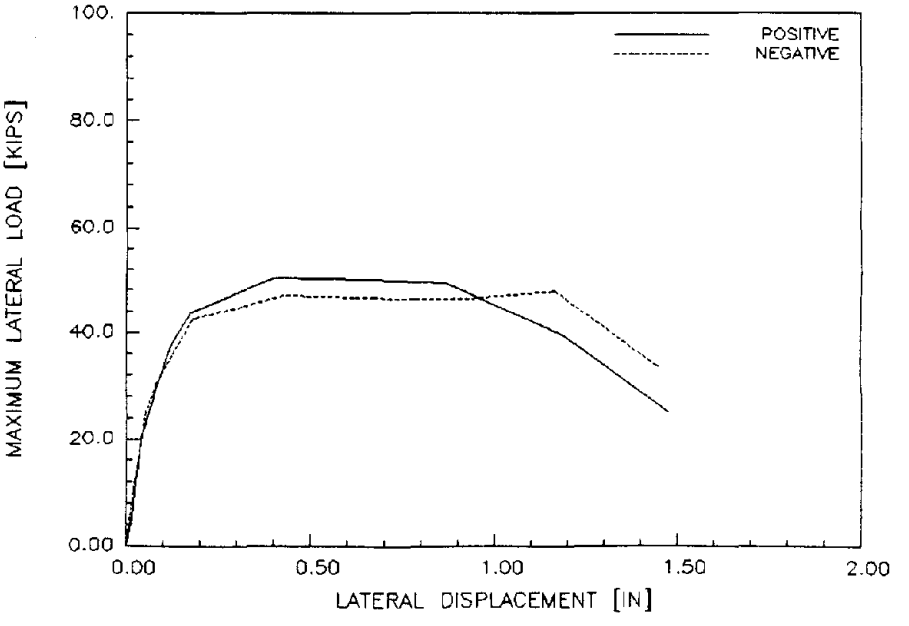

Figure B8 - Load Versus Displacement Envelopes of Specimen 8

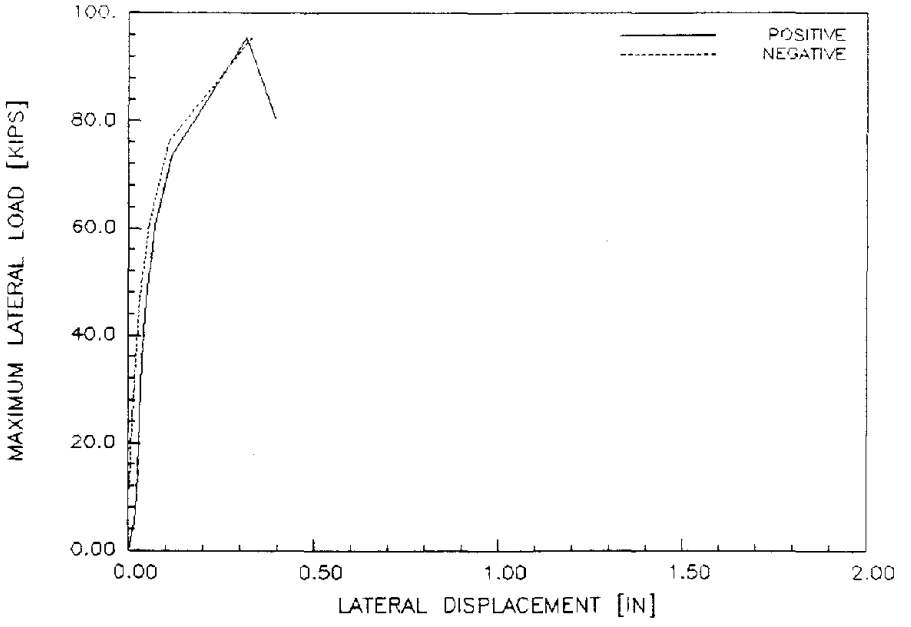

Figure B9 - Load Versus Displacement Envelopes of Specimen 9

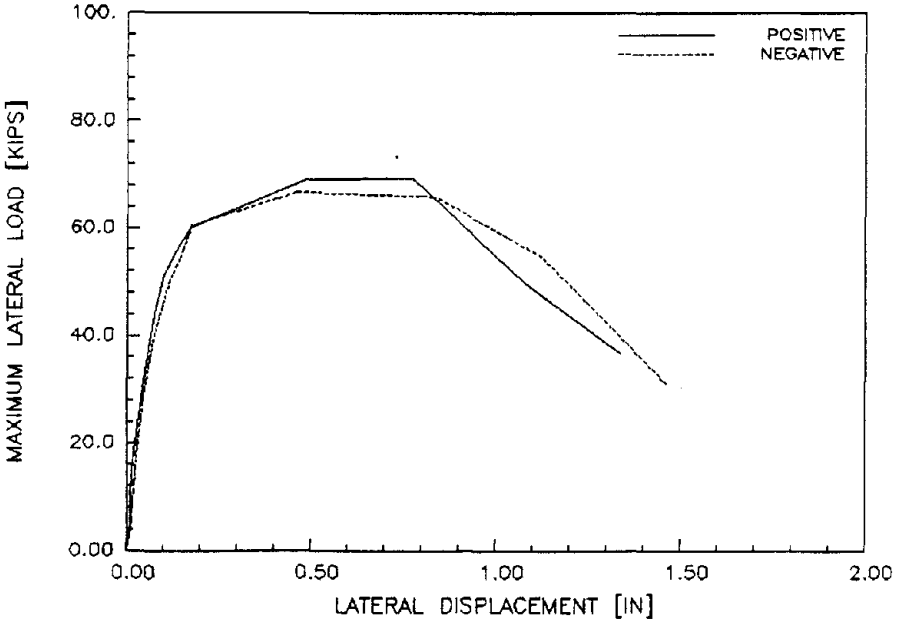

Figure B10 - Load Versus Displacement Envelopes of Specimen 10

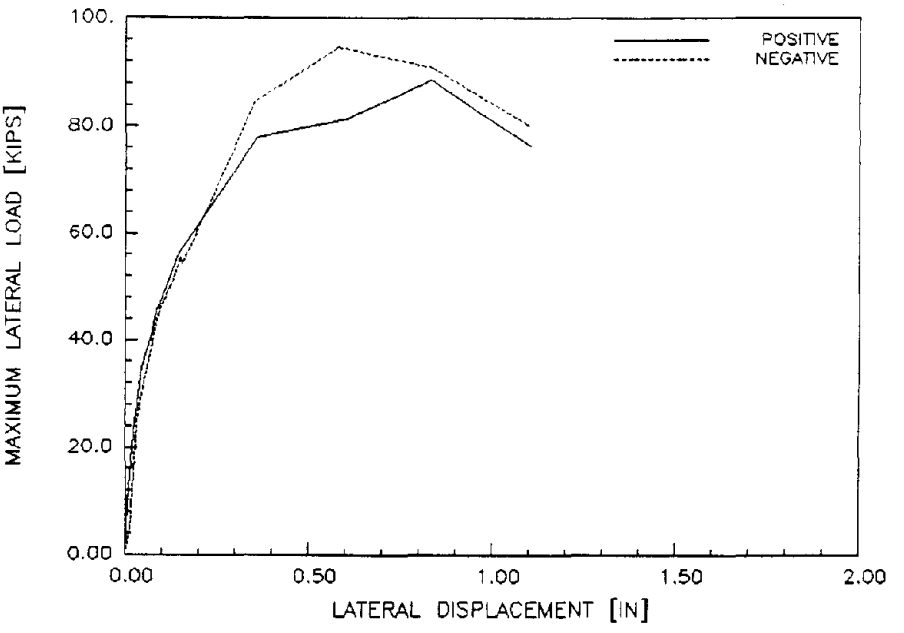

Figure B11 - Load Versus Displacement Envelopes of Specimen 11

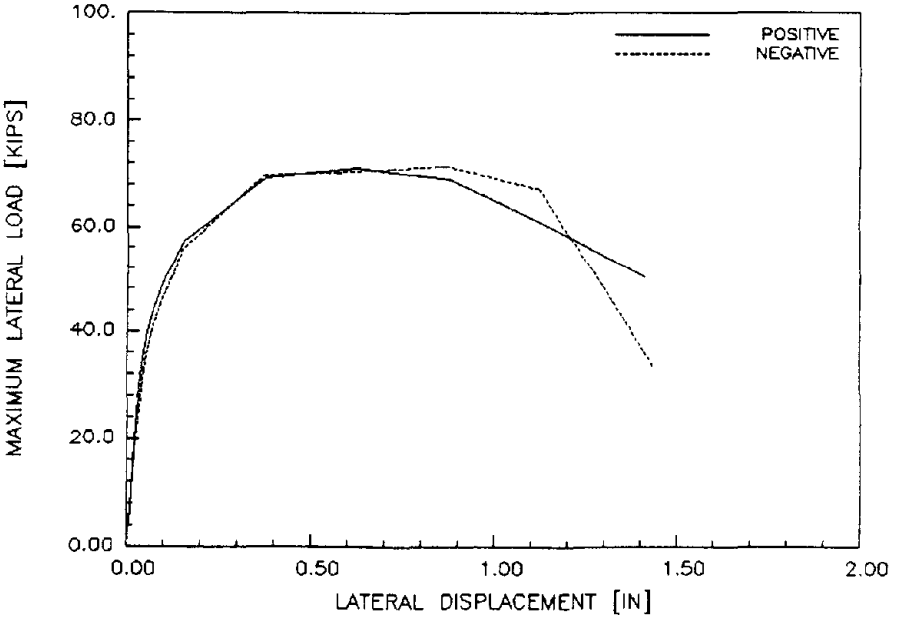

Figure B12 - Load Versus Displacement Envelopes of Specimen 12

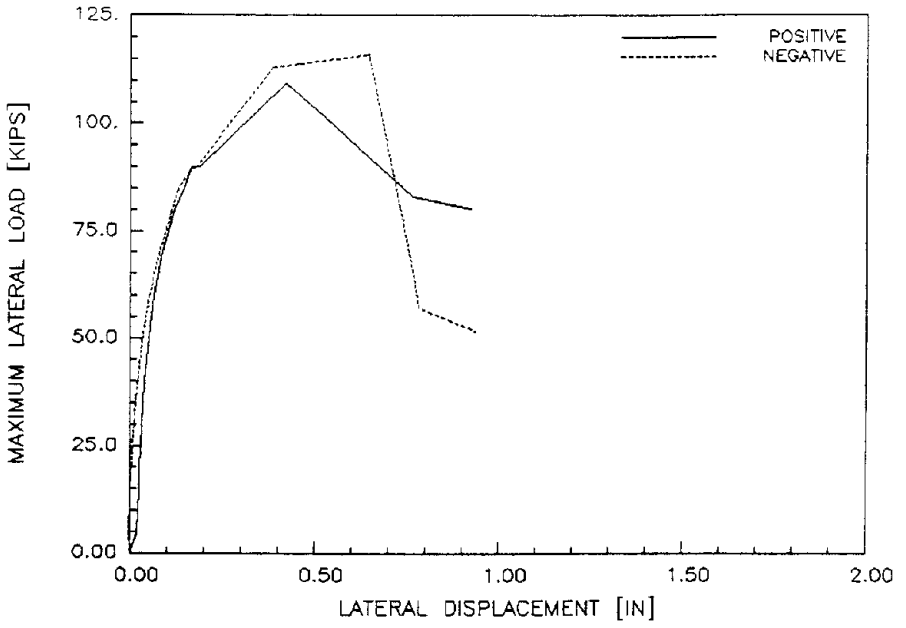

Figure B13 - Load Versus Displacement Envelopes of Specimen 13

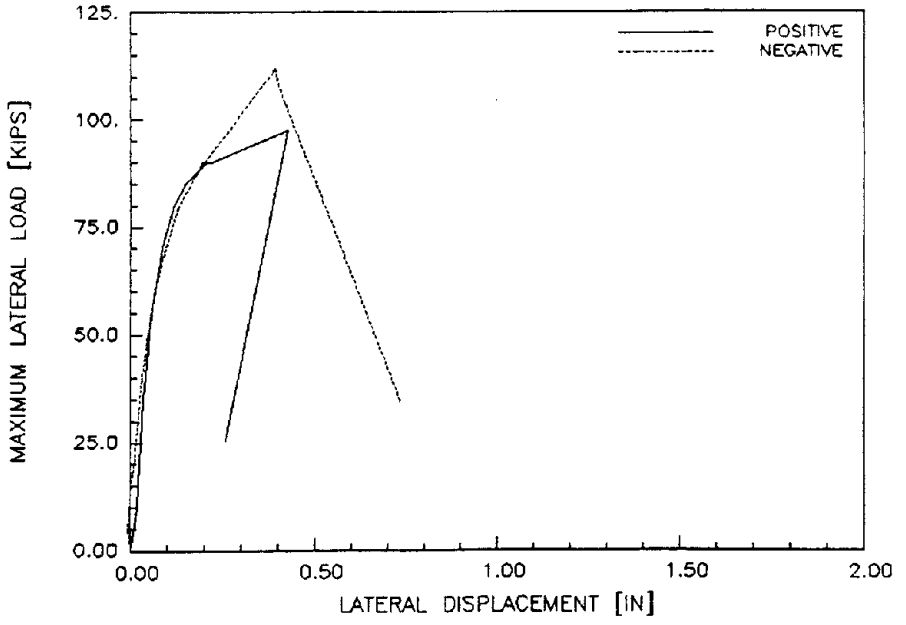

Figure B14 - Load Versus Displacement Envelopes of Specimen 14

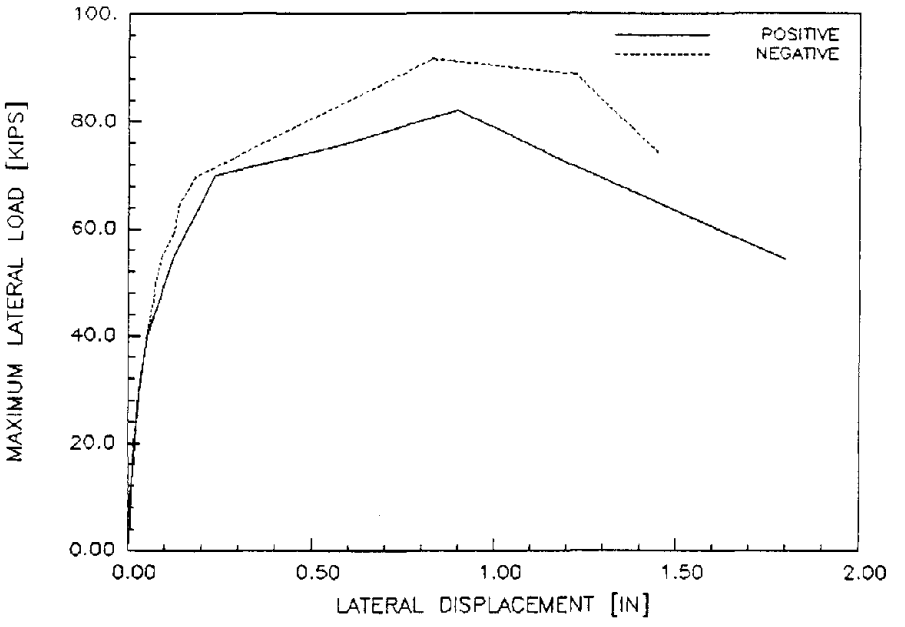

Figure B15 - Load Versus Displacement Envelopes of Specimen 15

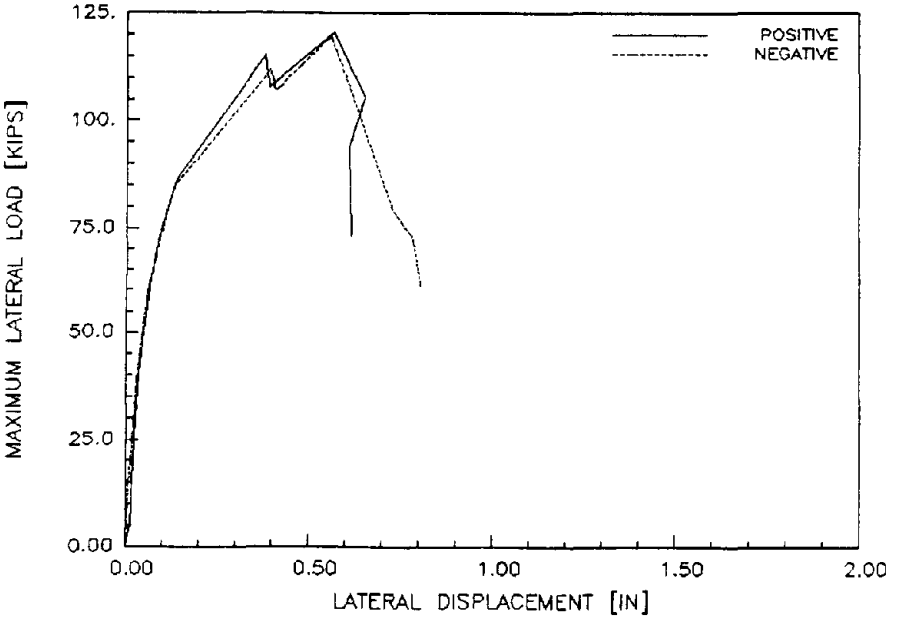

Figure B16 - Load Versus Displacement Envelopes of Specimen 16

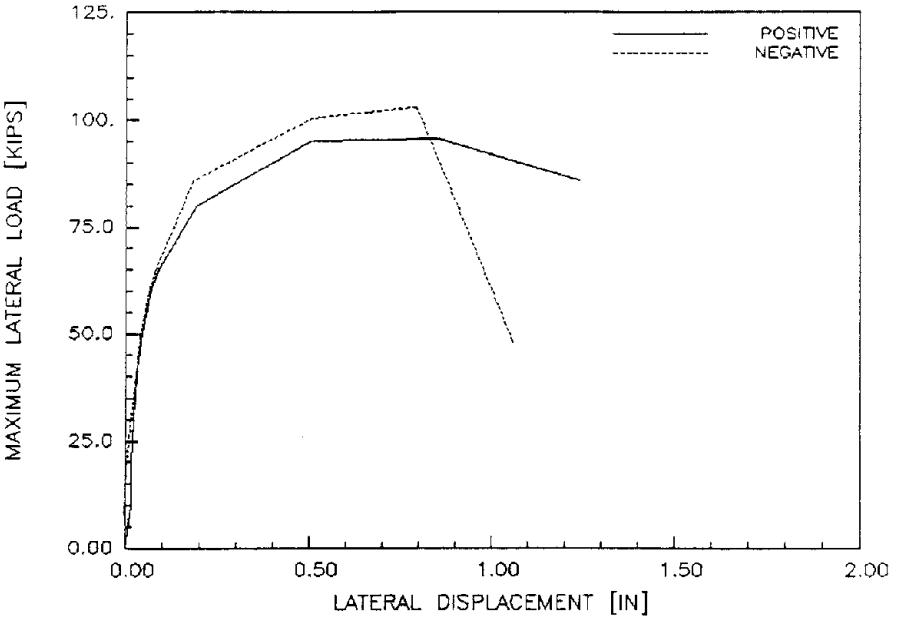

Figure B17 - Load Versus Displacement Envelopes of Specimen 17

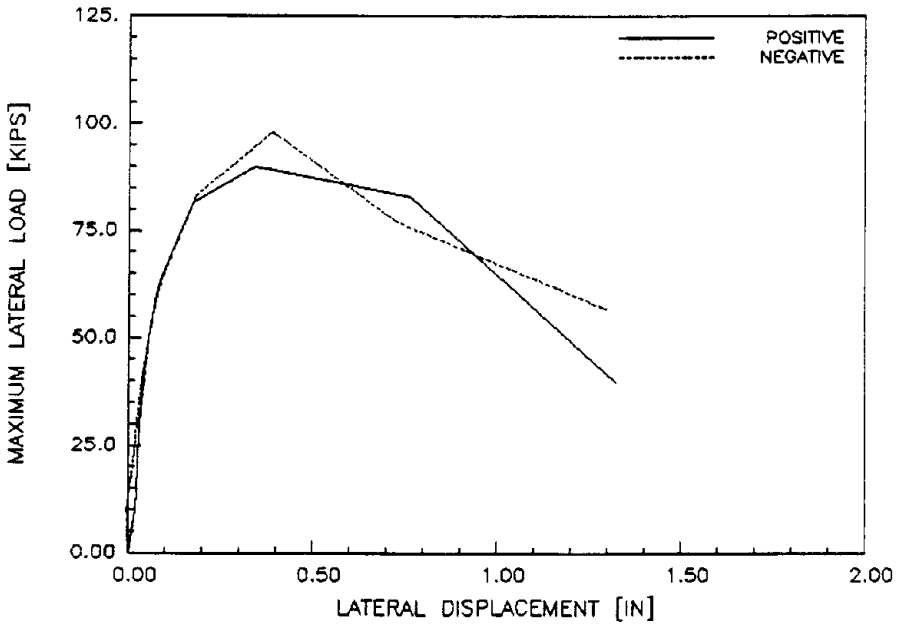

Figure B18 - Load Versus Displacement Envelopes of Specimen 18

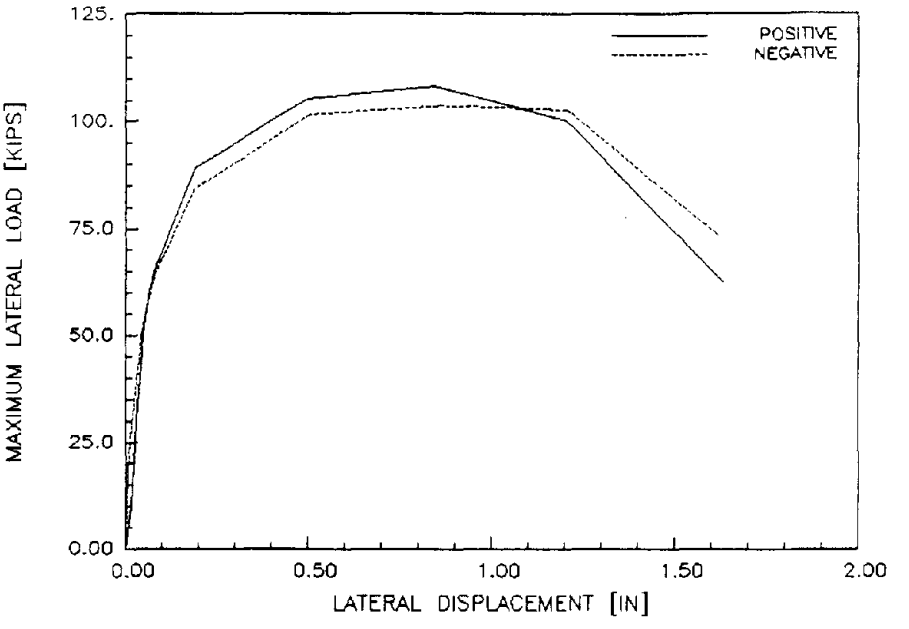

Figure B19 - Load Versus Displacement Envelopes of Specimen 19

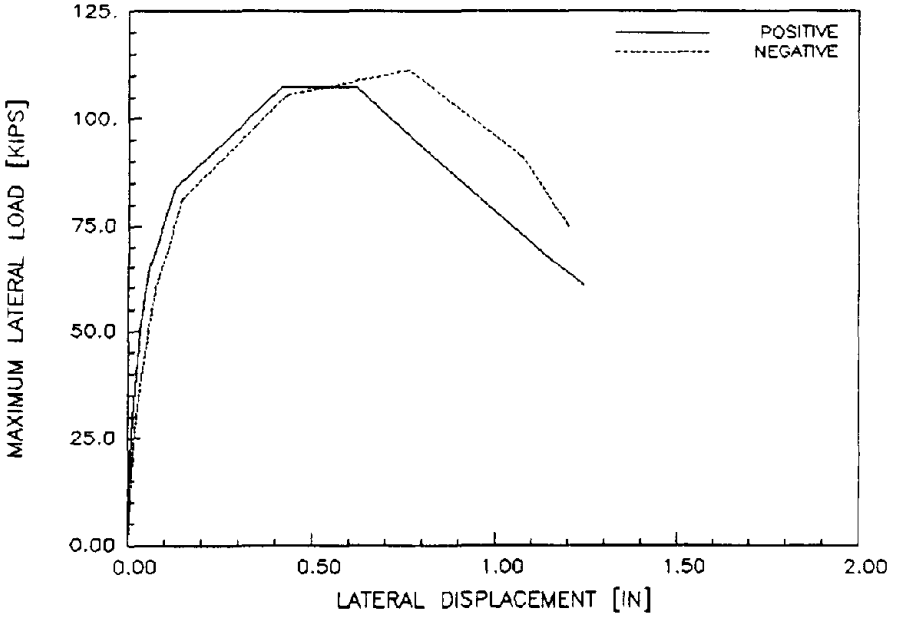

Figure B20 - Load Versus Displacement Envelopes of Specimen 20

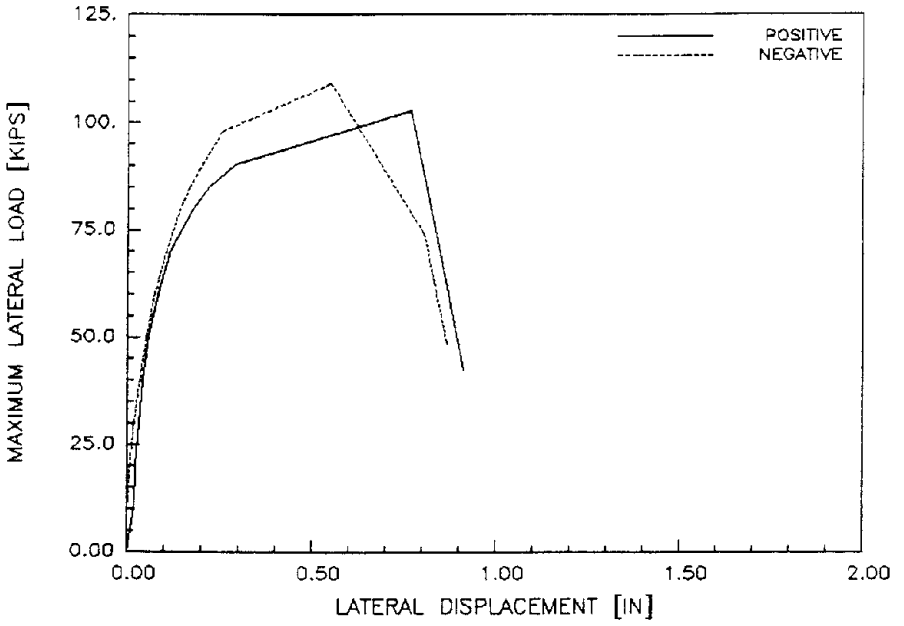

Figure B21 - Load Versus Displacement Envelopes of Specimen 21

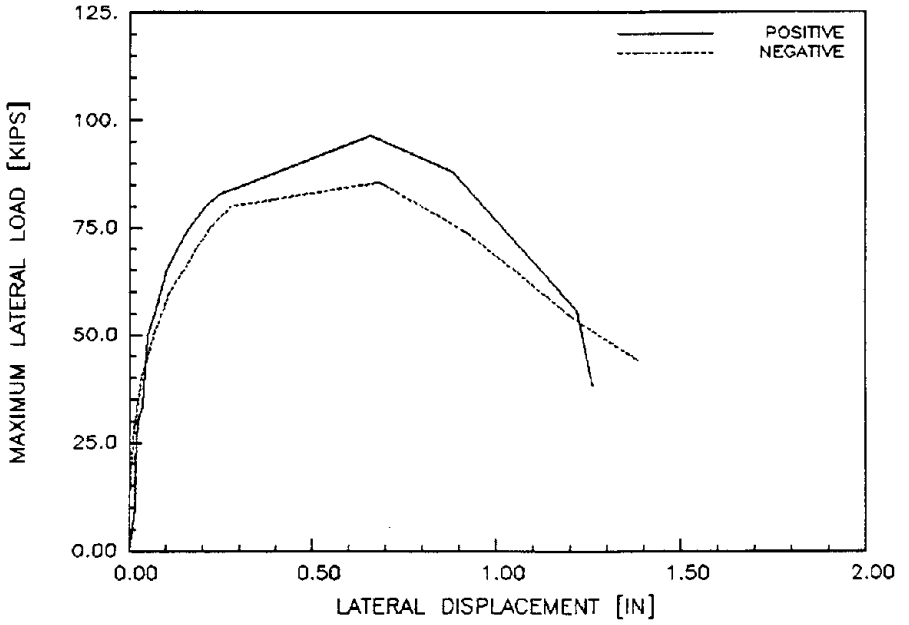

Figure B22 - Load Versus Displacement Envelopes of Specimen 22

REFERENCES

Annual Book of ASTM Standards. (1984 Ed.) American Society for Testing and Materials, Philadelphia.

Atkinson, R. H. and Kingsley, G. R. (1985). "A Comparison of the Behavior of Clay and Concrete Masonry in Compression." *Report No. 1.1-1*, U.S.-Japan Coordinated Program for Masonry Building Research, Atkinson-Noland & Associates, Boulder.

Bertero, V. V., Popov, E. P., and Wang, T. Y. (1974). "Hysteretic Behavior of Reinforced Concrete Flexural Members with Special Web Reinforcement." *Report No. UCB/EERC-74/9*, Earthquake Engineering Research Center, University of California, Berkeley.

Blume, J. A. and Proulx, J. (1968). "Shear in Brick Grouted Masonry Wall Elements." *Report*, Western States Clay Products Association, San Francisco.

Building Code Requirements for Reinforced Concrete (ACI 318-83). (Revised 1986) American Concrete Institute, Detroit, Michigan.

Cantu, E. and Macchi, G. (1979). "Strength and Ductility Tests for the Design of Reinforced Brickwork Shear Walls." *Proceedings*, Fifth International Brick Masonry Conference, Washington, DC.

Chen, S. W., Hidalgo, P. A., Mayes, R. L., Clough, R. W., and McNiven, H. D. (1978). "Cyclic Loading Tests of Masonry Single Piers, Vol. 2 - Height to Width Ratio of 1." *Report No. UCB/EERC-78/28*, Earthquake Engineering Research Center, University of California, Berkeley.

Giuffre', A., Macchi, G., and Modena, C. (1984). "Research on Reinforced Masonry Walls for Seismic Regions." *Proceedings*, CIB-3rd International Symposium on Wall Structures, Warsaw, Poland.

Hegemier, G. A., Nunn, R. O., and Arya, S. K. (1978). "Behavior of Concrete Masonry under Biaxial Stresses." *Proceedings*, North American Masonry Conference, The Masonry Society, University of Colorado, Boulder.

Hegemier, G. A., Seible, F., Nagy, G., Igarashi, A., and Latham, C. T., "Full Scale Simulated Seismic Testing of Reinforced Masonry Structures, Part II - Results of Pseudodynamic Tests of 3-Story Shear Wall," the Sixth Meeting of the Joint Technical Coordinating Committee on Masonry Research, U.S.-Japan Coordinated Program for Masonry Building Research, Port Ludlow, Washington, August 20-22, 1990.

Hidalgo, P. A., Mayes, R. L., McNiven, H. D., and Clough, R. W. (1978). "Cyclic Loading Tests of Masonry Single Piers, Vol. 1 - Height to Width Ratio of 2." *Report No. UCB/EERC-78/27*, Earthquake Engineering Research Center, University of California, Berkeley.

Hidalgo, P. A., Mayes, R. L., McNiven, H. D., and Clough, R. W. (1979). "Cyclic Loading Tests of Masonry Single Piers, Vol. 3 - Height to Width Ratio of 0.5." *Report No. UCB/EERC-79/12*, Earthquake Engineering Research Center, University of California, Berkeley.

Luders, C. and Hidalgo, P. (1988). "Seismic Behavior of Reinforced Masonry Walls." *Proceedings*, Ninth World Conference on Earthquake Engineering, Vol. VI, Tokyo-Kyoto, Japan.

Kaba, S. A. and Mahin, S. A. (1983). "Interactive Computer Analysis Methods for Predicting the Inelastic Cyclic Behavior of Structural Sections." *Report No. UCB/EERC-83/18*, Earthquake Engineering Research Center, University of California, Berkeley.

Kaminosono, T., et al. (1988). "Experimental Study on Seismic Performance of Reinforced Masonry Walls." *Proceedings*, Ninth World Conference on Earthquake Engineering, Vol. VI, Tokyo-Kyoto, Japan.

Kingsley, R. L., Tulin, L. G., and Noland, J. L. (1985). "Parameters Influencing the Quality of Grout in Hollow Clay Masonry." *Proceedings*, Seventh International Brick Masonry Conference, Melbourne, Australia.

Macchi, G. (1982). "Behavior of Masonry under Cyclic Actions and Seismic Design." *Proceedings*, Sixth International Brick Masonry Conference, Rome, Italy.

Matsumura, A. (1988). "Shear Strength of Reinforced Masonry Walls." *Proceedings*, Ninth World Conference on Earthquake Engineering, Vol. VI, Tokyo-Kyoto, Japan.

Mayes, R. L., Omote, Y., and Clough, R. W. (1976a). "Cyclic Shear Tests of Masonry Piers, Vol. 1 - Test Results." *Report No. UCB/EERC-76/8*, Earthquake Engineering Research Center, University of California, Berkeley.

Mayes, R. L., Omote, Y., and Clough, R. W. (1976b). "Cyclic Shear Tests of Masonry Piers, Vol. 2 - Analysis of Test Results." *Report No. UCB/EERC-76/16*, Earthquake Engineering Research Center, University of California, Berkeley.

Meli, R. (1973). "Behavior of Masonry Walls under Lateral Loads." *Proceedings*, Fifth World Conference on Earthquake Engineering, Rome, Italy.

Merryman, K. M., Leiva, G. Antrobus, N., and Klingner, R. E. (1990). "In-Plane Seismic Resistance of Two-Story Concrete Masonry Coupled Shear Walls," *Report No. 3.1(c)-1*, U.S.-Japan Coordinated Program for Masonry Building Research, University of Texas, Austin.

Noland, J. L. (1987). "A Review of the U.S. Coordinated Program for Masonry Building Research." *Proceedings*, Fourth North American Masonry Conference, The Masonry Society, University of California, Los Angeles.

Priestley, M. J. N. and Bridgeman, D. O. (1974). "Seismic Resistance of Brick Masonry Walls." *Bull. of the New Zealand National Society for Earthquake Engineering*, Vol. 7, No. 4.

Priestley, M. J. N. (1977). "Seismic Resistance of Reinforced Concrete Masonry Shear Walls with High Steel Percentages." *Bull. of the New Zealand National Society for Earthquake Engineering*, Vol. 10, No. 1.

Priestley, M. J. N. (1981). "Ductility of Unconfined and Confined Concrete Masonry Shear Walls," *The Masonry Society Journal*, Vol. 1, No. 2.

Priestley, M. J. N. and Elder, D. (1982). "Cyclic Loading Tests of Slender Concrete Masonry Shear Walls." *Bull. of the New Zealand National Society for Earthquake Engineering*, Vol. 15, No. 1.

Priestley, M. J. N. (1986). "Flexural Strength of Rectangular Unconfined Masonry Shear Walls with Distributed Reinforcement." *The Masonry Society Journal*, Vol. 5, No. 2.

Priestley, M. J. N. (1987). "The Role of Research in the Formulation of Masonry Design Procedures." *Proceedings*, Fourth North American Masonry Conference, The Masonry Society, University of California, Los Angeles.

Schneider, R. R. (1956). "Tests on Reinforced Grouted Brick Masonry Shear Panels." *Report*, California State Division of Architecture, Los Angeles, CA.

Scrivener, J. C. (1969). "Static Racking Tests on Masonry Walls." *Designing, Engineering and Constructing with Masonry Products*, Edited by Johnson, F. B., Gulf Publishing Co., Houston.

Sheikh, S. A. And Uzumeri, S. M. (1982). "Analytical Model for Concrete Confinement in Tied Columns." *Journal of Structural Engineering*, ASCE, Vol. 108, No. ST12.

Soric, Z. and Tulin, L. G. (1987). "Bond & Splices in Reinforced Masonry," *Report No. 6.2-2*, U.S.-Japan Coordinated Program for Masonry Building Research, University of Colorado, Boulder.

Sveinsson, B. I., McNiven, H. D., And Sucuoglu, H. (1985). "Cyclic Loading Tests of Masonry Single Piers, Vol. 4 - Additional Tests with Height to Width Ratio of 1." *Report No. UCB/EERC-85/15*, Earthquake Engineering Research Center, University of California, Berkeley.

Tassios, T. P., Vintzeleou, E., And Trohanis, A. (1984). "Reinforced Masonry Squat Walls under Horizontal Monotonic and Cyclic Loading." *Proceedings*, Eighth World Conference on Earthquake Engineering, Vol. V, San Francisco.

Tomazevic, M., Lutman, M., Velechovsky, T., And Zarnic, R. (1986). "Seismic Resistance of Reinforced Masonry Walls." *Report No. ZRMK/IKPI-86/04*, Institute for Structures and Earthquake Engineering, Ljubljana, Yugoslavia.

Tomazevic, M. And Lutman, M. (1988). "Seismic Resistance of Reinforced Masonry Walls." *Proceedings*, Ninth World Conference on Earthquake Engineering, Vol. VI, Tokyo-Kyoto, Japan.

Uniform Building Code. (1988 Ed.) International Conference of Building Officials, Whittier, CA.

Uniform Building Code Standards. (1985 Ed.) International Conference of Building Officials, Whittier, CA.

Wakabayashi, M. And Nakamura, T. (1984). "Reinforcing Principle and Seismic Resistance of Brick Masonry Walls." *Proceedings*, Eighth World Conference on Earthquake Engineering, Vol. V, San Francisco.

Williams, D. And Scrivener, J. C. (1973). "Response of Reinforced Masonry Shear Walls to Static and Dynamic Cyclic Loading." *Proceedings*, Fifth World Conference on Earthquake Engineering, Rome, Italy.

Woodward, K. And Rankin, F. (1985). "Influence of Block and Mortar Strength on Shear Resistance of Concrete Block Masonry Walls." *Report NBSIR 85-3143*, National Bureau of Standards, Gaithersburg, MD.